UNIVERSITY OF UDINE

Department of Agricultural, Food, Environmental and Animal Sciences
(DI4A)

Doctor of Philosophy in:
FOOD AND HUMAN HEALTH

XXXIII Cycle

Title of the thesis

Anticancer Activity and Structural Investigations of Novel Carbonyl Diphosphine Ruthenium(II) Complexes

Ph.D. Student:
Denise Lovison

Supervisor:
Prof. Walter Baratta

Co-Supervisor:
Prof. Giuseppe Damante

2021

TABLE OF CONTENTS

SUMMARY

The aim of this thesis was the synthesis of novel ruthenium complexes and the evaluation of their anticancer activity. Moreover, the behavior of these systems in water solution and towards different substrates was deeply studied. The work performed on this subject can be divided into four parts as follows:

1. The first part has concerned the synthesis and the characterization of three neutral ruthenium complexes of general formula [Ru(η^1-OAc)(CO)(dppb)(dkt)] (dkt = acetylacetonate, dibenzoylmethane, curcumin), trying to exploit the β-diketones properties as antioxidant, anti-inflammatory, anticarcinogenic and chemopreventive agents.
2. The second part has been focused on the synthesis and characterization of monocationic ruthenium complexes bearing diimine ligands in place of β-diketones. Once obtained the complex of formula [Ru(η^1-OAc)(CO)(dppb)(phen)]OAc and studied its reactivity, precise and rationalized modification on the ligands around the ruthenium center have been carried out, including phenanthroline functionalization, substitution of different anions, introduction of chiral diphosphines and replacement of the carbonyl with an isonitrile group. All these modifications were carried out after structure-activity relationship (SAR) evaluations.
3. During the third part, dicationic ruthenium complexes of general formula [Ru(CO)(dppb)(phen)(L)]$(PF_6)_2$ (L = 1,3,5-triaza-7-phosphaadamantane or pyridine) have been obtained exploiting a protic solvent like water, starting from [Ru(η^1-OAc)(CO)(dppb)(phen)]OAc.
4. The final part has regarded the evaluation of the anticancer activity of the novel ruthenium complexes against anaplastic thyroid cancer and colon carcinoma cell lines. In addition, for the most promising complexes, the capacity to induce apoptotic cell death and the antimetastatic properties were studied.

ABBREVIATIONS TABLE

Acac	Acetylacetonate
ATC	Anaplastic Thyroid Cancer
bpy	2,2'-bipyridine
DCM	dichloromethane
DFT	Density Functional Theory
dkt	diketone
dmso	dimethyl sulfoxide
dppb	1,4-Bis(diphenylphosphino)butane
dppy	2-(Diphenylphosphino)pyridine
dpqQx	dipyrido[3,2-a:2’,3’-c]quinoxalino[2,3-b]quinoxaline
en	ethylenediamine
GSH	glutathione (reduced)
GSSG	glutathione (oxidized)
HAS	Human Serum Albumin
IP	1*H*-imidazo[4,5-*f*][1,10]phenanthroline
MeOH	methanol
NMR	Nuclear Magnetic Resonance
NN	diamine
OAc	acetate
OPiv	pivalate
PARP	poly [ADP-ribose] polymerase
Phen	1,10-phenanthroline
PI	Propidium Iodide

PP	diphosphine
PTA	1,3,5-triaza-7-phosphaadamantane
Py	pyridine
PzPhen	pyrazino[2,3-*f*][1,10]phenanthroline
SAc	thioacetate
SAR	Structure-Activity Relationship
TIP	2-(thiophen-2-yl)-1*H*-imidazo[4,5-*f*][1,10]phenanthroline
TOF	Turnover frequency
TrxR	Thioredoxin Reductase

1 INTRODUCTION

1.1 METALS IN MEDICINE

In the late 1800´s, experiments carried out with blood samples revealed the existence of iron containing compounds in this fluid, proving the presence of metals in different enzymes. As a matter of fact, during the evolution, many metals have been incorporated into essential biological functions. Nowadays, it is well known that inorganic elements play different and important biological key roles, including stabilization of bone structure thanks to $CaCO_3$, transfer of electrons in cytochrome c, and redox reactions in metalloenzymes containing copper, iron, zinc and manganese[1]. Using their oxidation states, metals are able to control reversible binding of small molecules, like O_2 in hemoglobin, an iron containing protein. The typical coordination M-L bond can be much weaker than covalent bonding and this allows more flexibility in binding and dissociation of small molecules under biological conditions.

The fact that some metal ions are essential for life, also suggested the possibility of incorporating them into drugs. In the case of metallodrugs, the above mentioned M-L bond plays an important role in target recognition, particularly cell uptake and interaction with a large scale of biomolecules, undergoing a transformation in vivo before (in the case of the so called “prodrugs”) or after reaching its target, such as reduction or oxidation of the metal center, ligands substitution or reaction of the ligands[2-3]. In this way, we can increasingly make use of their unique properties in the development of potential novel therapies, taking into account the behavior of a metal complex, which is dependent on both its composition and the environment in which it finds itself. Control of different characteristics is important in the rational design of a metallodrug; among them, we should pay attention on the metal coordination number, the geometry, the oxidation state and the reactivity of the metal complex to predict features such as biochemical pathways and stability, biochemical pathways including cell uptake, metabolism and biological interactions. Predicting and controlling that behavior is one of the challenges for advancing the rational design of inorganic pharmaceuticals[3]. In this context, ligands can also represent organic drugs or small molecules (CO, NO)[4] and metals may also be used as multi-delivery systems in order to improve the drug’s specificity by extending ligand structures and facilitating transport to the site of action[5].

The first compound containing an inorganic element that was described to be used in medicine was Salvarsan, an arsenic compound used in the treatment of syphilis[6]. Salvarsan was synthesized and tested in the beginning of the 20th century by Ehrlich who was awarded the Nobel Prize in 1908 for his discovery of immunochemistry. He is considered the founder of chemotherapy, which he defined as “the use of drugs to injure an invading organism without injury to the host”. Ehrlich introduced the “magic bullet” concept, also known as “drug targeting”, nowadays the object of extensive research worldwide[5].

Nowadays, the application of metals for medical purposes ranges from anticancer, antimicrobial and antiarthritis agents to those used as contrast agents, radiopharmaceuticals and in chelation therapy (**Figure 1**).

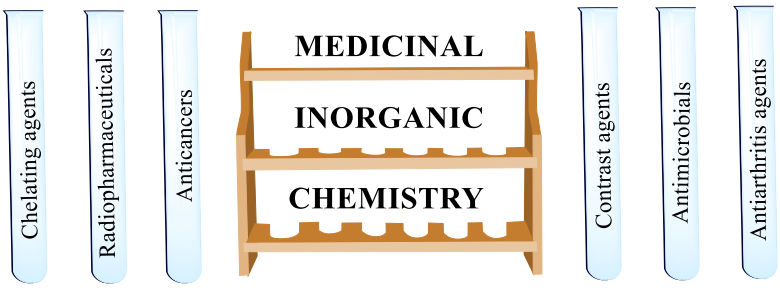

Figure 1. The most important areas of medicinal inorganic chemistry

Cancer is the hot topic in which metals have emerged as promising and viable therapeutic targets, due to a rapid increase in tumor cases worldwide. Most of the studied and approved anticancer drugs are organic molecules, although metallodrugs can cover a wider area of biological space possibilities, due to their ability to form structures with unique and defined shapes, where the metal can have the main purpose to organize the organic ligands in order to build small compounds with defined three-dimensional structures[3].

Even though metals can appear to be toxic at minimal dosage levels, they may not be equally dangerous for all organisms at all levels.

It has also been proven that toxic metal complexes can kill tumors at certain body locations. There is still an indispensable need for the development and screening of potential anticancer agents.

1.2 THE DISCOVERY OF CISPLATIN

Medicinal inorganic chemistry as a discipline is considered to have boosted with the discovery of the anticancer properties of cisplatin.

Cisplatin or cis-diamminedichloroplatinum(II) is a platinum-based anti-cancer complex which continues to be the most successful drug used for the treatment of several cancers, including testicular, ovarian, bladder, cervical, head and neck and small-cell lung tumors, either as a first-line treatment or in combination with other anti-cancer drugs[7].

The discovery of the anticancer properties of cisplatin represents the main milestone in the history of anticancer drugs, which led to the expansion of the family of platinum compounds. Cisplatin is a neutral square planar platinum complex with the metal in the +2 oxidation state. It was first synthesized in 1844 by Peyrone and its antiproliferative activity was discovered by Rosenberg, a biophysics researcher at Michigan State University, in 1965 while he was studying the effect of electric current on Escherichia coli using platinum electrodes[8]. He found out that the process of cell division was influenced and inhibited by the electrical field, so he thought he might have found a way to control cell growth with electrical currents. Finally, he realized that electricity had nothing to do with it and that cell division was blocked not by the electric field, but by a platinum compound released from the electrodes. In this way, Dr. Rosenberg's team identified the compound that influenced cell division and it was later named “cisplatin” (**Figure 2**).

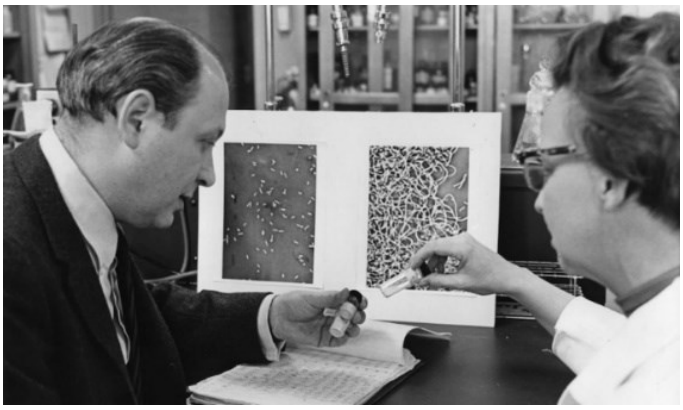

Figure 2. Chemistry professor Barnett Rosenberg and his colleague Loretta VanCamp observing that cisplatin inhibits cell division.

Dr. Rosenberg then wondered whether cisplatin would also block cell division in tumors, testing it in a sarcoma mouse model. He and his colleagues found that it was able to attack

and regress cancer. The mice tolerated the drug in low doses, but, more importantly, the tumors responded to cisplatin and decreased[7]. In six months, the mice remained healthy and showed no return of the tumors. Cisplatin was licensed for medical use in 1978/1979.

1.3 MECHANISM OF ACTION OF CISPLATIN

Cisplatin administration protocols currently include an intravenous infusion. Since this method is far from ideal, requiring patient hospitalization, research has been carried out to find an alternative administration route. A release-controlled formulation of cisplatin with reduced toxicity has recently been developed. The complex is encapsulated inside nano-scale liposomal carriers and administered to the patient via nebulization. This new approach is currently undergoing phase I clinical trials[9]. In the bloodstream, the high physiological chloride concentration (ca. 100 mM) ensures that the complex remains neutral until it enters the cell, preventing the hydrolysis. The mechanism by which cisplatin enters cells is still under debate. Originally, it was thought to enter cells by passive diffusion, being a neutral molecule[10]. Recently, researchers discovered that cisplatin might pass the cell membrane via active transport mediated by copper transporter Ctr1p present in yeast and mammals[11]. The very low chloride concentration in the cells (~3mM) facilitates water interaction with the platinum coordination sphere, forming several cationic and aquated species which are able to react with the nucleophilic sites in the cell, where nuclear DNA is the most preferential and cytotoxic target[10] (**Figure 3**).

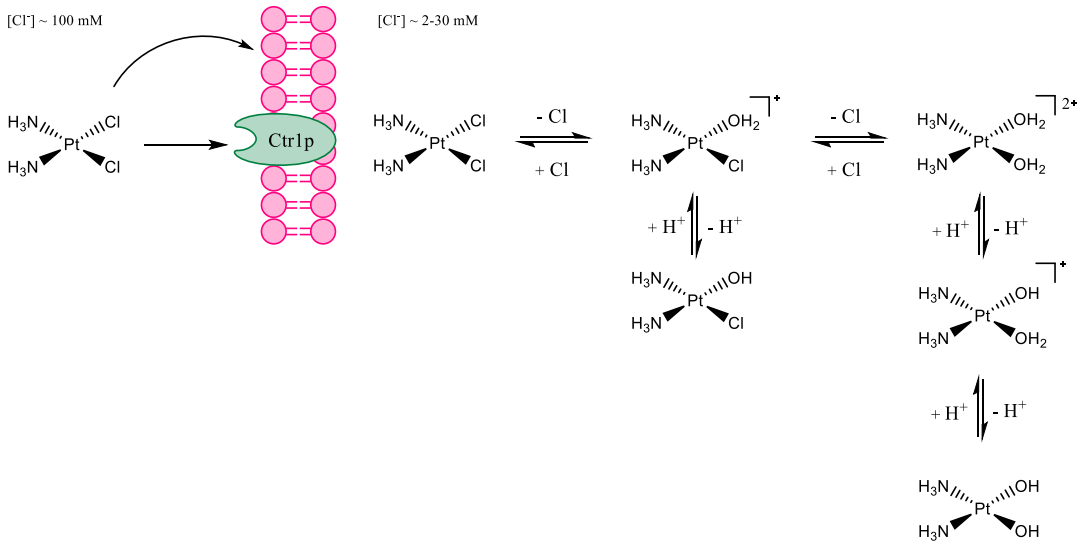

Figure 3. Cisplatin transport mediated by copper transporter Ctr1p and aquated species in cellular environment.

Cisplatin can bind to nucleic acids, proteins and sulfur-containing biomolecules, such as glutathione (GSH)[12]. The ultimate target of cisplatin, which triggers its cytotoxicity, is generally accepted to be nucleic acids[7]. Cisplatin binds to nuclear DNA and forms covalent crosslinks with the nucleobases. The $[Pt(NH_3)_2]^{2+}$ unit binds covalently to the N-7 of the imidazole rings of purine bases (guanine (G) or adenine (A)) via electrostatic interaction of the positively charged complex[10].

There are three different types of aquated cisplatin crosslinking to DNA. Monoadducts are formed when one molecule of water is lost from the aquated cisplatin, which then tends to react and form crosslinks with DNA. Intrastrand crosslinks are formed when two chloride ligands of the aquated cisplatin are replaced by purine nitrogen atoms on adjacent bases of the same DNA strand. These crosslinks are referred to as 1,2-d(GpG) crosslinks and almost all cisplatin DNA crosslinks are of this type. Additional DNA crosslinks include the 1,2 or 1,3 interstrand crosslinks[10, 13] (**Figure 4**).

The formation of such cisplatin-DNA adducts causes a significant distortion of the helical structure leading to replication arrest, transcription inhibition, cell cycle arrests, and eventually cell death by apoptosis.

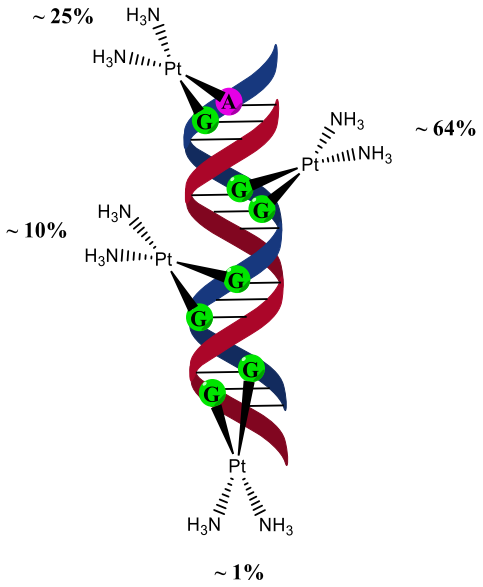

Figure 4. Binding mode of cisplatin with nucleobases on DNA helix.

1.4 CURRENT PLATINUM CHEMOTHERAPEUTIC DRUGS

More than half of patients with cancer receive chemotherapy. Among the available therapies ‘‘platinum chemotherapy’’ is the term used for cancer treatment where one of the chemotherapeutic drugs is a platinum derivative. Cisplatin, the most widely known metal-based anticancer drug, has been the treatment of choice for several type of cancers during the past 30 years, giving characteristic relief and modest improvement in survival[5]. Although cisplatin is efficacious against the vast majority of cancers, it also gives non-cancer cell toxicity, causing severe adverse effects, including peripheral neuropathy, myelotoxicity, nephrotoxicity and ototoxicity in patients. In order to minimize the side effects of cisplatin, to enhance the therapeutic index, and for application against cisplatin-resistant tumors, a second generation of platinum-based anticancer agents were subsequently developed, including carboplatin and oxaliplatin, approved for medical use in 1986 and 1996, respectively, and registered worldwide[13-14] (**Figure 5**).

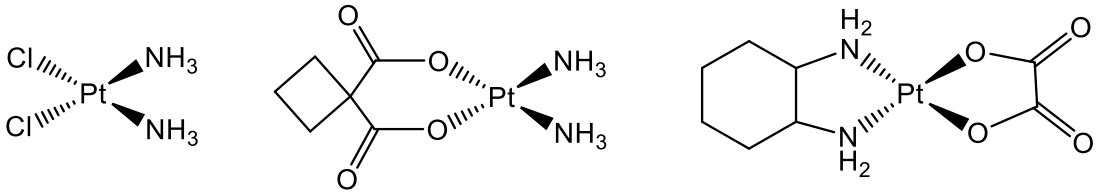

Cisplatin Carboplatin Oxaliplatin

Figure 5. Chemical structures of cisplatin, carboplatin and oxaliplatin.

The chelate effect of the six member ring in carboplatin is thought to reduce the reactivity of the platinum drug, decreasing its nephrotoxicity and ototoxicity, although it is able to inhibit synthesis of RNA, DNA, and protein in cells, preventing the tumor spreading.

Oxaliplatin has modest activity against advanced colon or rectal cancer that has metastasized, it is often given in combination with other anticancer drugs (fluorouracil and leucovorin). It is believed to work by blocking the duplication of DNA[15].

Several platinum compounds are currently under clinical evaluation, including orally administered satraplatin (*cis*,*trans*-[$PtCl_2(\eta^1\text{-}OAc)_2(NH_3)$(cyclohexylamine)) which is the only platinum drug available for oral administration to the patient[16]. It contains a Pt(IV) center that after the action of redox proteins it is reduced to Pt(II), the active form. It showed promising activity against hormone refractory prostate cancer. A trinuclear platinum complex, triplatin

tetranitrate[17] was also developed and tested against various types of cancer. However, severe side effects including nausea and diarrhea stopped it in phase III clinical trials.
In general, it has been shown that the platinum drugs lose their therapeutic benefits after the initial success because of the intrinsic resistance acquired by the malignant tissues, making platinum-based drugs ineffective and causing treatment failure. The vast majority of platinum compounds synthesized for cancer therapy have been abandoned because of low efficacy, high toxicity, and/or low water solubility[2, 5].

1.5 RUTHENIUM-BASED ANTICANCER DRUGS AS ALTERNATIVE TO CISPLATIN

The antitumor mechanisms of platinum complexes, especially the DNA binding modes and DNA replication suppression, are of great importance for the rational design of novel compounds. It is necessary to highlight that the main goal of developing non-platinum metal anticancer molecules is to contrast tumors that are resistant to Pt drugs. Non-platinum compounds may be expected to have anticancer activity and toxic adverse effects markedly different from those of Platinum drugs for their distinct coordination geometries, binding preferences, and ligand exchange rates, so leading to other mechanisms of action and, as a consequence, to different biological properties[18].
Along with the extensive ongoing research for the development and modification of suitable platinum drugs, ruthenium compounds have also shown promising results as anticancer agents, raising great interest against a number of cancer cell lines. Ruthenium(II) and (III) complexes have different ligand-exchange kinetics to those of platinum(II) complexes, making them the first choice in the search for compounds that display similar biological effects to platinum(II) drugs[5, 18]. Since very few metal drugs reach the biological targets without being modified, it was found that most of them undergo interactions with macromolecules such as proteins, or with small S-donor compounds, or water. This kind of interactions are essential to determine the biological activity and to induce the desired therapeutic effect[19-20].
The ruthenium center, predominantly octahedral, exists in different oxidation states, namely Ru(II), Ru(III) and Ru(IV), where Ru(III) complexes tend to be more biologically inert than the related compounds containing Ru(II) and Ru(IV) ones. Once into the biological environment, the redox potential of a ruthenium complex can be modified by varying the

ligands. In healthy cells, the reduction of Ru(III) to Ru(II) is a very easy process run by glutathione, ascorbate and proteins involved in the mitochondrial electron-transfer chain, while Ru(II) is quickly oxidized back to Ru(III) by means of molecular dioxygen and cytochrome oxidase present in tissues.

Ruthenium(II) complexes are generally more reactive than the corresponding ruthenium(III) and their activation by reduction was proposed by Clarke and coworkers[21]. These authors suggested, for Ru(III) chloride complexes, that aquation was preceded by *in vivo* reduction to ruthenium(II), releasing the chloride anions and affording aqua species that are capable of coordinating to the biological targets. Thus, the reduction of relatively inert Ru(III) complexes by glutathione is more important in the hypoxic environment of solid tumors thanks to the altered metabolism associated with cancer which results in lower oxygen concentration[22].

Another property that makes ruthenium suitable for medical uses, is its ability to selectively bind biomolecules, including transferrin and albumin, two proteins employed to solubilize and transport iron[23]. Rapidly dividing cells, such as cancer cells, require greater quantity of iron, so they increase the number of transferrin receptors on their surfaces; this implies that, possibly, the amount of ruthenium taken up by this cancer cells is greater than the healthy ones[24]. This selectivity of the drug towards the diseased cells would explain the low toxicity of many ruthenium compounds, compared to platinum ones. However, besides the similarities between Fe and Ru ions (size, charge, coordination geometry), their coordination chemistry is quite different in terms of thermodynamics and kinetics. In addition, it is not easily understood how ruthenium species with residual ligands and different net charge, can compete for the binding sites of Fe^{2+}/Fe^{3+} proteins and enzymes[25].

One of the main features of cancer cells is the loss of control on the cell cycle division, leading to a high rate of proliferation. Taking into account this aspect and considering this process regulated by DNA, many ruthenium compounds have been designed to have high selectivity in binding DNA. The electron-deficient metal atoms might act as electron acceptors for electron-rich DNA nucleophiles[5].

Based on the suitable properties of ruthenium, different approaches are nowadays adopted for the design of new anticancer compounds, although the biological target(s) and mechanism of action of such ruthenium complexes are largely unknown.

1.5.1 NAMI-A

The first approved ruthenium complex in clinical trials, NAMI-A, (*trans*-[Ru(III)Cl_4(dmso-S)(Im)](ImH), Im = imidazole) has attracted a lot of attention in the medicinal inorganic chemistry scientific community as promising anticancer drug candidate (**Figure 6**).

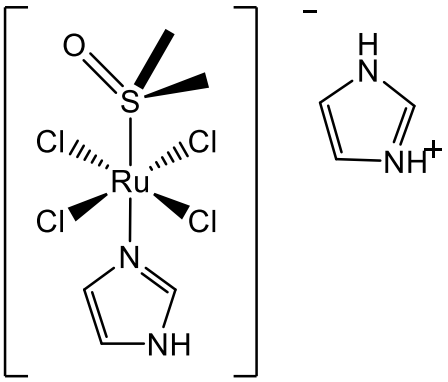

NAMI-A

Figure 6. Chemical structure of NAMI-A.

It shows low potency towards cancer cells in vitro, however, in vivo, it has significant efficacy in inhibiting tumor spread in metastatization process, demonstrating excellent and selective activity against lung metastasis of a number of solid metastasizing tumors[5]. In particular, NAMI-A is basically non-cytotoxic against solid tumor, and metastasis reduction (up to 100 %) take place without significant reduction of primary tumor growth, thus suggesting the occurrence of a different pathway from that of Pt anticancer drugs, even at the beginning[26]. Indeed, the lack of cytotoxicity towards solid tumor is due to the fact that NAMI-A undergoes extracellular metabolization and its metabolites, namely the aquated and the reduced forms, interact mainly with targets in the cell membrane without being internalized by cells, trigging integrin activation, actin nucleation and microfilament elongation, which are related with adhesion in cancer cells. The mechanisms of action of NAMI-A are not fully understood, but aquation is thought to be an important step for its activation, forming a reactive aqua species which are able to interact with biomolecules[18]. NAMI-A undergoes two well-separated steps of hydrolysis, as shown in **Scheme 1.**

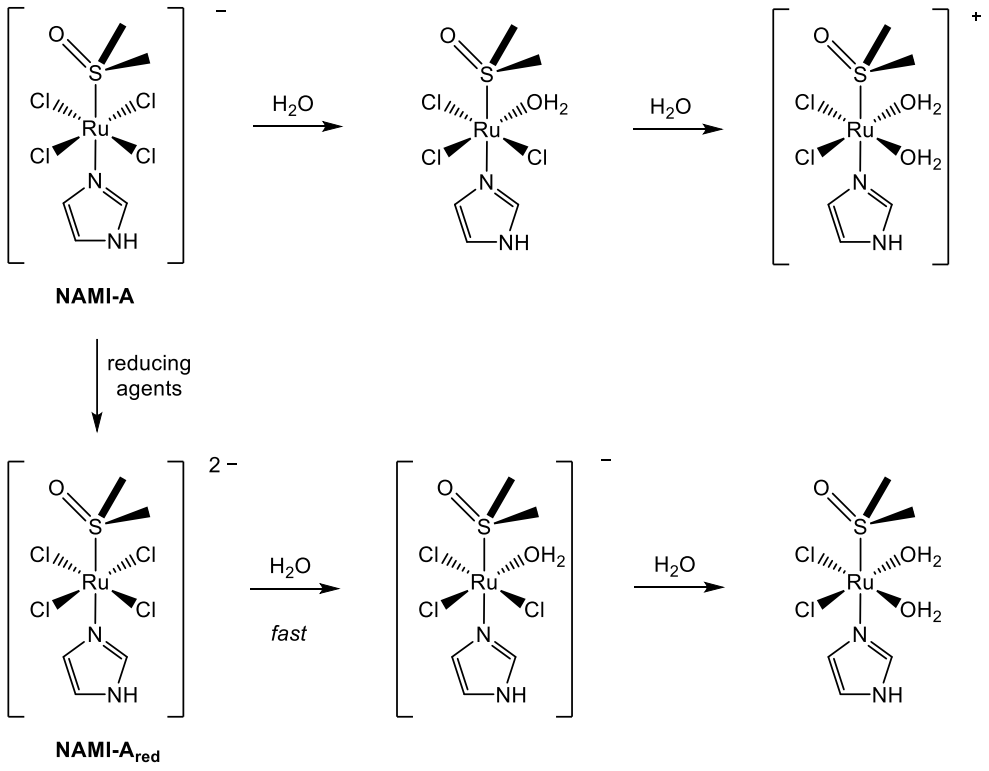

Scheme 1. The mechanism of hydrolysis and activation of NAMI-A at pH = 7.4.

At physiological pH, biological reducing agents such as glutathione, reduce NAMI-A to dianionic Ru(II) specie (NAMI-A_{red}), which then undergoes a two-step chloride hydrolysis. However, the reduction of the complex is not responsible of its activity, instead, the anti-metastatic activity of NAMI-A is strictly related to the presence of the dmso ligand[27].

Recently, the ligand-exchange process between NAMI-A and human serum albumin (HAS) was investigated, using electron paramagnetic resonance spectroscopy (EPR). NAMI-A demonstrated to bind selectively the protein side chain, at level of the imidazole ring of histidine, via hydrophobic interactions[28]. Other possible paths, related to cellular uptake, is the transient blocking of the cell cycle progression at the G2-M premitotic phase, DNA and RNA binding once it enters the cancer cells[20]. Finally, NAMI-A metabolites are responsible for low and reversible side effects on kidneys, where high concentration of ruthenium was found, suggesting kidneys as the main pathway of ruthenium excretion.

1.5.2 Arene ruthenium complexes

Recently, a new class of organometallic Ru(II)-arene compounds, developed by the groups of Sadler and Dyson, demonstrated promising anticancer activity *in vitro* and *in vivo*.

The Ru(II)-arene complexes have the general formula [(η^6-arene)Ru(X)(Y)(Z)], and the geometry of these half-sandwich compounds can be described as pseudo-tetrahedral (piano-stool geometry) assuming that the arene ligand occupies one coordination position. The ligands X and Y are usually two monodentate ligands or a neutral or mono-anionic N,N-, N,O-, or O,O-bidentate ligand which helps to control stability and the kinetics of ligand-exchange[29]. Z typically represents a leaving group such as a halide (Cl, Br, I) and the hydrolysis of Ru-Z bond is affected by pH and Z concentration in the cellular environment. The activation of this class of complexes, is believed to involve rapid hydrolysis of the Ru-Cl bond, thus generating an active Ru–OH_2 specie. This process is not allowed in the extracellular environment ([Cl^-] = 0.1 M) but becomes possible inside the cells, where [Cl^-] is much lower (4-25 mM). The pK_a values of the [(η^6-arene)Ru(en)(H_2O)]$^{2+}$ aqua species are commonly between 7 and 8, and thus at physiological pH the Ru-OH_2 specie largely prevails over the less reactive Ru–OH specie[5] (**Scheme 2**).

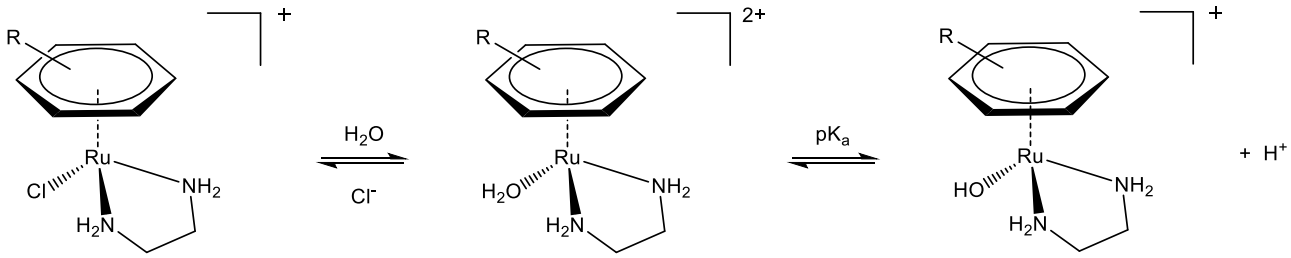

Scheme 2. Hydrolysis of Ru-Cl bond in arene ruthenium complexes inside the cell environment.

The arene rings (benzene, p-cymene, biphenyl, etc.) are the core component of arene Ru(II) complexes where their hydrophobic nature facilitate the entry of Ru(II) complexes into cells. Different Ru(II)-arene complexes are able to exert activity in vitro and in vivo against a range of cancer cell lines: the anticancer activity of this class of complexes was first reported in 2001 by Sadler, who was investigating the RAED family of complexes [(η^6-arene)Ru(en)X]$^+$ (X = halide, en = ethylenediamine)[30]. In particular, Sadler's group reported that the variation in the leaving group, the N,N-chelating ligand and the arene ring can have a significant effect on the chemical and biological activity. They explored the ability of the RAED type complexes in targeting human ovarian cancer cell line A2780 and the cisplatin-resistant

variant A2780cis with significant growth delay both in vitro and in vivo. Cytotoxicity increases with the hydrophobicity of the arene ligands when evaluated against the human ovarian cancer cells A2780: compounds with p-cymene or biphenyl have EC_{50} values in the range of 6–9 μM, similar to that of carboplatin, while compounds with tetrahydronaphthalene are equipotent with cisplatin (EC_{50} = 0.6 μM). For this type of complexes, nuclear DNA is mostly the main target. Their reactivity toward DNA was tested against nucleotides and a DNA 14-mer. Both [(η^6-arene)Ru(en)]–nucleobase and –nucleoside adducts have been isolated and characterized by X-ray crystallography, revealing the preferential formation of monofunctional adducts with the *N7* atom of guanine residues, via hydrogen bonding between the carbonyl of guanine and the NH of en, and π- π stacking between the arene ligand and the nucleobase[5, 30]. The interactions between the [(η^6-arene)Ru(en)X]Y complexes with other biologically relevant molecules and potential targets including cytochrome c, the amino acids histidine, cysteine and methionine, and the tripeptide glutathione, have also been investigated. Overall, the results suggest that, in the cell, DNA and RNA are the preferred targets. In addition, cell biological studies have revealed cross-resistance with adriamycin but not with cisplatin, which was also confirmed in vivo.

1.5.3 RAPTA-type ruthenium complexes

The half-sandwich RAPTA-type compounds of general formula [(η^6-arene)$RuCl_2$(PTA)] (RAPTA = ruthenium-arene PTA) developed by the group of Dyson, are the most well-known, characterized by a hydrophilic monodentate phosphane ligand PTA (1,3,5-triaza-7-phosphaadamantane), which confers high water solubility to the complexes[31]. RAPTA-C is the milestone of this class of organometallic, half-sandwich compounds (**Figure 7**). In vitro, RAPTA-C does not show significant cytotoxicity, but it is able to inhibit lung metastasis in mice bearing MCa mammary carcinoma, while having only mild effects on the primary tumor[32].

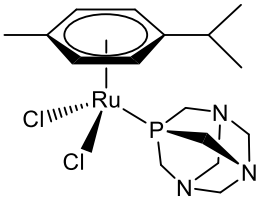

RAPTA-C

Figure 7. Chemical structure of RAPTA-C complex.

RAPTA-type complexes undergo hydrolysis in vivo and it depends on the pH and the amount of chloride present in the solution. Due to this behavior, other Ru(II) compounds containing PTA have been investigated for their DNA-binding properties: for instance, the replacement of the chloride ligands of RAPTA-C with bidentate oxalate o diamine species, modify their solution behavior, making them more inert towards aquation processes, displaying efficacy similar to RAPTA-C in vitro[33]. More recently, the closely similar toluene derivative [(η^6-toluene)$RuCl_2$(PTA)] (RAPTA-T) was subject of *in vitro* and *in vivo* investigations. *In vitro*, RAPTA-T apparently lack of cytotoxicity, but it interacts with extracellular matrix components, probably inhibiting some steps of the metastatic process[34]. *In vivo* the activation of RAPTA-T is believed to occur through the hydrolysis of the chloride ligands and in some cases the loss of the arene ring was observed, while the PTA ligand is bound very strongly. Its behavior is quite similar to NAMI-A, both in vitro and in vivo, which is surprising due to the structural differences. As well as NAMI-A, RAPTA-T inhibits lung metastasis formation without affecting the primary tumor significantly[35]. In addition, it was found that RAPTA derivatives can also interact with histone proteins in A2780 cells such as glutathione transferase, lysozyme, cathepsin B and TrxR, suggesting that RAPTA derivatives are able to induce cell death via multiple modes of action[36-37].

1.5.4 Polypyridyl ruthenium complexes

Complexes with bidentate chelating ligands $[Ru(chel)_3]^{2+}$ have been the most studied among the transition metal-based luminophores. Ru(II) polypyridyl complexes frequently contain chelating ligands such as bipyridine, 1,10-phenanthroline, imidazophenanthroline and their derivatives, forming lipophilic and cationic Ru(II) tris(bidentate) complexes, strictly octahedral in their geometry[38]. Dwyer and co-workers demonstrated that the enantiomers of these chiral complexes (Δ, Λ isomerism) may display different biological activity and different intracellular localization[39]. Zeng et al. demonstrated that complex Λ-$[Ru(polypy)_3]^{2+}$ mainly located in the cell nucleus, inhibit the growth of MDAMB-231 cancer cells[40]; by contrast, Δ-$[Ru(polypy)_3]^{2+}$ mostly accumulated in the cytoplasm and displayed no significant cytotoxicity (**Scheme 3**).

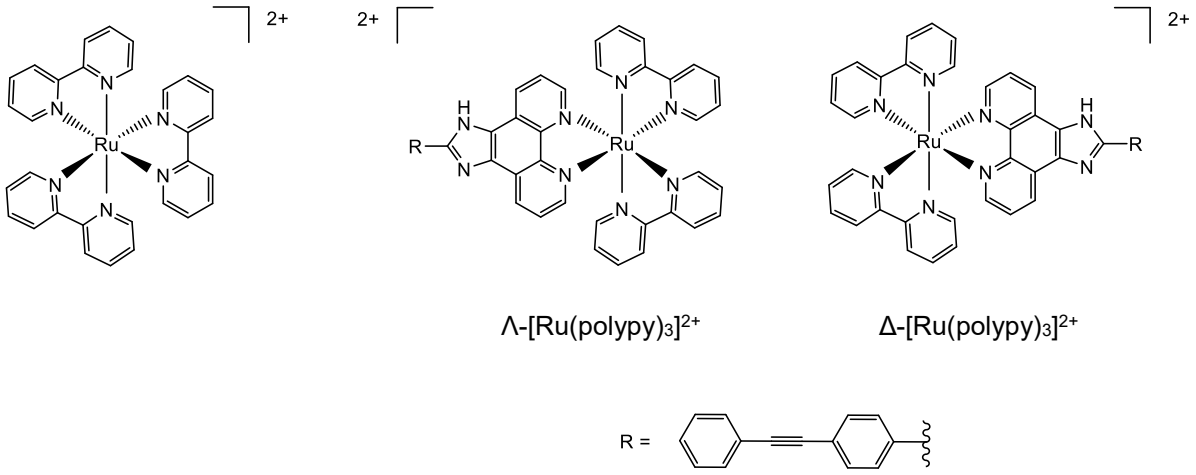

Scheme 3. $[Ru(bpy)_3]^{2+}$ as general example of polypyridyl ruthenium complexes and Δ, Λ isomerism of complex $[Ru(polypy)_3]^{2+}$.

These results revealed that chirality can affect the uptake and intracellular interactions of Ru complexes, leading to different anticancer efficacy. As a source of positive charges and stable molecular construction, non-covalent interactions (e.g. intercalation, groove binding, electrostatic interaction, etc.) are possible when a planar aromatic ligand is inserted between adjacent base pairs in the DNA double helix, via π-stacking interactions. In this way, the progression of the replication fork is stopped, leading to alterations of the tertiary structure of the DNA and consequently hindrance of biological functions[41].

Moreover, complexes bearing phenanthroline derivatives have shown antimetastatic properties, with significant suppressive effects on cell invasion and migration *in vitro*.

The mechanism of the interaction of $[Ru(chel)_3]^{2+}$ with living cells has been thoroughly studied via fluorescence spectroscopy, in order to elucidate the cellular uptake and toxicity mechanisms. $[Ru(phen)_3]^{2+}$ (phen = 1,10-phenanthroline) is able to intercalate into double stranded DNA, but only with low changes in the absorption/emission properties of the luminophore and with weak binding constant. In 1990 Friedman *et al.* described Ru(II) phenazine complex as stronger DNA intercalating agent[42]. This complex, in aqueous buffer is luminescent only upon DNA intercalation and, in addition, it is sensitive to the changes of the helix structure: the emission ranges from 628 to 640 to 650 nm in the presence of B, Z and A form helices, respectively.

In addition, ruthenium(II) complexes containing polypyridyl and cyclometalated ligands have been employed as photosensitizers in photodynamic therapy and have been proven to interact with other biological molecules, including proteins and G-quadruplex[42-43].

2 SAR EVALUATIONS ON THE DESIGN OF NOVEL RUTHENIUM COMPLEXES.

During the last decade, the group of organometallic chemistry of the University of Udine has developed a new class of extremely efficient bifunctional catalysts based on ruthenium and osmium, containing the 2-aminomethylpyridine (ampy) motif, namely the cis-$MCl_2(PP)(ampy)$[44-45] (M = Ru, Os) and the cationic carbonyl [RuCl(CO)(PP)(ampy)]Cl complexes[46]. These catalysts are highly efficient for the (asymmetric) transfer hydrogenation (TH) and hydrogenation of aldehydes and ketones and are complementary to the well-known Noyori *trans*-[$RuCl_2$(PP)(diamine)] and [(η^6-arene)RuCl(NN)] complexes[47-50]. The ampy systems showed an outstanding catalytic performance, allowing very fast reduction of carbonyl compounds with high reaction rate (TOF up to 10^5 h^{-1}) and high catalyst productivity (substrate/catalyst up to 10^4). Enantiomerically pure alcohols (*ee* up to 99 %) have also been obtained through the chiral version of this class of catalysts, achieving high stereoselective control of the reaction. Interestingly, the ruthenium anticancer complexes described by Sadler, were developed as modification of the ruthenium arene TH catalysts [(η^6-arene)RuCl(NN)] for ketones reduction by the Noyori group.

Moving the interest toward the synthesis of novel anticancer ruthenium complexes, we decided to maintain a precise configuration, introducing modifications to the different ligands around the ruthenium center in [RuX(CO)(PP)(NN)] complexes. The design and the structure-activity relationship (SAR) was elucidated by the analysis of the ability to induce cell viability decrease in cancer cell lines, which demonstrated that determined features are necessary to achieve a high anticancer activity (**Figure 8**).

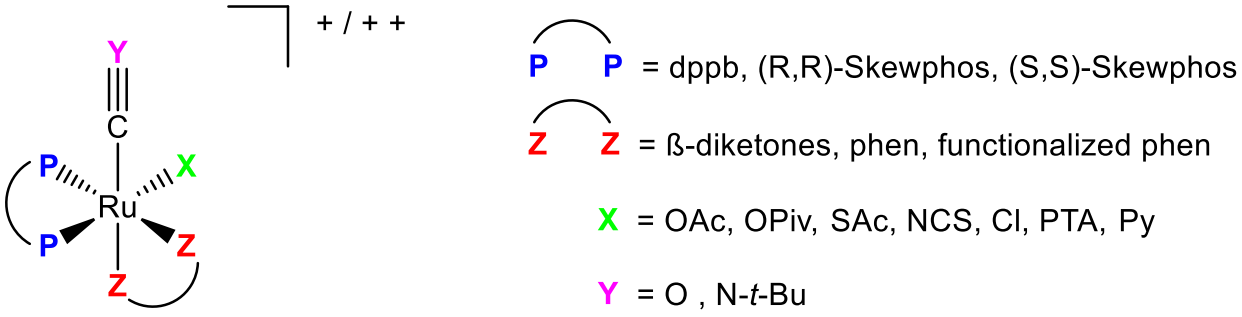

Figure 8. General structure of the ruthenium complexes reported in this work.

In particular, the cationic nature and the presence of a lipophilic diphosphine are properties which were maintain for the development of each ruthenium complex in this work. Both of these features may be responsible for the diffusion through the cell membrane, taking into account that cancer cells have more negative plasma membrane potential than normal cells and therefore lipophilic cationic metal complexes often preferentially accumulate in cancer cells. During this study, dppb (1,4-bis(diphenylphosphino)butane) ligand was largely used for the series of the synthetized complexes. Once established its efficacy as strong and stabilizing ligand, dppb was substituted with two very similar but enantiomeric diphosphine, such as (R,R)-Skewphos ((2R,4R)-2,4-Bis(diphenylphosphino)pentane) and (S,S)-Skewphos ((2S,4S)-2,4-Bis(diphenylphosphino)pentane), which induced chirality on the ruthenium centre[46, 51]. Surprisingly, the couples of ruthenium enantiomers exhibited significant differences in activity toward cancer cells.

In addition, ligands such as β-diketones or the planar aromatic phenanthroline were combined to the diphosphine group.

Different anionic species were substituted in the position *trans* to a diphosphine P atom. Especially OAc, OPiv and SAc anions demonstrated the best activity as anticancer agents, while the substitution with neutral species (1,3,5-triaza-7-phosphaadamantane phosphine (PTA) or pyridine), forming robust dicationic complexes, led to a low anticancer activity.

The presence of a carbonyl group was maintained as apical ligand, which demonstrated to be essential in that position for the activity of this class of complexes. The substitution of the CO specie with a *t*-butyl isonitrile ligand did not affected the stability nor the high anticancer activity, thus broadening the class of Ru complexes containing functionalized biological substrates, selectively targeting cancer cells or biomolecules involved in cancer growth.

The better activity demonstrated by the complexes bearing phenanthroline or functionalized phenanthrolines can possibly be related to the interaction with the DNA helix via intercalation, stalling the replication fork and blocking the cell cycle, although protein or peptide adduct formation via substitution of the carboxylate anion with cysteine residues or glutathione and their activation can also be involved in apoptosis.

3 RESULTS AND DISCUSSION

3.1 NEUTRAL B-DIKETONES RUTHENIUM(II) COMPLEXES.

3.1.1 State of the art.

The β-diketone scaffold is not very common in nature although it is the main feature of a series of naturally occurring compounds, such as curcumin and its derivatives. Curcumin (curcH) and its naturally analogues are some of the bioactive ingredients derived from the rhizome of *Curcuma longa*, and have been used in traditional Indian and Chinese medicines. These natural products and their synthetic analogues have been extensively studied in the last decade with an exponentially increasing number of publications on this topic[52]. Natural curcumin derivatives have been shown to possess free-radical-scavenging and antioxidant, anti-inflammatory, anticarcinogenic and chemopreventive properties, as well as neuroprotective characteristics, based on simultaneously acting on several molecular targets. Conversely, Curcumin and other curcuminoids show also some disadvantages, such as poor solubility in water, poor absorption, rapid metabolism and rapid clearance, so there is increasing interest in the coordination chemistry of such ligands in combinations with several metal ions, with the aim of overcoming these drawbacks and disadvantages, improving its bioavailability[53]. β-diketones represent one of the oldest classes of chelating ligands, but their coordination chemistry continues to attract much interest, due to the possible structural functionalization of such ligands and the potential applications of their metal derivatives in new fields of technology and as scaffolds for anticancer drug design[54]. In 2004 Sadler reported the first example, in the form of anticancer (arene)Ru(II) acetylacetonate[55] complex **a** (**Scheme 4**), displaying an increased rate and extent of hydrolysis (i.e., replacement of Cl^- with a water molecule) to form complex **b** and different selectivity toward DNA nucleobases.

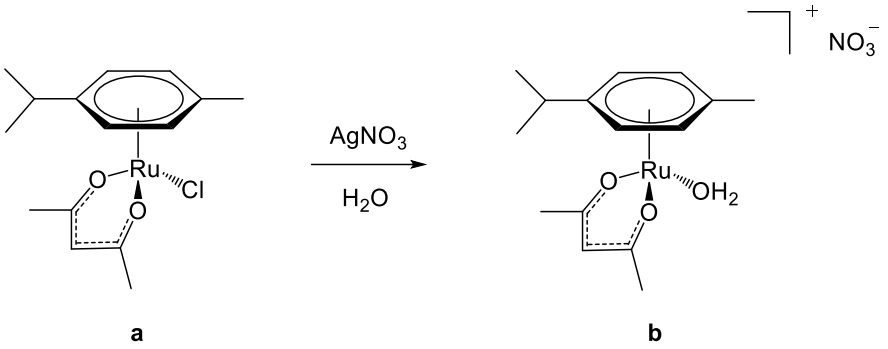

Scheme 4. Hydrolysis of Sadler's (arene)Ru(II) acetylacetonate complex **a**.

In 2012, the group of Pettinari investigated the biological activity of the neutral (p-cymene)Ru(II) curcumin complex **c**[56-57] (**Figure 9**), showing in vitro antiproliferative activity on different five cancer cell lines, with a preference for the colorectal tumor HCT116, followed by breast MCF7 and ovarian A2780 cell lines, whereas the human glioblastoma U-87 and lung carcinomaA549 lines are less sensitive.

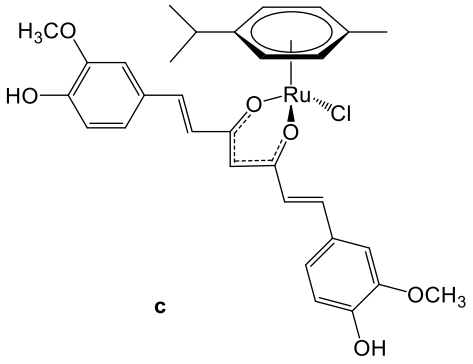

Figure 9. Chemical structure of Pettinari's (p-cym)Ru(II) curcumin complex **c**.

In a recent study carried by Lippard's group, several diketones were studied as chelating ligands[2]. Different diketones featuring methyl, phenyl and trifluoromethyl substituents, were taken into account to form complexes of general formula $[Pt(NH_3)_2(dkt)]NO_3$. The influence of the lipophilicity on the toxicity of the complexes, was studied, and it was found out that the CF_3 and Ph substituents increase lipophilicity and improve cellular uptake.

3.1.2 Synthesis and characterization.

Among the active ruthenium catalysts developed by the group of Udine, complexes containing diphosphines and carbon monoxide in combination with acetate ligands, were used as precursors for the synthesis of novel anticancer complexes, exploiting one acetate substitution by means of acidic ligands, which can protonate and displace acetate.

In the view of extending the reactivity of the [Ru(η^1-OAc)(η^2-OAc)(CO)(dppb)] (**1**) compound[46], we investigated the preparation of the corresponding β-diketones derivatives from acetylacetonate, dibenzoylmethane and curcumin, in order to study the effects of neutral complexes on cancer cell viability. Reaction of [Ru(η^1-OAc)(η^2-OAc)(CO)(dppb)] (**1**) with 1 equivalent of acetylacetonate (acac) in methanol at 60 °C, afforded the neutral derivative [Ru(η^1-OAc)(CO)(dppb)(acac)] (**2**), isolated in 42% yield by displacement of one acetate ligand (eqn. 1).

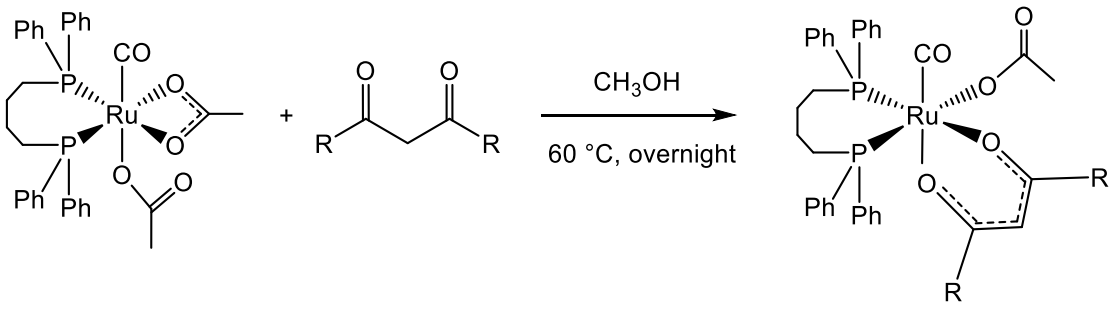

(1)

1 **2 - 4**

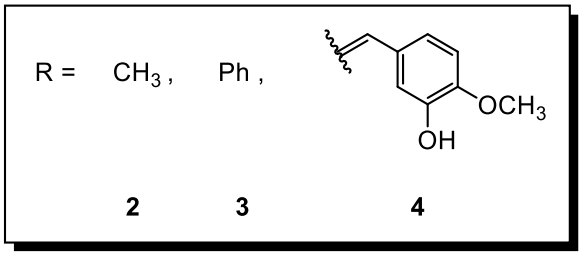

The $^{31}P\{^1H\}$ NMR spectrum of **2** in $CDCl_3$ displays two doublets at δ 43.2 and 41.9 ppm ($^2J_{PP}$ = 29.5 Hz) for the P atoms trans to N and O, respectively, thus excluding a *trans* arrangement of the CO and OAc ligands (**Figure 10**).

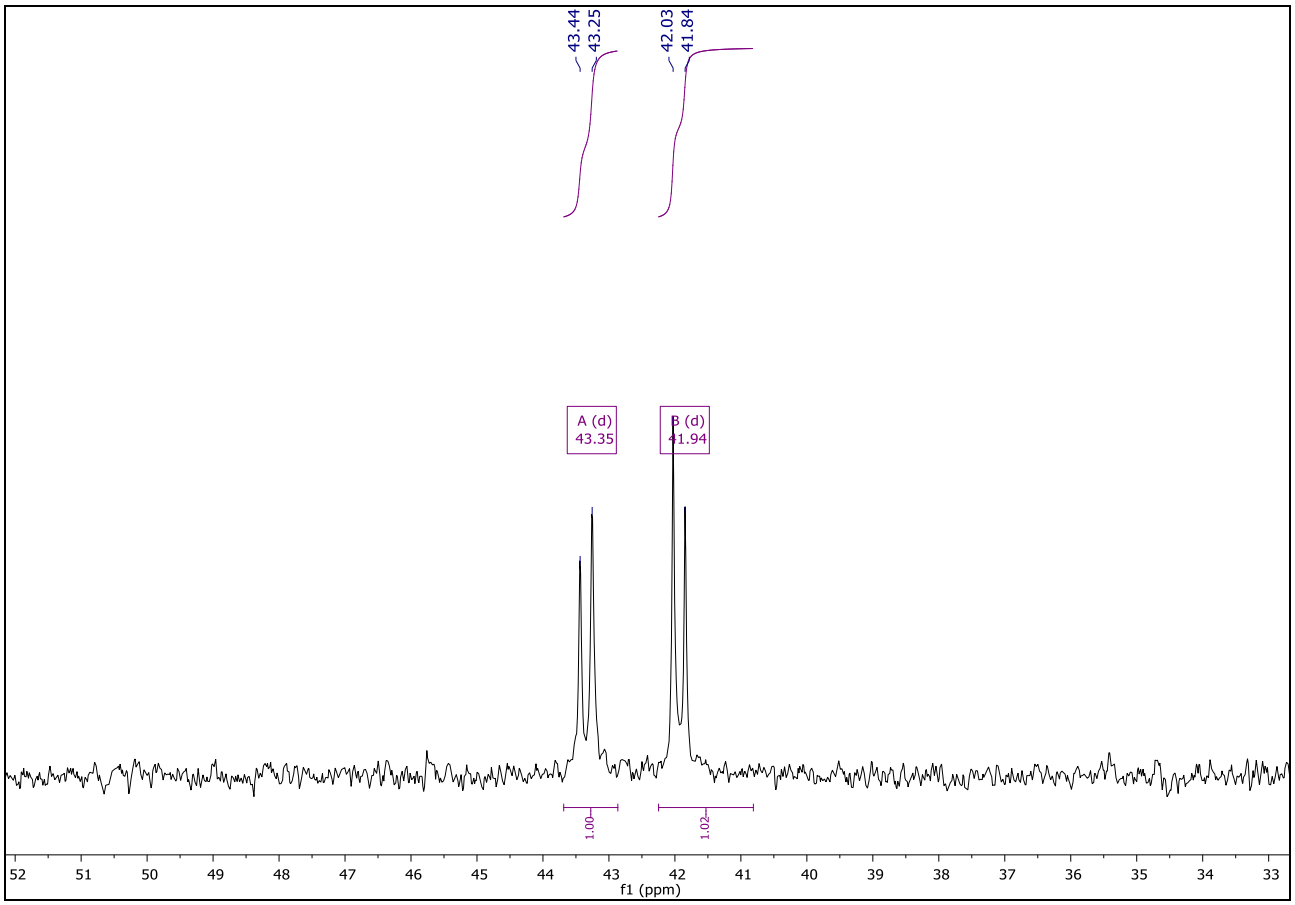

Figure 10. $^{31}P\{^{1}H\}$ NMR spectrum of complex [Ru(η^{1}-OAc)(CO)(dppb)(acac)] (**2**) in $CDCl_3$.

The ^{1}H NMR resonances at δ 1.62 and δ 1.56 ppm have been attributed to the acac CH_3 moieties, while the singlet at δ 1.39 ppm corresponds to the coordinated OAc. The signal at δ 4.92 ppm is related to the acac CH in alpha position (**Figure 11**).

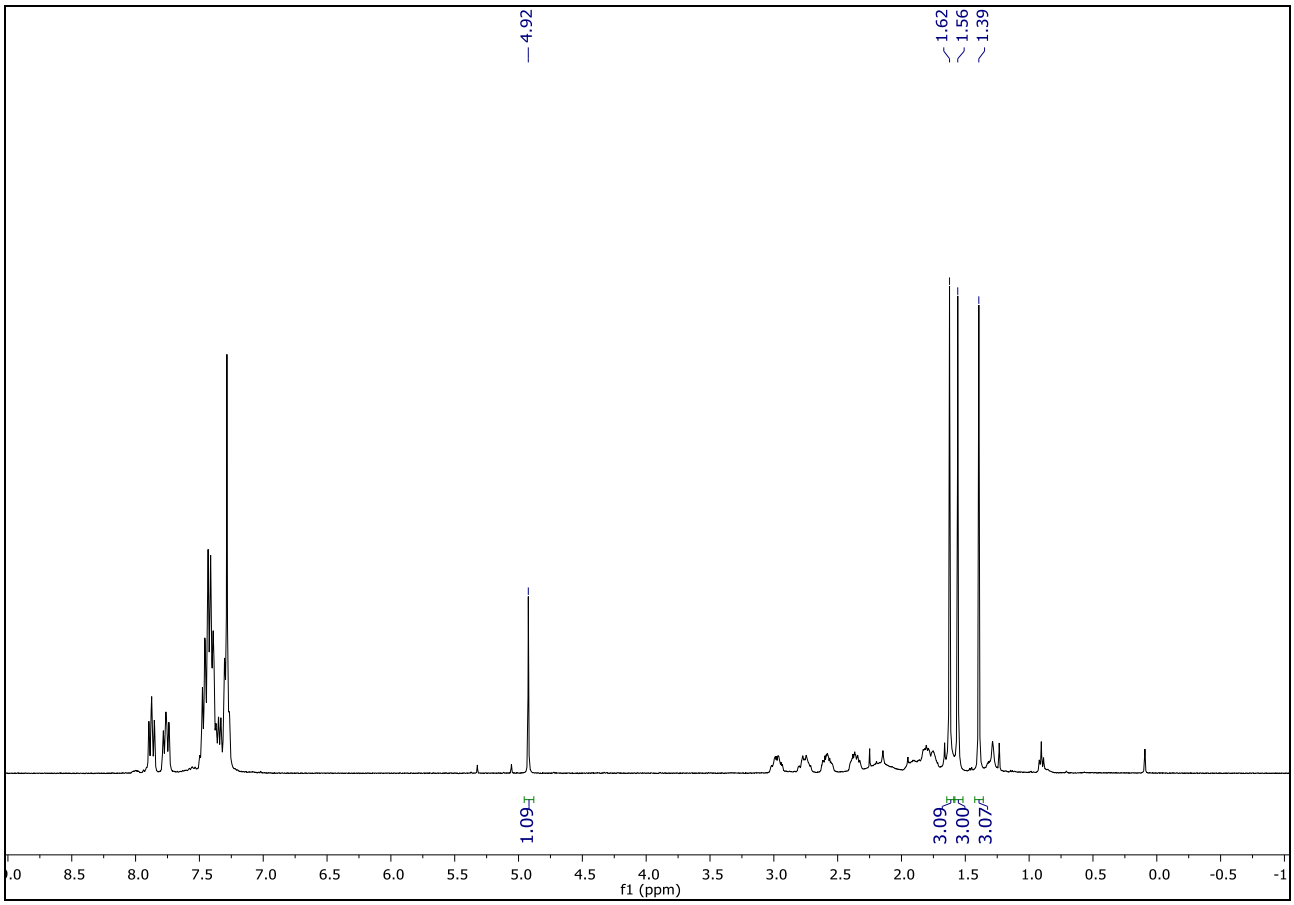

Figure 11. ^{1}H NMR spectrum of complex [Ru(η^{1}-OAc)(CO)(dppb)(acac)] (**2**) in $CDCl_3$.

In the $^{13}C\{^{1}H\}$ NMR spectrum the triplet at δ 204.9 ppm ($^{2}J_{CP}$ = 16.7 Hz) corresponds to the CO cis to the two P atoms, whereas the singlets at δ 187.0, 184.3 and 176.6 ppm correspond to the acac and acetate CO carbon atoms, respectively (**Figure 12**).

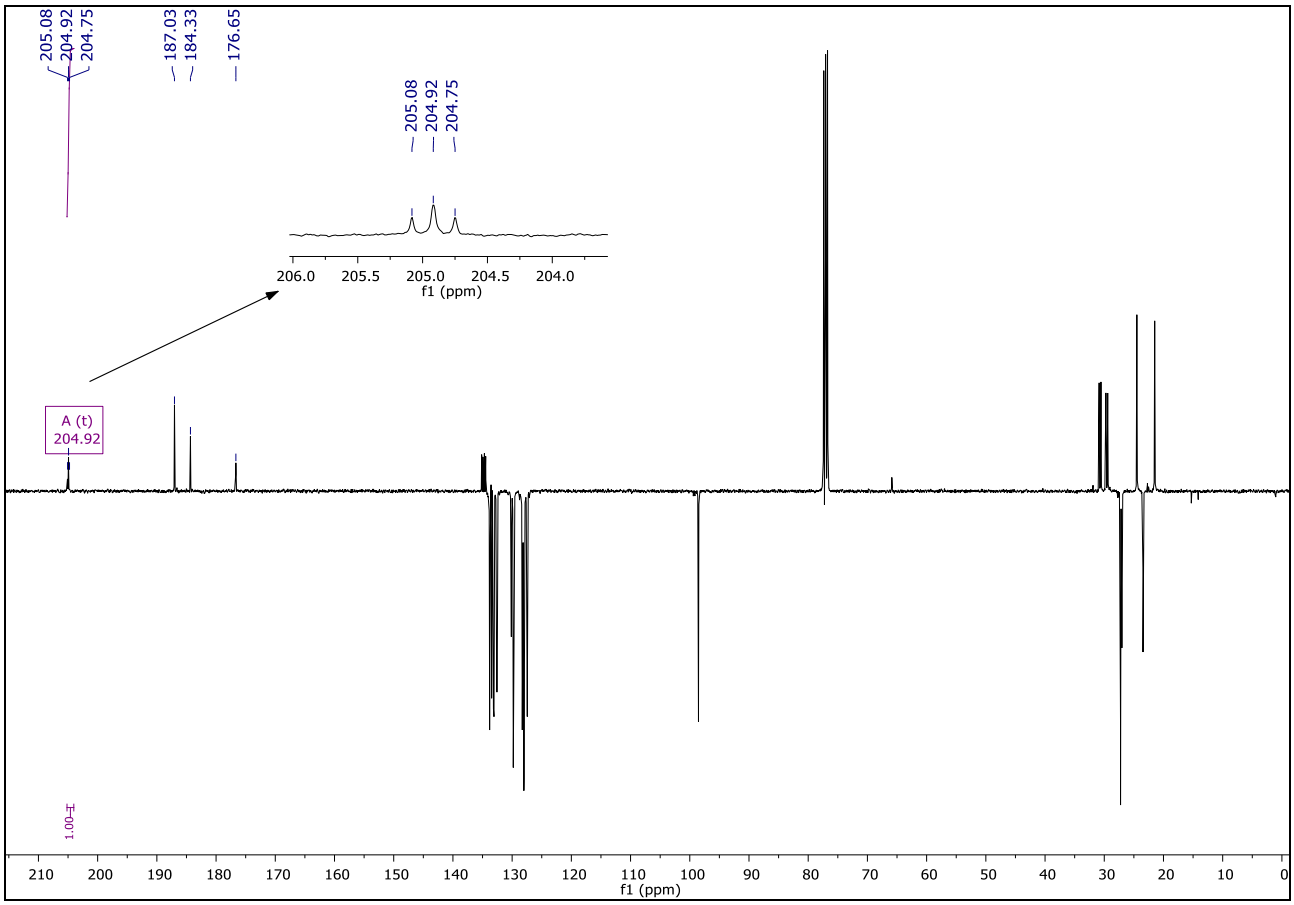

Figure 12. $^{13}C\{^{1}H\}$ NMR spectrum of complex [Ru(η^{1}-OAc)(CO)(dppb)(acac)] (**2**) in $CDCl_3$.

In order to enlarge the number of β-diketones complexes, the dibenzoylmethane derivative [Ru(OAc)(Odbm)(CO)(dppb)] (**3**) was prepared in 63% yield by treating **1** with dibenzoylmethane (1 equiv.) in methanol at 60 °C overnight (eqn. 1). Likewise **2**, the $^{31}P\{^{1}H\}$ NMR spectrum of **3** in $CDCl_3$ shows two doublets at δ 44.6 and 40.9 ppm ($^{2}J_{PP}$ = 29.5 Hz). In the ^{1}H NMR spectrum, the singlet at δ 1.62 ppm corresponds to the coordinated OAc methyl group, whereas the singlet at δ 6.32 ppm has been attributed to the Odbm CH in alpha position, in line with the data of **2**. Likewise complex **3**, the curcumin ruthenium complex [Ru(OAc)(Ocurc)(CO)(dppb)] (**4**) was synthesized by the reaction of **1** with curcumin (1 equiv.) in methanol at 60 °C and isolated in 53% yield (eqn. 1). In the $^{31}P\{^{1}H\}$ NMR spectrum, **4** shows two doublets at δ 44.7 and 41.1 ppm ($^{2}J_{PP}$ = 31.0 Hz), which are very close to those of **3**. ^{1}H NMR measurements, display two singlet at δ 3.97 and 3.87 ppm for the curcumin OCH_3 groups, while the signal at δ 1.78 ppm can be assigned to the OAc. The signal at δ 5.26, similarly to complex **2,** was attributed to the curcumin CH of the β-diketone function. The carbonyl resonance in $^{13}C\{^{1}H\}$ NMR spectrum, appears as a broad

signal at δ 204.8, while the singlets at δ 179.2, 178.0 and 175.7 ppm are for the curcumin CO, OAc and the second curcumin CO, respectively.

Complexes **2** and **3** display relatively high solubility in several organic solvents, including alcohols (methanol and ethanol), chloroform, dichloromethane, acetone and dimethylsulfoxide. Conversely, complex **4** is poorly soluble in chlorinated solvent (chloroform and dichloromethane) and acetone, while demonstrated moderate solubility in alcohols. In addition, the solutions of **2** and **3** are relatively stable in air at room temperature for days, whereas complex **4** demonstrated no stability in solution and it is sensitive when exposed to the sun light.

3.2 MONOCATIONIC DIIMMINE RUTHENIUM(II) COMPLEXES.

3.2.1 State of the art.

Metal compounds containing ligands such as diimine, carbon monoxide and phosphine, which exhibit DNA interaction and antitumor properties, have attracted great interest so far. In addition, an enhancement of the cellular uptake is expected for lipophilic drugs displaying an overall positive charge, facilitating diffusion through the cell membrane.

Recently, Batista *et al.* have reported the synthesis of cationic complexes [RuCl(CO)(dppb)(NN)][PF_6] (NN = bpy and phen) in different isomeric forms (**Figure 13**), revealing that the presence and the position of CO ligand are relevant for the activity against *Trypanosoma cruzi* parasite[58]. These findings presented, demonstrated that the use of carbonyl ligand provides stability and pharmacological properties to ruthenium diphosphine diimine complexes. None of these complexes was found to be more cytotoxic than cisplatin and oxaliplatin in hepatocellular carcinoma.

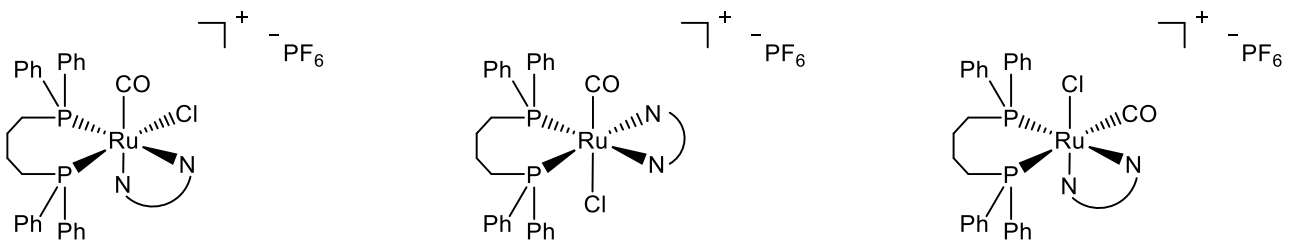

Figure 13. [RuCl(CO)(dppb)(NN)][PF_6] isomers proposed by Batista and coworkers.

In 2017, they also described the synthesis of a DNA-intercalating agent [Ru(Cl)(CO)(dppb)(dpqQX)]PF_6 (dpqQX = dipyrido[3,2-*a*:2',3'-*c*]quinoxalino[2,3-*b*]quinoxaline) (**d**) (**Figure 14**), with EC_{50} values as low as 0.10 ± 0.22 and 0.41 ± 0.02 μM against MDA-MB-213 and MCF-7 breast cancer cells, respectively[59]. In addition, DNA affinity studies suggest interactions between the metal complex **d** and the DNA double helix, acting as intercalating agent. In fact, ruthenium complexes with 1,10-phenanthroline derivatives exhibit high redox potential, photochemical and photophysical properties, and consequently possible effects as DNA linkers.

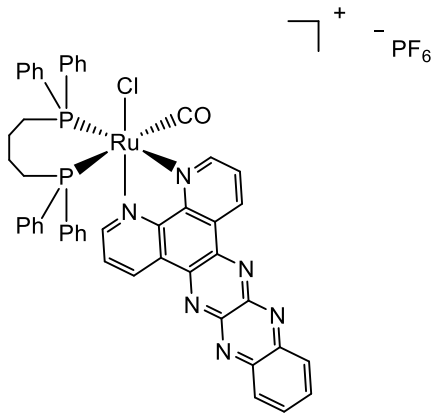

d

Figure 14. Chemical structure of the DNA-intercalating agent [Ru(Cl)(CO)(dppb)(dpqQX)]PF_6 (**d**).

Recently, Cominetti and Batista's group described the synthesis of novel ruthenium complexes [Ru(SO_4)(dppb)(bpy)], [Ru(CO_3)(dppb)(bpy)], [Ru(C_2O_4)(dppb)(bpy)] and the cationic [Ru(CH_3CO_2)(dppb)(bpy)][PF_6]. They studied the relationship between the complexes with different oxygen containing ligands and the effects on MCF-10A breast tumor, ranging from 31 to 49 μM of EC_{50} values[60].

3.2.2 Synthesis and characterization of monocationic phenanthroline ruthenium(II) complexes.

The synthesis of complex Ru$(OAc)_2(CO)(PPh_3)_2$ was previously reported by Wilkinson[61] by bubbling CO through a solution of [Ru(η^2-OAc)$_2(PPh_3)$][62] in MeOH and resulting in a

colourless precipitate. This complex was applied successfully as precursor for the synthesis of [Ru(OAc)$_2$(CO)(PP)] type complexes with a number of diphosphines (PP) in Baratta's research group[46], via the substitution of triphenylphosphine with PP. In this section the 1,4-bis(diphenylphosphino)butane (dppb) ruthenium derivative was used as precursor for the synthesis of monocationic ruthenium complexes of general formula [RuX(CO)(dppb)(phen)]Y (X = Y = OAc, OPiv, SAc, and NCS; X = Cl and Y = PF_6)[63].

Treatment of [Ru(η^1-OAc)(η^2-OAc)(CO)(dppb)] (**1**) complex with phen (1 equiv.) in methanol at 60 °C afforded the thermally stable cationic complex [Ru(η^1-OAc)(CO)(dppb)(phen)]OAc (**5**), isolated in 83% yield by displacement of one acetate ligand (eqn. 2).

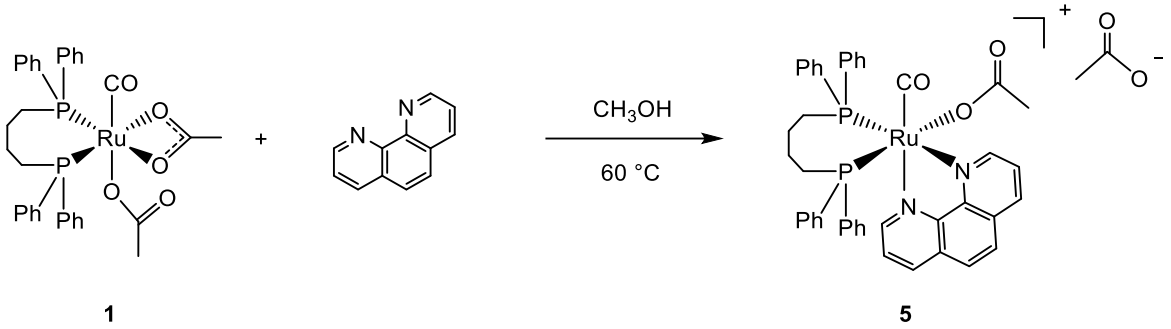

1 **5** (2)

The $^{31}P\{^1H\}$ NMR spectrum of **5** in CD_2Cl_2 displays two doublets at δ 32.4 and 29.1 ppm ($^2J_{PP}$ = 21.4 Hz) for the P atoms trans to N and O atoms, respectively, consistent with a *cis* arrangement of the acetate and CO ligands. The ^1H NMR signals at *δ* 1.86 and *δ* 1.44 ppm correspond to the free and coordinated OAc moieties, respectively. In order to demonstrate the cationic nature of this complex, **5** was dissolved in methanol-d_4 and sodium acetate (1-15 equiv.) was added portion wise. ^1H NMR studies showed an increase of the signal at *δ* 1.91 compared to that at *δ* 1.42 ppm, indicating that one acetate is free and not coordinated to ruthenium. In the $^{13}C\{^1H\}$ NMR spectrum the doublet of doublets at *δ* 204.3 ppm ($^2J_{CP}$ = 16.6 and 14.1 Hz) was attributed to the axial CO *cis* to the dppb P atoms, whereas the singlets at *δ* 176.6 and 176.0 ppm correspond to the carboxylate carbon atoms of the free and coordinated OAc, respectively. In addition, the structure of the cationic complex **5** was confirmed by a single crystal X-ray diffraction experiment, where the ruthenium metal centre was observed in a slightly distorted octahedral environment with the phen ligand *trans* to one P atom and the CO ligand. The Ru1–N1 and Ru1–N2 bond distances are 2.119(3) and 2.160(3) Å, respectively, as result of the strong *trans* influence exerted by the diphosphine and CO ligands, respectively (**Figure 15**).

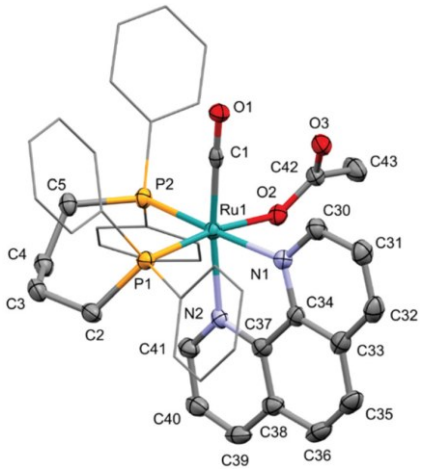

Figure 15. Molecular structure of **5** as determined by single crystal X-ray diffraction. Hydrogen atoms and the OAc counterion are omitted, and the phenyl groups are simplified as wireframes for clarity.

As for the N atom *trans* to P, also the coordinated acetate shows a reasonably long Ru1–O2 bond length (2.134(3) Å) due to the presence of a *trans* phosphine. This would suggest the facile dissociation of the OAc ligand as demonstrated from the studies in water and in methanol in presence of other anionic species (OPiv, SAc, SCN and Cl). As a matter of fact, [Ru(η^1-OAc)(CO)(dppb)(phen)]OAc **5** promptly reacts with alkali metal salts (i.e. NaOPiv and KSCN), affording the derivatives [RuX(CO)(dppb)(phen)]X by displacement of OAc. In addition, X-ray analysis shows an intramolecular π–π-interaction between a phenyl group of the dppb and one heterocyclic phenanthroline ring, as also inferred from the high field ^{1}H NMR signals of the *ortho* phenyl protons (*δ* 6.84–6.23 ppm).

The pivalate derivative [Ru(η^1-OPiv)(CO)(dppb)(phen)]OPiv (**6**) was prepared in 78% yield by treating the precursor **1** with NaOPiv (10 equiv.) in methanol at 60 °C for 48 h by displacement of OAc (**Scheme 5**).

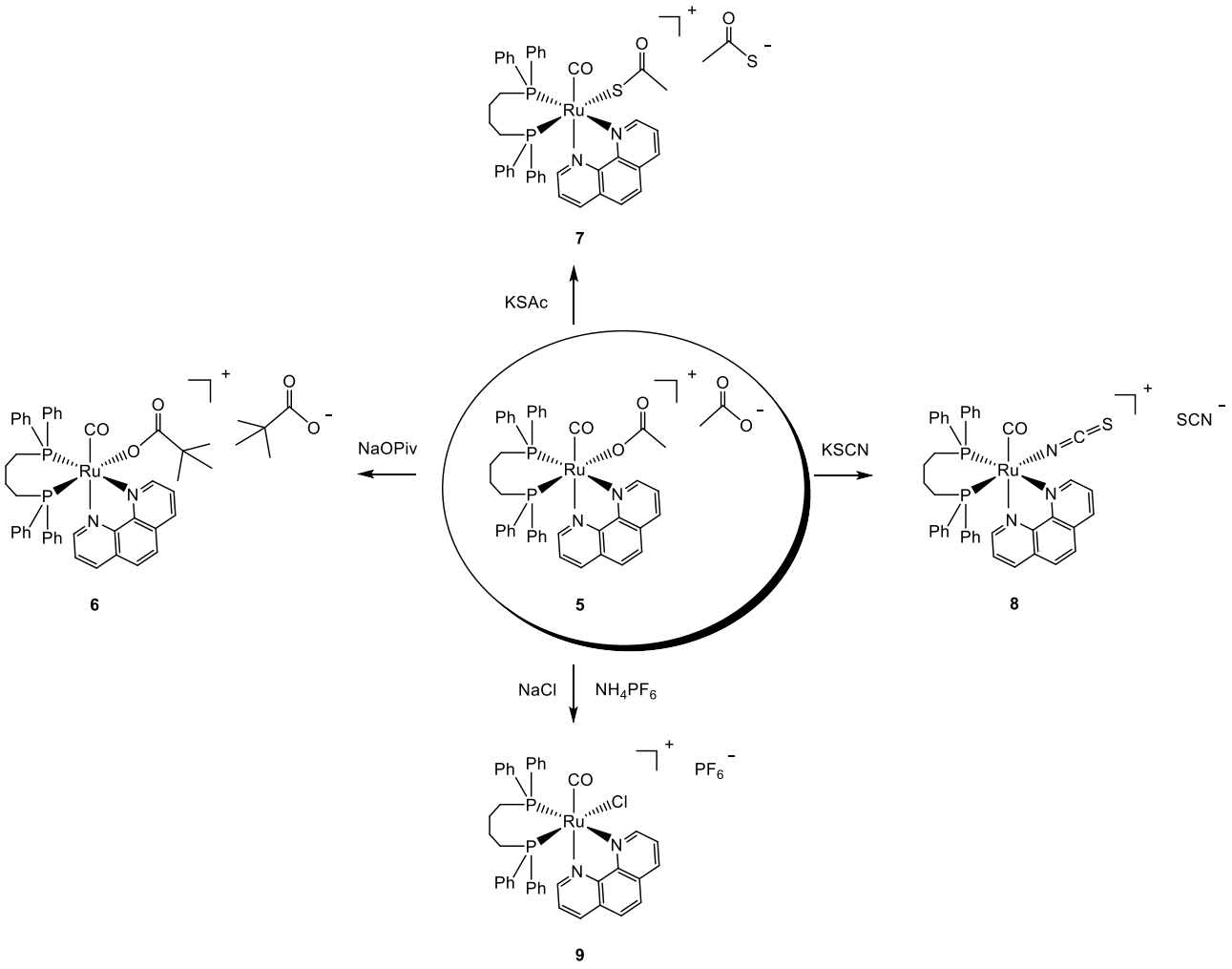

Scheme 5. Syntheses of complexes **6**-**9** from **5** by displacement of the coordinated acetate in MeOH at 60 °C.

The $^{31}P\{^{1}H\}$ NMR spectrum of **6** in CD_2Cl_2 shows two doublets at δ 32.6 and 29.8 ppm ($^{2}J_{PP}$ = 22.1 Hz) which are values very close to those of **5** (**Figure 16**).

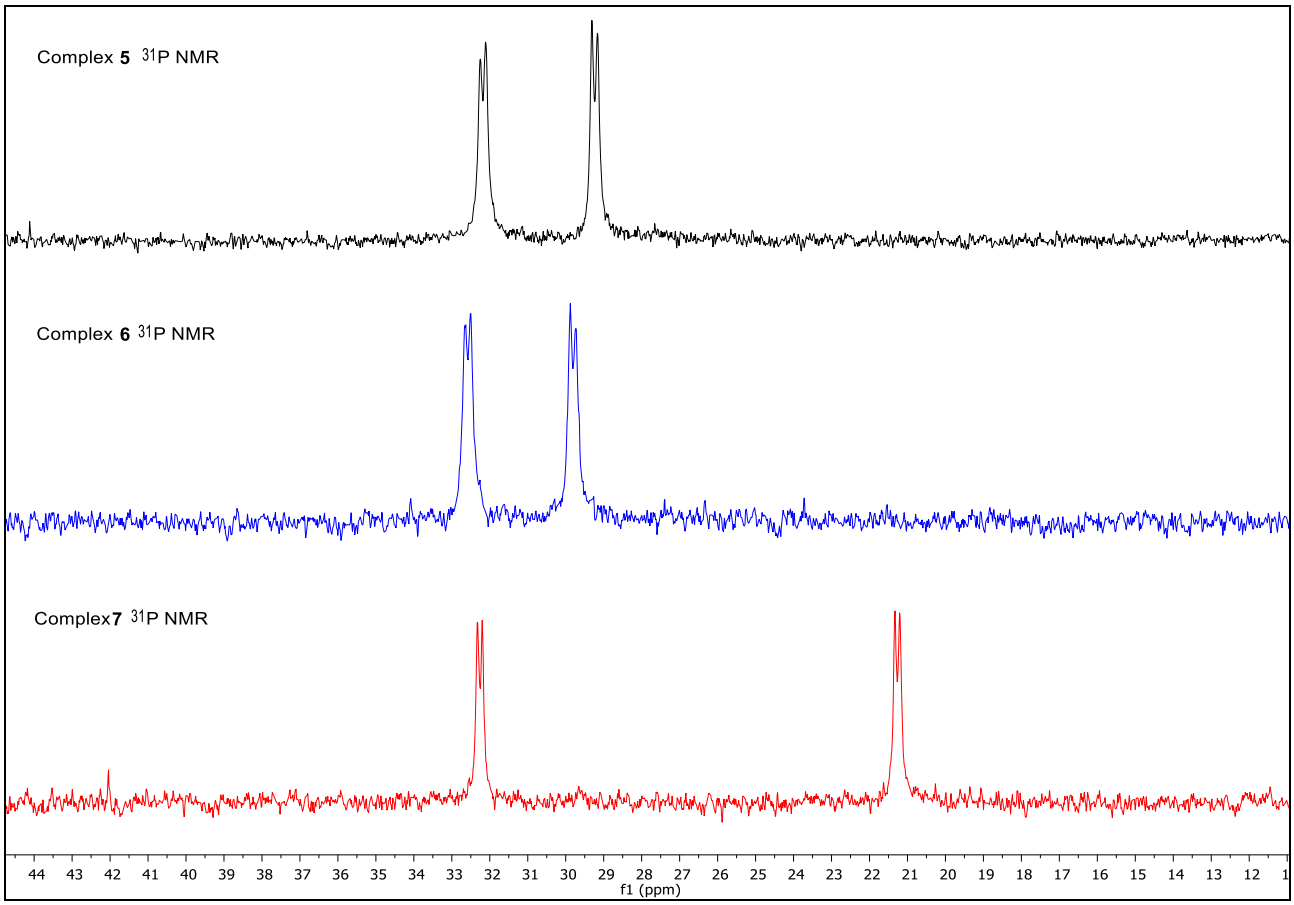

Figure 16. Comparison of $^{31}P\{^{1}H\}$ NMR spectra of complexes **5**-**7** in CD_2Cl_2.

In the ^{1}H NMR spectrum, the two singlets at *δ* 1.14 and 0.30 ppm correspond to the methyl groups of the free and coordinated pivalate, respectively. The presence of these two distinct singlets for the coordinated and free carboxylate in acetate **5** and pivalate **6** derivatives indicates that no rapid exchange between the inner and outer sphere anions occurs at room temperature in dichloromethane on the NMR time scale.

Similarly to **6**, the thioacetate derivative [Ru(η^{1}-SAc)(CO)(dppb)(phen)]SAc (**7**) was synthesized by means of the reaction between **5** and KSAc (10 equiv.) in methanol at 60 °C and isolated in 80% yield (**Scheme 5**). Complex **7** displays two $^{31}P\{^{1}H\}$ NMR doublets at *δ* 32.2 and 21.3 ppm ($^{2}J_{PP}$ = 21.5 Hz) for the P atoms *trans* to N and S, respectively. It is worth to observe that the P atom trans to S is at high field compared to the chemical shift value of the P *trans* to an O atom in complexes **5** and **6** (*δ* = 29.1 and 29.8 ppm, respectively) (**Figure 16**). The ^{1}H NMR singlets at *δ* 2.02 and 1.97 ppm correspond to the free and coordinated thioacetate methyls, while in the $^{13}C\{^{1}H\}$ NMR spectrum, the CO carbon appears as a doublet of doublets at *δ* 204.2 ppm ($^{2}J_{CP}$ = 17.3 and 12.0 Hz), and the free and coordinated thioacetate carbonyl moieties appear as singlets at *δ* 202.5 and 173.9 ppm, respectively.

The isothiocyanate derivative [Ru(NCS)(CO)(dppb)(phen)]SCN (**8**) was obtained as a pale yellow precipitate (80% yield) by treating **5** with KSCN (10 equiv.) in methanol at 60 °C overnight (**Scheme 5**). The $^{31}P\{^{1}H\}$ NMR spectrum of **8** in $CDCl_3$ shows the presence of two isomers in about 10/1 molar ratio with a doublet at δ 30.9 ppm ($^{2}J_{PP}$ = 21.9 Hz) and a broad peak at δ 30.2 ppm for the main species, and two doublets at δ 29.7 and 28.6 ppm ($^{2}J_{PP}$ = 21.8 Hz) for the minor species (**Figure 17**).

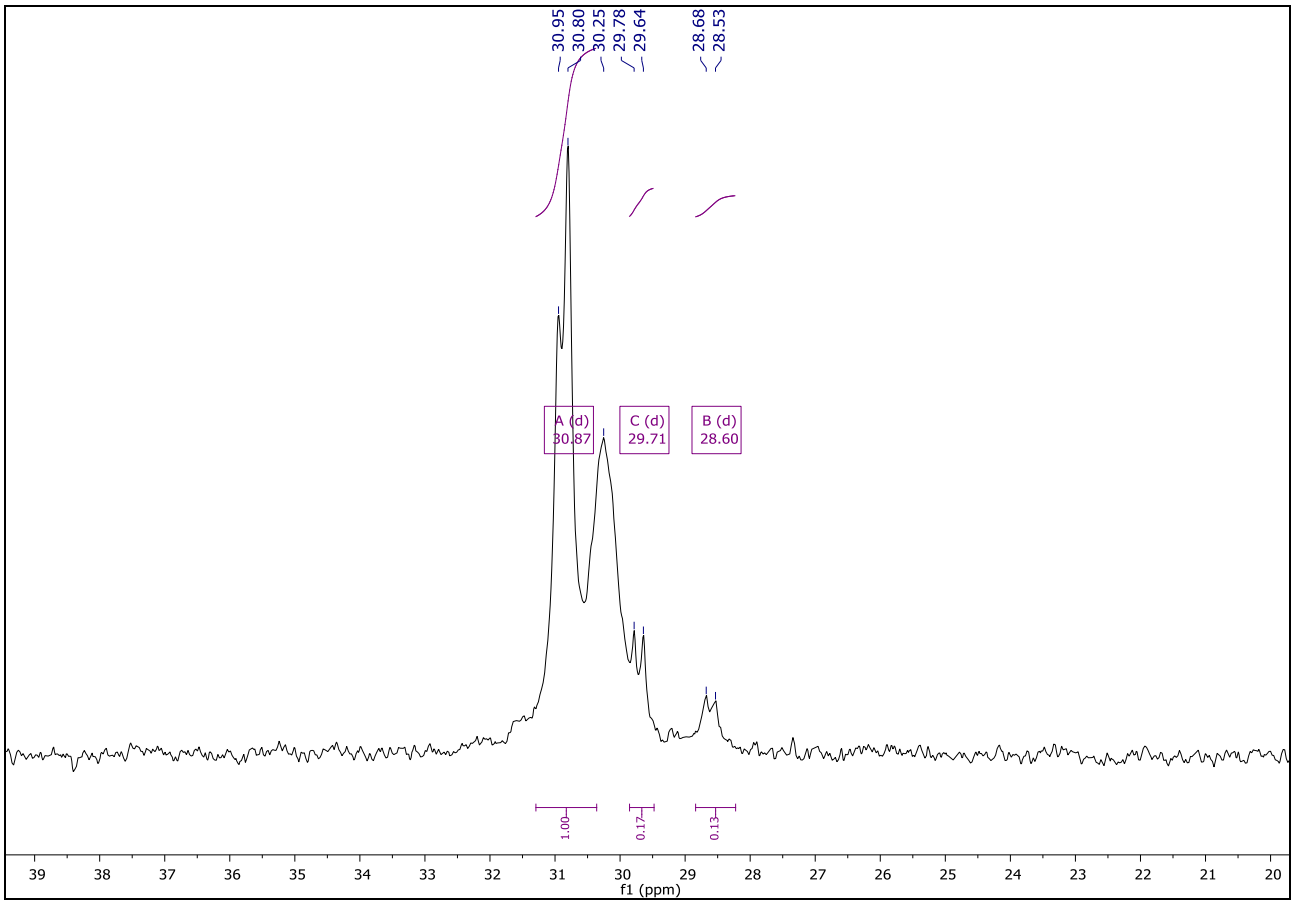

Figure 17. $^{31}P\{^{1}H\}$ NMR spectrum of complex [Ru(NCS)(CO)(dppb)(phen)]SCN (**8**) in $CDCl_3$.

The presence of two isomers in the same molar ratio has also been observed from ^{1}H NMR measurements and it was attributed to the ruthenium isothiocyanate (Ru-NCS, major isomer) and ruthenium thiocyanate (Ru-SCN) species. Conversely, the NMR spectra of **8** in CD_2Cl_2 (broad singlet at δ_P 30.6 ppm, δ_C = 139.6 ppm for NCS) are consistent with a fast equilibrium on the NMR time scale occurring in solution between the Ru-NCS and Ru-SCN species, with a higher rate in CD_2Cl_2 compared to $CDCl_3$. The single crystal X-ray diffraction data of **8** show two crystallographically independent molecules of the complex in the

asymmetric unit, with the ruthenium center in a slightly distorted octahedral environment (**Figure 18**).

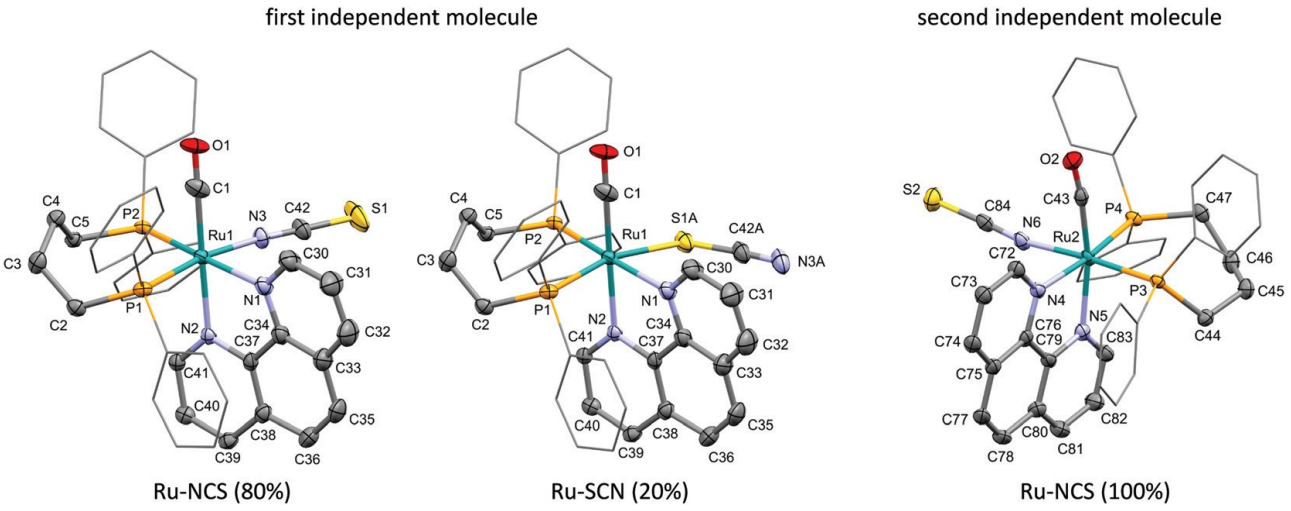

Figure 18. Molecular structure of **8** in the solid state. Left and centre: the first independent molecule in the asymmetric unit showing the disordered Ru-NCS (ca. 80%) and Ru-SCN (ca. 20%) binding isomers; right: the second independent molecule exhibiting only the Ru-NCS isomer. Hydrogen atoms and the SCN counterions are omitted, and the phenyl groups are simplified as wireframes for clarity.

In the first molecule, the binding isomerism of the thiocyanate ligand is observed (**Figure 18**, left and center). Hereby, the ligand is disordered across both binding modes and could be successfully modelled with ca. 80% binding via N (Ru1–N3) and ca. 20% binding via S (Ru1–S1A). In the second molecule, the thiocyanate ligand coordinates exclusively via the N atom with a Ru–N bond length of 2.1126(19) Å (Ru2–N6) and a Ru–N–C angle of 162.90(18)° (**Figure 18**, right). Consequently, the N-bound isomer is favored compared to the S-bound isomer showing an overall ratio of about 9 : 1 in the solid state. The solid state and solution data are consistent with the formation of Ru-NCS as the main species, which in solution equilibrates with the Ru-SCN one. The binding isomerism of thiocyanate complexes has been previously reported, including examples in which an exchange between the N and S mode occurs in solution[64-66].

Finally, the reaction of **5** with NaCl (10 equiv.) in methanol and subsequent treatment with NH_4PF_6 (6 equiv.) at 60 °C (4 h) affords the complex [Ru(Cl)(CO)(dppb)(phen)][PF_6] (**9**) as a yellow precipitate (89% yield) by displacement of the acetate with the chloride ligand

(**Scheme 5**). This complex was previously prepared by Batista, using the dinuclear carbonyl derivative [$Ru_2Cl_4(CO)_2(dppb)_3$] as the starting material[58].

3.2.2.1 Reactivity and studies in solution

Complexes **5–9** display relatively high solubility in several media, including alcohols (methanol and ethanol), chloroform, dichloromethane, acetone, dimethylsulfoxide, and acetonitrile, with the exception of **8** and **9** that are poorly soluble in MeOH and $CHCl_3$, respectively. Furthermore, the solutions of **5**-**9** are relatively stable in air at room temperature for days. To establish the coordination ability of the anionic ligands, control NMR experiments have been carried out to study the exchange reactions of **5–9** with the appropriate ligands in CD_3OD at 60 °C. Thus, while **5** reacts easily with NaOPiv, KSAc, KSCN and NaCl by displacement of the coordinated acetate (**Scheme 5**), treatment of chloride **9** with KSCN leads to the substitution of Cl by NCS, affording the isothiocyanate **8**. Conversely, **8** cleanly reacts with NaSAc affording **7** via substitution of NCS by SAc, but no reaction of **8** with NaCl has been observed, indicating that NCS is more strongly coordinating than Cl. Finally, **7** does not react with NaOAc, NaOPiv, KSCN and NaCl under the same reaction conditions, indicating that SAc is the strongest ligand. Thus, according to these results, the following sequence of donor ability can be proposed for this class of ruthenium complexes: OAc ≤ OPiv < Cl < NCS < SAc. Interestingly, carboxylate derivatives **5** and **6** that show the weakest carboxylate ligands are highly soluble in water. The $^{31}P\{^1H\}$ NMR spectrum of pivalate **6** (3.3 mM) in D_2O at 37 °C shows a new pair of doublets at δ 38.8 and 24.9 ppm ($^2J_{PP}$ = 26.4 Hz), without any significant change after 72 h. In the ^1H NMR spectrum, **6** displays one singlet at *δ* 1.11 ppm corresponding to the pivalate tert-butyl group, in contrast to two singlets observed for **6** in CD_2Cl_2, indicating that in water the pivalate ligand of **6** is not coordinated to ruthenium, in accordance with the strong ionic hydrogen bond interaction of $RCOO^-$ with H_2O and RCOOH. Interestingly, thermodynamic studies show that hydrate carboxylates ($RCOO^-$ HOH) can lead to the displacement of water with the formation of strongly stabilized $RCOO^-$ HOOCR species[67-68].

Complex **6** in H_2O gives a pH value of about 4.2, which is close to that of a buffer solution of pivalic acid – pivalate (pK_a of HOPiv = 5.03)[69], and is consistent with the formation of the

hydroxo species [Ru(OH)(CO)(dppb)(phen)]OPiv (**6-OH**), in equilibrium with the aquo complex, stabilized by the hydrogen bonds of pivalate with water and pivalic acid (**Scheme 6**).

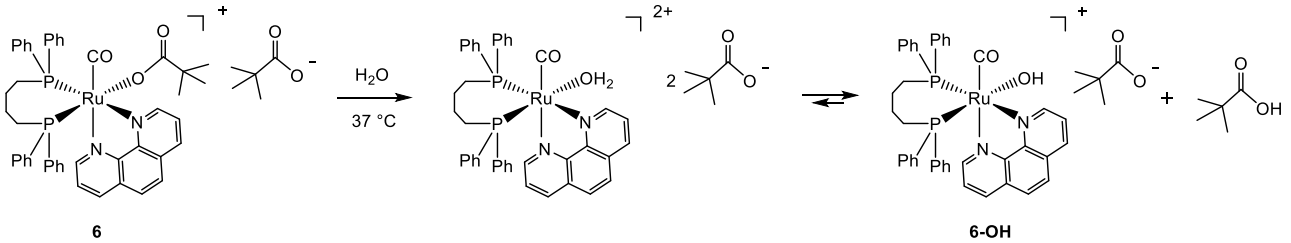

Scheme 6. Reaction of complex **6** with H_2O.

It is worth noting that for tumor or inflammatory tissues the extracellular pH range is about 6.5-6.9, which is lower than pH = 7.4 of normal tissues because of the rapid cell metabolism and therefore pH becomes a feasible endogenous trigger for a stimuli-responsive prodrug. By dissolution of the acetate **5** in D_2O, the $^{31}P\{^1H\}$ NMR spectrum reveals the presence of three species, namely **5** (δ 32.6 and 28.8 ppm, with $^2J_{PP}$ = 25.8 Hz), [Ru(OH)(CO)(dppb)(phen)]OAc (**5-OH**) (δ 38.7 and 24.9 ppm with $^2J_{PP}$ = 27.0 Hz, similar to **6-OH**), at about 3/1 molar ratio, in addition to a third uncharacterized species (broad signals at δ 36.0 and 27.0 ppm) in about 10% molar amount. Conversely, the thioacetate **7** and the isothiocyanate **8**, which show moderate solubility in water and can be solubilized by the addition of dmso-d_6 (one equiv.), do not show exchange reactions with D_2O or dmso-d_6 as inferred from $^{31}P\{^1H\}$ and ^1H NMR measurements.

In addition, the acetate **5** is completely stable in CH_3CN and no substitution of the acetate has been observed even at 70 °C for 12 h. Interestingly, the addition of CH_3CN (10 equiv.) to **5** in D_2O solution leads to the displacement of the acetate at room temperature within hours, affording $[Ru(NCCH_3)(CO)(dppb)(phen)](OAc)_2$, as inferred from NMR measurements. This suggests that water has a strong effect in enhancing the lability of **5**, facilitating the acetate substitution reactions, possibly through the formation of the hydroxo/aquo species (**Scheme 7**).

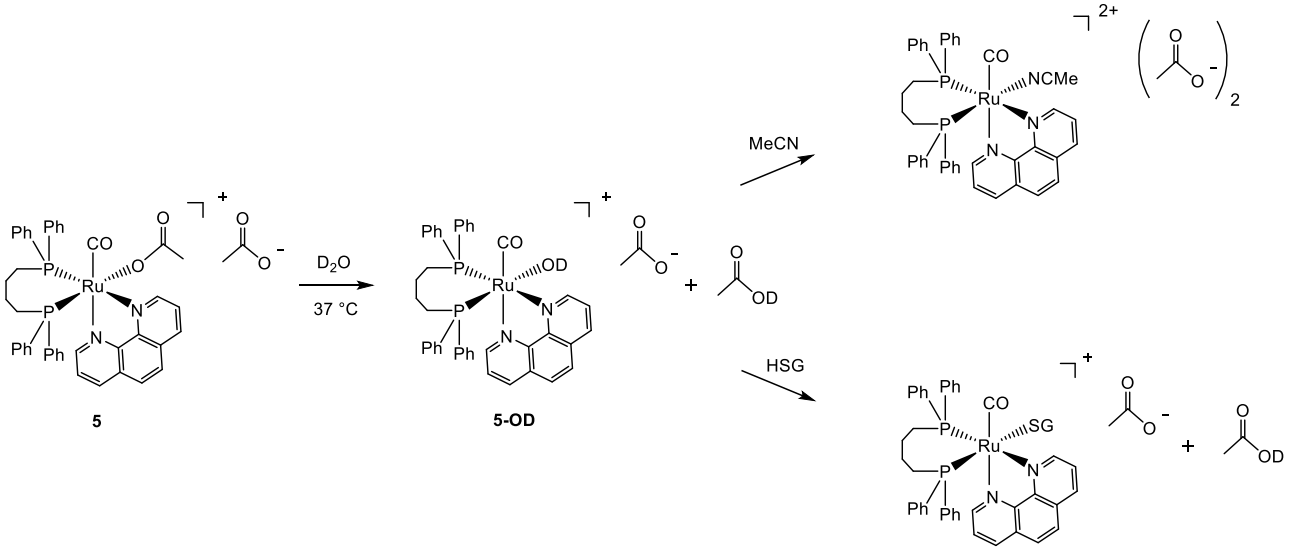

Scheme 7. Reaction of compound **5** with MeCN and HSG in D_2O.

On account of the easy substitution of the carboxylate ligands in complexes **5** and **6** in water, the reaction of glutathione (GSH), which is the most abundant thiol in animal cells (0.5 to 10 mM), was investigated in D_2O. Thus, the reaction of **5** with GSH (2 equiv.) in D_2O at 37 °C, suddenly affords a new species by displacement of the coordinated acetate showing one signal for the free acetate, as inferred from ^{1}H NMR measurements. The $^{31}P\{^{1}H\}$ NMR spectrum shows two broad signals at δ 29.0 and 24.1 ppm, close to those of the thioacetate **7** and consistent with the formation of the [Ru(SG)(CO)(dppb)(phen)](OAc) species. Identical behaviour has been observed for the reaction of pivalate **6** with GSH, while complex **7** does not react with GSH under these experimental conditions (GSH/Ru = 2), indicating that GSH easily protonates carboxylates **5** and **6**, but not the thioacetate **7**.

3.2.2.2 Structural isomerism

The investigation of this class of ruthenium complexes was extended to the isomerism of [Ru(η^1-OAc)(CO)(dppb)(phen)]OAc complex (**5**), which was previously described presenting the facial (*fac*) disposition of P, P and C atoms. In this section, the meridional (*mer*) PPC isomer **5a** is described, in order to highlight the different behaviour in solution and as cytotoxic agent.

[Ru(η^2-OAc)$_2$(dppb)] precursor[70] was treated with phen (1 equiv.) in methanol at 60 °C to afford the monocationic [Ru(η^2-OAc)(dppb)(phen)]OAc (**10**), isolated in 88% yield (eqn. 4).

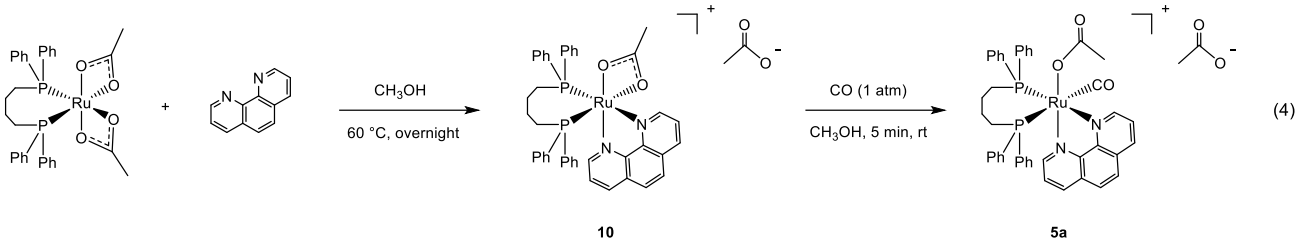

(4)

The $^{31}P\{^{1}H\}$ NMR spectrum of **10** in CD_2Cl_2 displays two doublets at δ 48.9 and 47.8 ppm ($^{2}J_{PP}$ = 33.6 Hz), consistent with the presence of a N and O ligands *trans* to the two P atoms, while the ^{1}H NMR resonances at δ 1.87 and δ 1.17 ppm correspond to the free and coordinated OAc moieties, respectively. As a matter of fact, NMR studies carried out in methanol-d_4 reveal that the addition of sodium acetate (1-5 equiv.) to **10** leads to a gradual increase of the signal at δ 1.91 compared to that at δ 1.18 ppm, indicating that one acetate is not coordinated to ruthenium, in line with the investigations performed on complex **5**. These studies reveal that the cationic form of **10** with a η^2-acetate is preferred to the neutral one in which two acetates are η^1-coordinated in a *cis* arrangement.

Complex **10** in methanol under CO atmosphere (1 atm) at room temperature, gave the *mer* PPC isomer [Ru(η^1-OAc)(CO)(dppb)(phen)]OAc **5a** (eqn. 3). This is due to the *trans* effect exerted by the phosphine, which allows the facile opening of the η^2-OAc, with consequent insertion of CO ligand, a process which is favoured by the interaction of methanol with acetate via hydrogen bonds.

The $^{31}P\{^{1}H\}$ NMR spectrum of **5a** in CD_3OD shows two doublets at δ 44.6 and 2.9 ppm ($^{2}J_{PP}$ = 29.0 Hz), for the P atoms *trans* to N and C ligands, respectively, demonstrating a mer PPC arrangement (**Figure 19**).

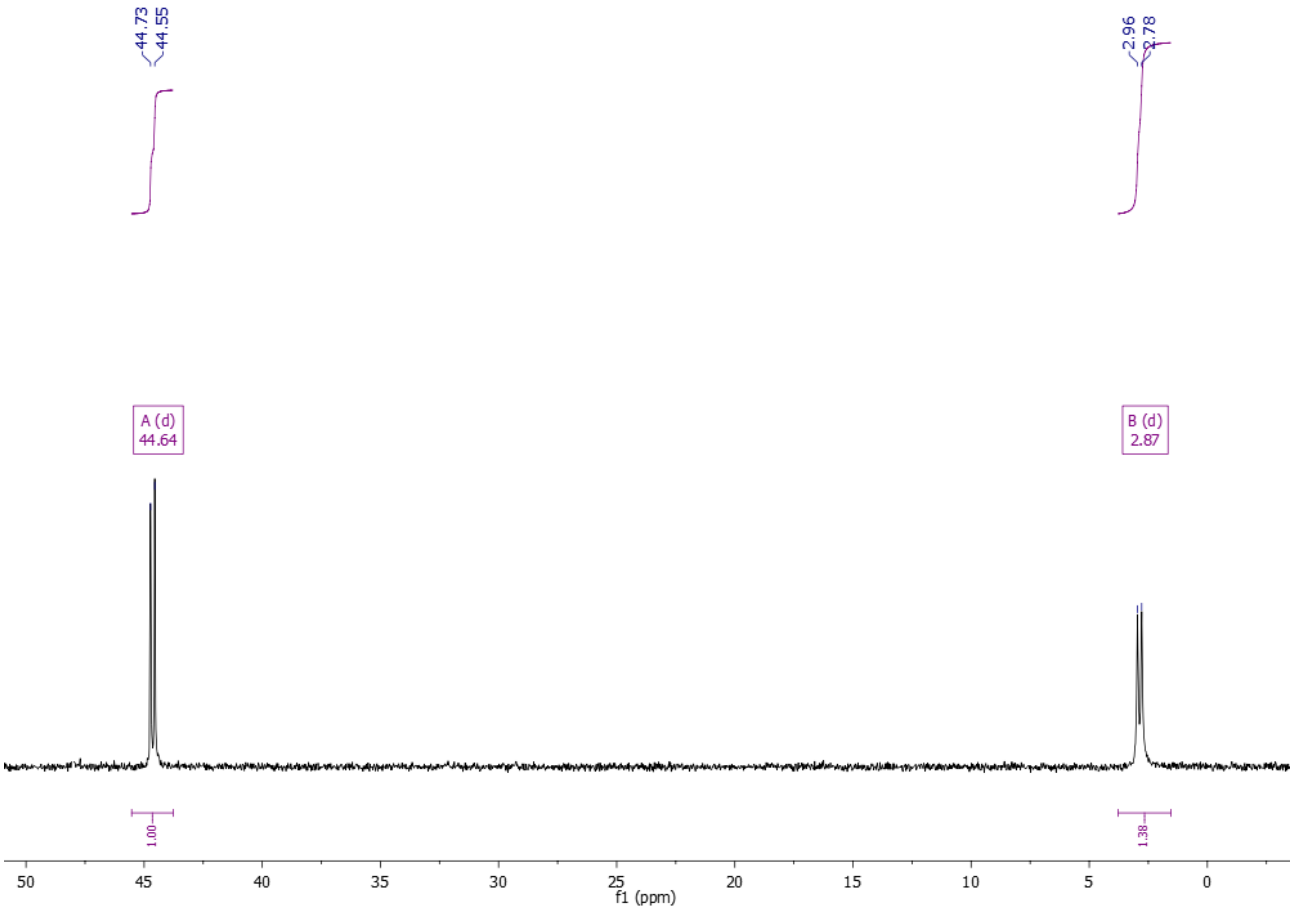

Figure 19. $^{31}P\{^{1}H\}$ NMR spectrum of **5a** in CD_3OD.

The ^{1}H NMR singlets at δ 1.91 and 1.78 ppm in CD_3OD, correspond to the free and coordinated axial acetate, respectively, and similar behaviour has been observed in protic solvents such as D_2O and ethanol-d_6. Surprisingly, in dichloromethane, chloroform and toluene, the bidentate chelation mode of the dppb is lost (eqn. 5).

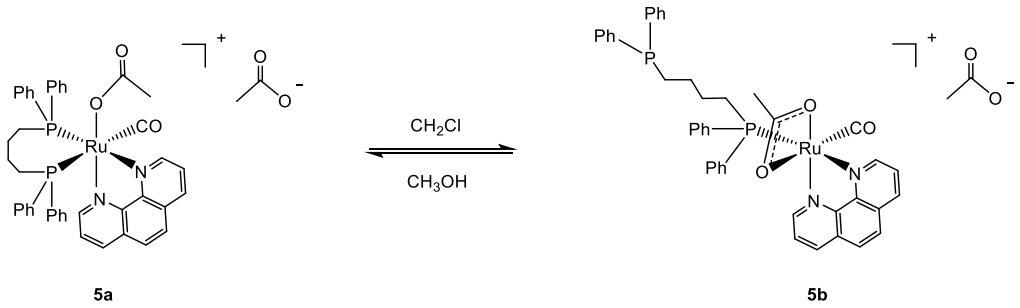

(5)

In CD_2Cl_2 complex **5a** displays two $^{31}P\{^{1}H\}$ NMR singlets at δ 37.3 and -16.4 ppm, suggesting that dppb is coordinated to ruthenium centre only with one P atom, *trans* to N (**Figure 20**).

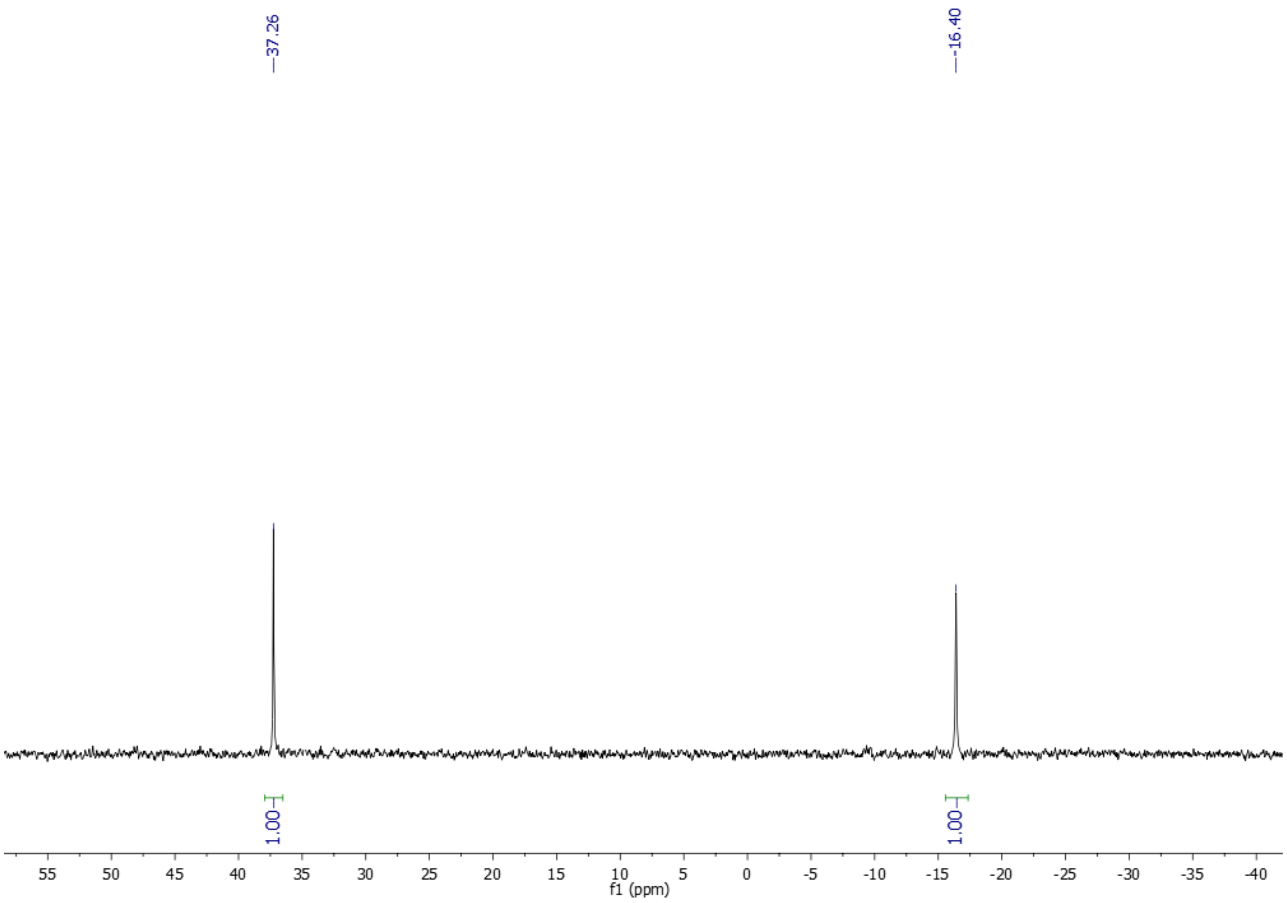

Figure 20. $^{31}P\{^{1}H\}$ NMR spectrum of **5a** in CD_2Cl_2.

This is due to the strong *trans* effect exerted by CO ligand. Also in this case, the cationic nature of **5a** is demonstrated by ^{1}H NMR singlets at δ 1.94 and 1.41 ppm for the free and η^2-coordinated OAc, respectively. This behaviour of **5a** is reversible as revealed by addition of CD_3OD in large amount in the NMR tube (150 equivalents with respect to **5a**).

It is worth noting that the carbonylation of **10** in CH_2Cl_2 instead of methanol is very slow and after 12 hours under 1 atm of CO, $^{31}P\{^{1}H\}$ NMR measurement revealed only the 50% of conversion of **10** to **5b**, with the additional formation of other not characterized species. These results indicate/confirm that protic solvents play a crucial role in enhancing the reactivity of ruthenium acetate complexes via strong hydrogen bond interactions and slippage of the acetate from η^2 to η^1 coordination mode.

3.2.2.3 Phenanthroline functionalization

With the aim to provide versatile new ligand frameworks for the straightforward linkage of cytotoxic ruthenium complexes with functional molecules, the development of functionalized imidazophenanthroline (IP) scaffolds has been studied. The choice for the IP or IP-phenyl ligands can reserve desired properties as already described in literature covering the creation of highly potent drug candidates and imaging agents. The functionalized imidazophenanthroline were synthetized according to the literature methods, utilizing optimized protocols[71]. Phenanthroline-5,6-dione was suspended in acetic acid with the desired substituted aldehyde (formaldehyde, thiophene-2-carbaldehyde and 4-(trifluoromethyl)benzaldehyde), in presence of ammonium acetate, in order to obtain 1*H*-imidazo[4,5-*f*][1,10]phenanthroline (IP), 2-(thiophen-2-yl)-1*H*-imidazo[4,5-*f*][1,10]phenanthroline (TIP) and 2-(4-(trifluoromethyl)phenyl)-1*H*-imidazo[4,5-*f*][1,10]phenanthroline (p-CF_3PIP) (eqn. 6).

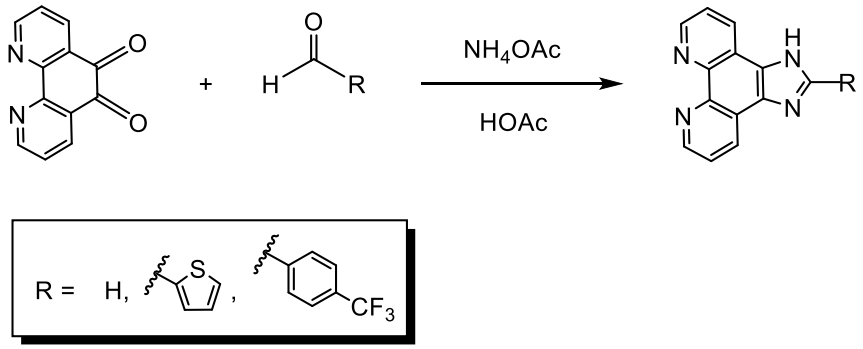

(6)

The obtained substituted imidazophenanthroline reacts with complex [Ru(η^1-OAc)(η^2-OAc)(CO)(dppb)] (**1**) in methanol at 60 °C, following the synthetic method of **5**, in order to obtain [Ru(OAc)(CO)(dppb)(IP)] (**11**), [Ru(OAc)(CO)(dppb)(TIP)] (**12**) and [Ru(OAc)(CO)(dppb)(p-CF_3PIP)] (**13**) (eqn. 7).

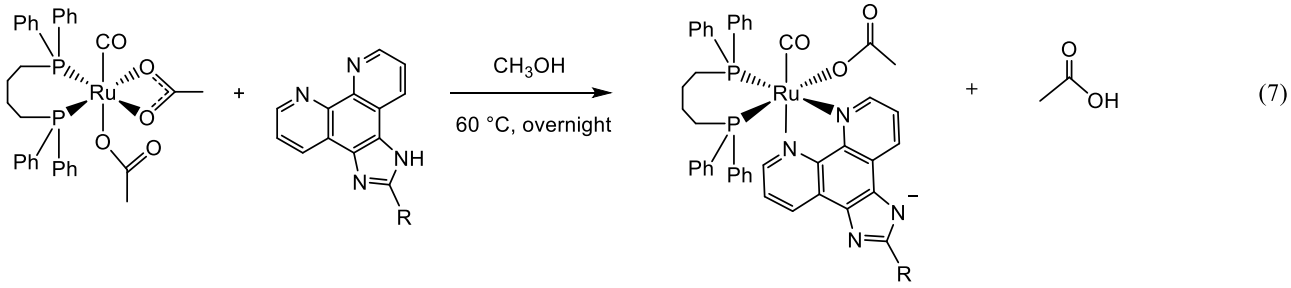

(7)

1

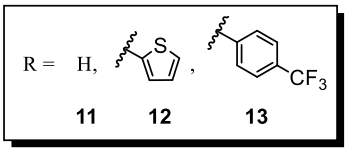

Surprisingly, the attitude of this class of complexes was not to form a cationic derivative as shown for complex **5**. By contrast, ^{1}H NMR evidences demonstrated the formation of neutral derivatives, as inferred from the absence of the OAc signal at *δ* 1.86 ppm, while all the three complexes present the coordinated OAc resonances between 1.45 and 1.47 ppm. This is probably due to the acidic proton of the NH imidazo-ring, which protonate the free acetate, forming acetic acid as by-product (eqn. 6).

The ^{31}P{^{1}H} NMR spectrum of **11** in CD_2Cl_2 displays two doublets at *δ* = 33.6 and 27.6 ppm ($^{2}J_{PP}$ = 23.0 Hz). Similarly, derivative **12** shows ^{31}P{^{1}H} NMR resonances at *δ* = 32.5 and 28.6 ppm (d, $^{2}J_{PP}$ = 24.5 Hz), while complex **13** at *δ* = 34.1 and 27.3 ppm (d, $^{2}J_{PP}$ = 23.4 Hz), confirming a geometry similar to that described for the cationic complexes.

These imidazophenanthroline complexes are air stable and soluble in the main organic solvents, including alcohols (methanol and ethanol), acetone, dichloromethane, chloroform and dimethyl sulfoxide, except for complex **12**, which is not soluble in chlorinated solvents. Unlike the majority of cationic complexes previously described, complexes **11**-**13** are not soluble in water, which is also probably responsible of their diminished effect on the cancer cell viability decrease (see section 4).

In order to overcome the problem of the formation of neutral complexes, the imidazophenanthroline ligand was replaced by pyrazino[2,3-*f*][1,10]phenanthroline ligand[72], which was synthetizes according to literature methods starting from phenanthroline-2,5-dione and ethylenediamine (eqn. 8).

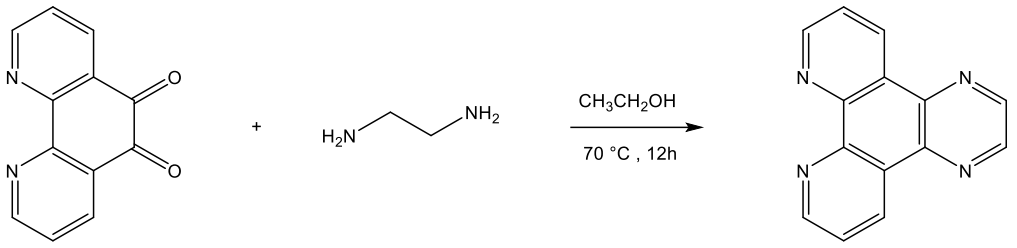

(8)

[Ru(η^1-OAc)(η^2-OAc)(CO)(dppb)] complex (**1**) was treated with pyrazino[2,3-*f*][1,10]phenanthroline (1 equiv.) in methanol at 60 °C for 12 hours, to afford the cationic derivative [Ru(OAc)(CO)(dppb)(PzPhen)]OAc (**14**) isolated in 89% yield (eqn. 9). Differently from imidazophenanthroline complexes, complex **14** displays high solubility in water and in the main organic media (alcohols, chlorinated solvents, acetone, dmso). Furthermore, the solutions of **14** are stable in air at room temperature for days.

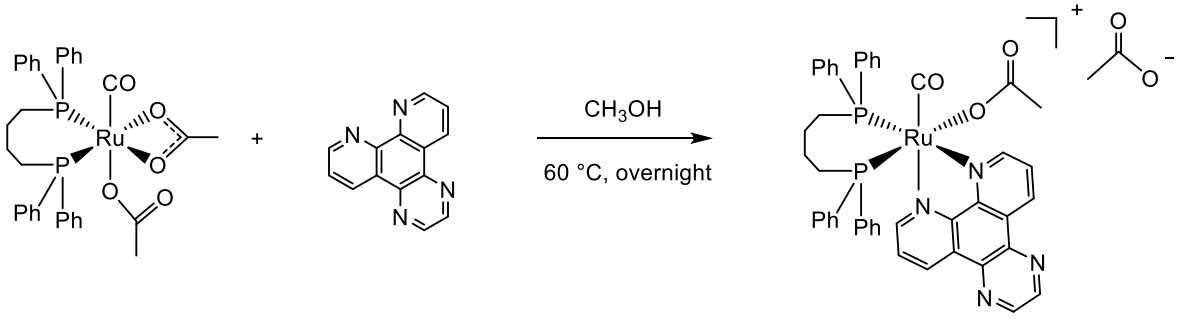

1 **14**

(9)

The $^{31}P\{^1H\}$ NMR spectrum of **14** in $CDCl_3$ shows two doublets at δ 31.7 and 29.6 ppm ($^2J_{PP}$ = 23.5 Hz), which are very close to those of the corresponding phenanthroline complex **5**. In the ^1H NMR spectrum, the two singlets at *δ* 1.99 and 1.50 ppm correspond to the methyl groups of the free and coordinated acetate, respectively, in line with the data of the previously described cationic acetate complexes. In the $^{13}C\{^1H\}$ NMR spectrum, the CO carbon appears as triplet at *δ* 204.1 ppm ($^2J_{CP}$ = 15.0 Hz), whereas the free and coordinated acetate carbonyl moieties appear as singlets at *δ* 177.2 and 176.5 ppm, respectively. Similarly to complex **5**, by dissolution of **14** in D_2O, the $^{31}P\{^1H\}$ NMR spectrum reveals the presence of two species, specifically **14** (*δ* 31.6 and 29.1 ppm, with $^2J_{PP}$ = 25.0 Hz) and [Ru(OH)(CO)(dppb)(PzPhen)]OAc (**14-OH**) (*δ* 37.5 and 25.2 ppm with $^2J_{PP}$ = 28.7 Hz, similar to **5-OH**), in about 80% and 10% in molar amount, respectively, in line with the studies carried out with **5** and **6**.

3.2.2.4 Isocyanide ruthenium complexes

On account of the high activity of this class of phenanthroline complexes, the subsequent step was to functionalize the main structure of the synthetized complexes, in order to optimize selectivity and targeting. Since the functionalization of phen ligand did not lead to better results in terms of cytotoxicity, the substitution of the carbonyl ligand with a functionalized isocyanide was considered as a challenging target.

First of all, the preparation of an alkyl-isocyanide was tested to consolidate the synthetic pathway for obtaining this new class of complexes.

$[Ru(\eta^2\text{-}OAc)_2(PPh_3)]$ reacted with *t*-butyl isocyanide (1 equiv.) in suspension in methanol at room temperature, to afford the air stable $[Ru(\eta^2\text{-}OAc)(\eta^1\text{-}OAc)(CN\text{-}t\text{-}Bu)(PPh_3)_2]$ (**15**), isolated in 90% yield by η^2-OAc opening (eqn. 10).

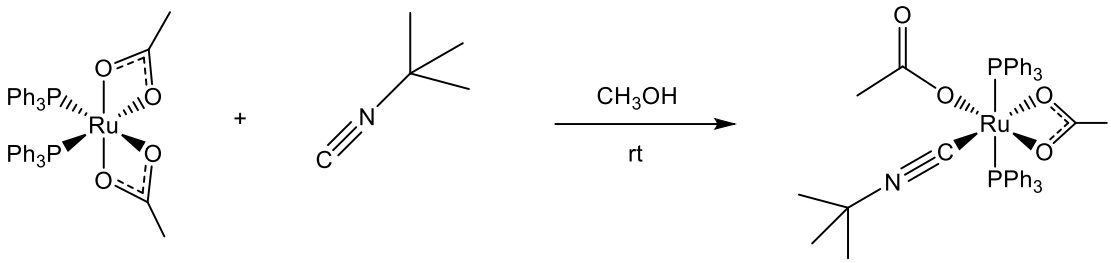

(10)

15

The $^{31}P\{^1H\}$ NMR spectrum of **15** in CD_2Cl_2 displays one singlet at δ 41.2 ppm for the two P atoms of PPh_3, whereas the ^1H NMR resonances at δ 0.75 and 0.78 ppm are attributed to the two acetates and to the isocyanide *t*-butyl group, respectively. In $^{13}C\{^1H\}$ NMR spectrum the R-NC carbon atom appears as triplet at δ 132.7 ($^2J_{CP}$ = 19.8 Hz), while the singlets at δ 180.9 and 161.1 ppm correspond to the carboxylate carbon atoms of OAc groups.

Complex **15** reacted with dppb (1 equiv.) in toluene at 100 °C to afford $[Ru(\eta^1\text{-}OAc)(\eta^2\text{-}OAc)(CN\text{-}t\text{-}Bu)(dppb)]$ **(16)** in 83% yield, by displacement of PPh_3 ligands (eqn. 11).

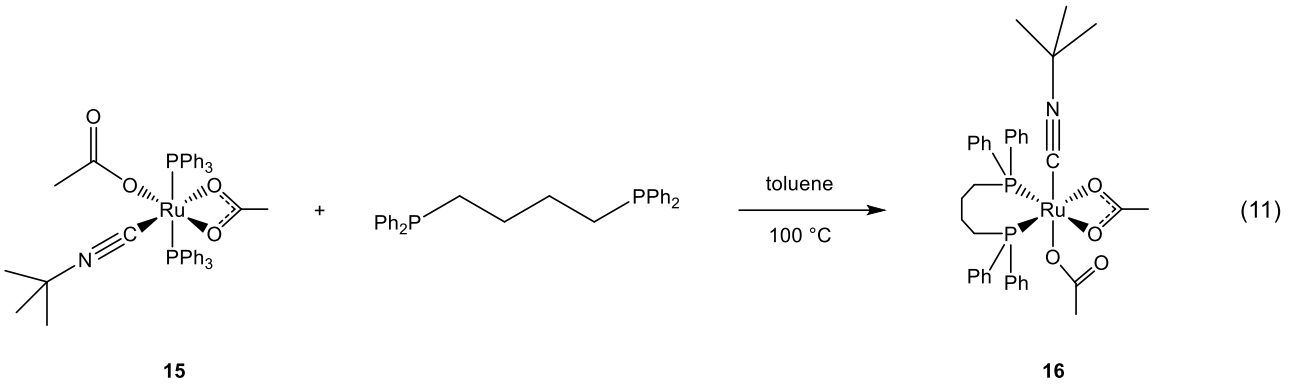

15 **16**

The $^{31}P\{^{1}H\}$ NMR spectrum in CD_2Cl_2 shows a broad signal at *δ* 51.9 ppm indicating a fluxional behaviour due to the rapid exchange between η^1-OAc and η^2-OAc. The signals of the CO acetate carbons were not detectable in the $^{13}C\{^{1}H\}$ NMR spectrum, regardless of the deuterated solvent, concentration, duration and relaxation time selected for the analysis, confirming a rapid exchange of the OAc groups on the NMR time scale at RT. On the other hand, ^{1}H NMR spectrum exhibits a singlet at *δ* 1.46 ppm for the protons of both acetate ligands.

The subsequent reaction of **16** with phenanthroline (1 equiv.) in methanol at 60 °C afforded the stable cationic derivative [Ru(OAc)(CN-*t*-Bu)(dppb)(phen)]OAc (**17**), isolated in 79% yield after displacement of one acetate ligand (eqn. 12).

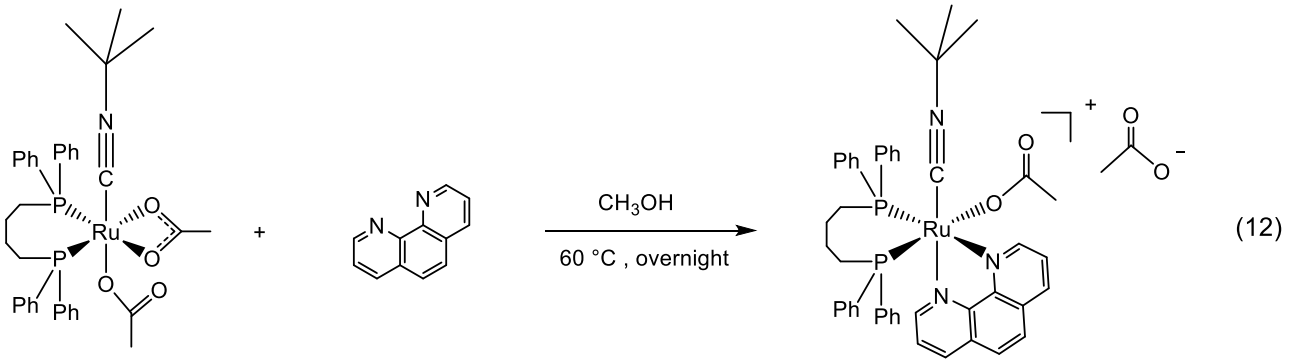

16 **17**

The $^{31}P\{^{1}H\}$ NMR spectrum in CD_2Cl_2 displays two doublets at *δ* 41.8 and 29.9 ppm ($^{2}J_{PP}$ = 26.5 Hz) for the P atoms *trans* to N and O, respectively, consistent with a *cis* arrangement of the acetate and CN-*t*-Bu ligands. Interestingly, these chemical shift values are quite different if compared to those of the relate complex bearing carbonyl (**5**), in particular the P atom *trans* to phenanthroline N atom is very deshielded with respect to that of **5** (*δ* 32.4

ppm). Also in this case, in the ^{1}H NMR spectrum it is possible to distinguish the resonances at *δ* 1.84 and 1.40 ppm of the free and coordinated OAc moieties, respectively, and the signal of the isocyanide t-butyl group at *δ* 1.44 (9 protons). Unlike the fluxional precursor **16**, in $^{13}C\{^{1}H\}$ NMR spectrum of **17** can be distinguished the signals at *δ* 176.6 and 176.4 ppm for the carboxylate carbon atoms of the free and coordinated OAc, respectively, while the triplet at *δ* 154.2 ppm ($^{2}J_{CP}$ = 18.4 Hz) corresponds to the CN-*t*-Bu *cis* to the two P atoms. The high solubility and stability in water of this isocyanide derivative arouse great interest toward this new class of complexes for their application in biological conditions and in light of an optimal bioavailability. In fact, differently from comparable complex **5**, which forms 3 species in water solutions (see section 3.2.2.1), complex **17** in D_2O solution (4 mM) at 37 °C, leads to the immediate formation of only one new compound, characterized by a new pair of doublets at *δ* 47.9 and 27.2 ppm ($^{2}J_{PP}$ = 33.8 Hz) in $^{31}P\{^{1}H\}$ NMR spectrum, without any significant change for days. In the ^{1}H NMR spectrum, **17** displays the singlets at *δ* 1.82 and 1.29 ppm for the acetate and the isocyanide *t*-Bu group, respectively. Differently from what observed in the spectrum in CD_2Cl_2 with the presence of two singlets given by the free and coordinated acetate, indicating that in D_2O the OAc ligand is not coordinated to ruthenium. Complex **17** in H_2O shows a pH value of 4.6, which is close to the value of a buffer solution of acetic acid – acetate (pKa HOAc = 4.75)[69], and is consistent with the formation of the hydroxo specie [Ru(OH)(CN-*t*-Bu)(dppb)(phen)]OPiv (**17-OH**) (**figure 21**).

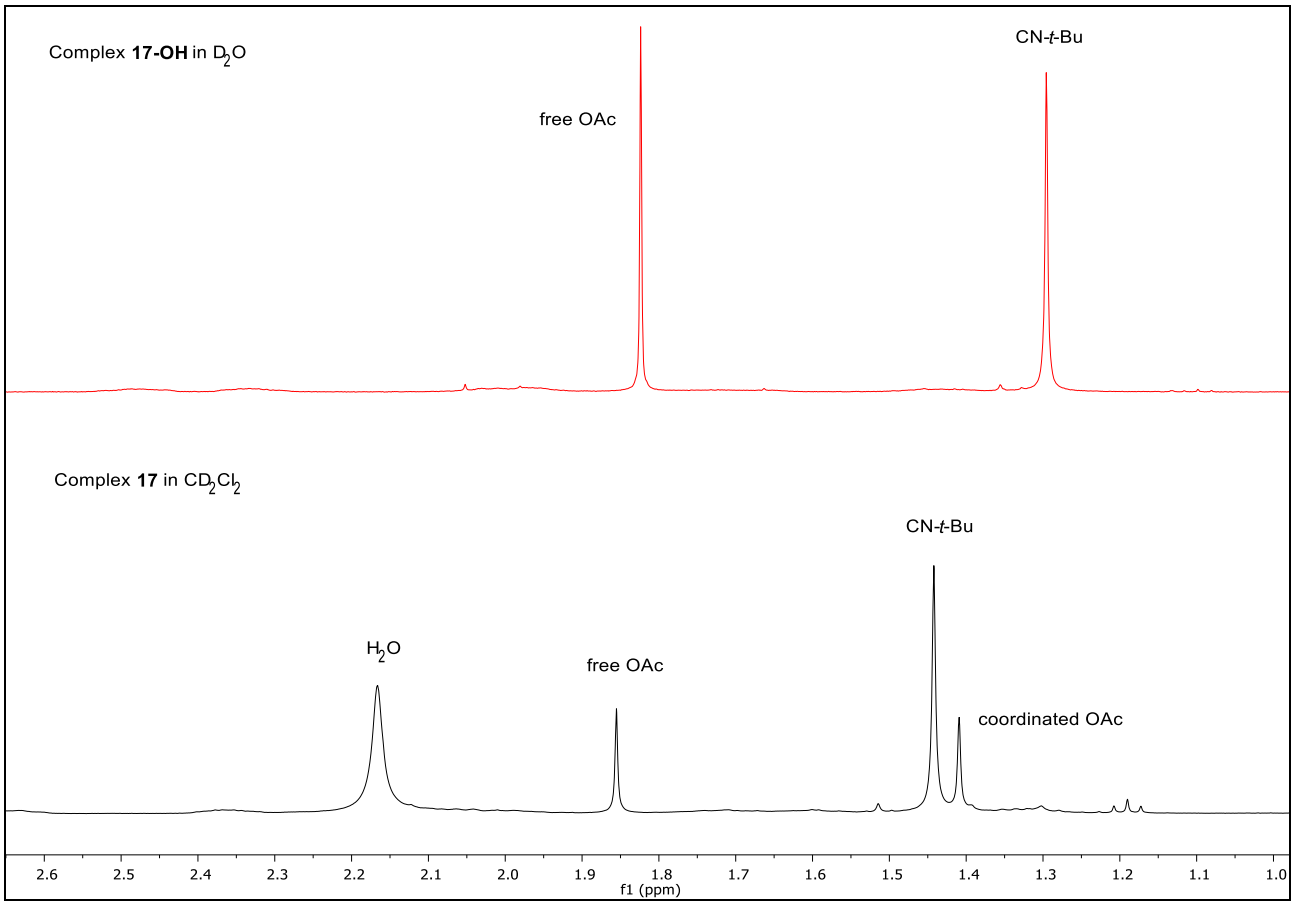

Figure 21. ^{1}H NMR in the range of 2.6-1.0 ppm of **17** in CD_2Cl_2 (down) and the formation of **17-OH** specie in D_2O (up).

This suggests once again that water has a strong effect in enhancing the lability of this class of complexes, facilitating the acetate substitution reactions by means of the strong ionic hydrogen bond interaction of $RCOO^-$ with H_2O.

3.2.3 Synthesis and characterization of chiral monocationic phenanthroline ruthenium(II) complexes.

The control of the configuration at the ruthenium center in octahedral complexes is a key challenge that can be exploited for different applications in the field of catalysis, materials sciences and pharmacology.

Based on these considerations, we synthetized the chiral ruthenium complexes of the above-mentioned class and studied their reactivity and properties. The introduction of a chiral diphosphine such as (R,R)-Skewphos or (S,S)-Skewphos leads to a diasteroselective synthesis, inducing chirality to the ruthenium center.

Herein the synthesis of chiral cationic complexes of general formula [RuX(CO)((R,R)-Skewphos)(phen)]Y and [RuX(CO)((S,S)-Skewphos)(phen)]Y (where X = Y = OAc, OPiv, SAc) is reported, as well as their biological behaviour, demonstrating a different activity for the two enantiomers.

The chiral acetate complex [Ru(η^1-OAc)(η^2-OAc)((R,R)-Skewphos)(CO)][46] (**1R**) was treated with phenanthroline (1 equiv.) in methanol at 60 °C to afford the cationic enantiomer [Ru(η^1-OAc)(CO)((R,R)-Skewphos)(phen)]OAc (**18R**), isolated in 87% yield. In a similar way, the complex [Ru(η^1-OAc)(CO)((S,S)-Skewphos)(phen)]OAc (**18S**) was prepared from [Ru(η^1-OAc)(η^2-OAc)((S,S)-Skewphos)(CO)] (**1S**) and phenanthroline and isolated in 91% yield (eqn. 13).

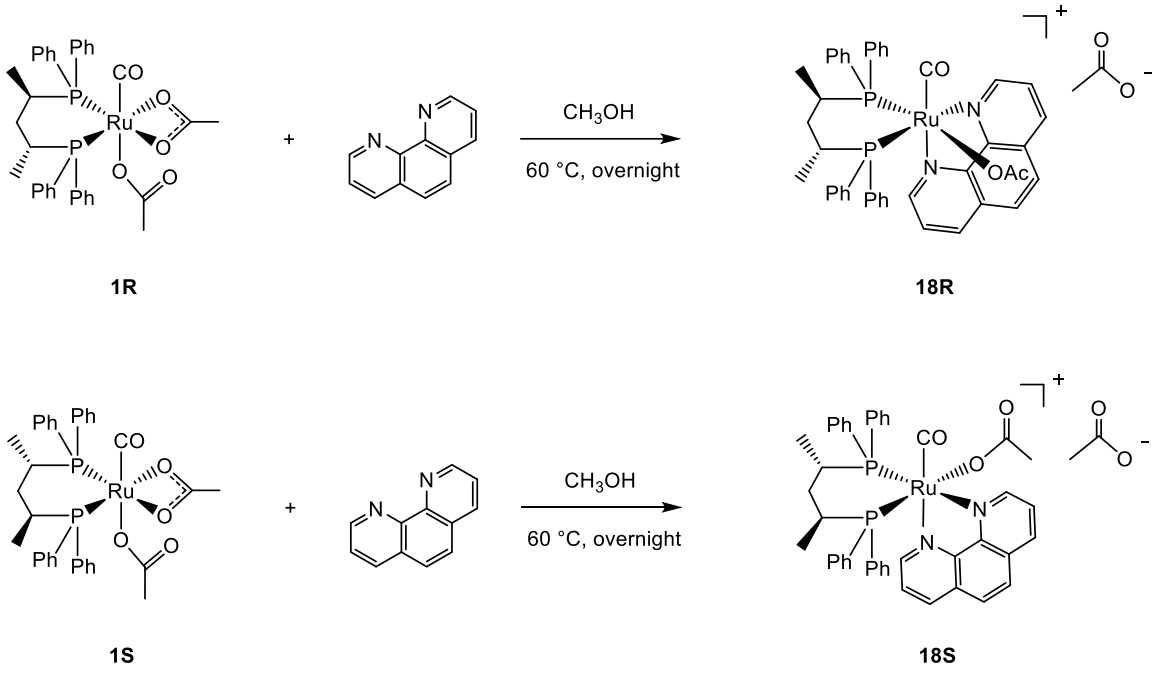

1R **18R**

(13)

1S **18S**

3.2.3.1 NMR evaluations

The $^{31}P\{^1H\}$ NMR spectra of **18R** in $CDCl_3$, displays two very close doublets at δ 42.9 and 41.0 ppm (d, $^2J_{PP}$ = 32.2 Hz) for the P atom *trans* to N and O atoms, respectively.

The attribution of P atoms was confirmed by 2D ^{31}P-^1H HMBC spectrum, where the $^{31}P\{^1H\}$ NMR doublet at δ 42.9 ppm shows a long range coupling with the *ortho* phenanthroline proton at δ 8.75 in ^1H NMR spectrum. The ^1H NMR CH and CH_3 proton signals of (R,R)-Skewphos backbone at δ 3.43 and 1.16 ppm, respectively, can be easily attributed to the

adjacent P atom displaying a $^{31}P\{^{1}H\}$ NMR signal at *δ* 42.9 ppm. Conversely, the $^{31}P\{^{1}H\}$ NMR doublet at *δ* 41.0 ppm is for the P *trans* to acetate singlet at *δ* 1.19 ppm bound to the CH moiety at *δ* 2.91 ppm and bearing the CH_3 at 0.82 ppm (**Figure 22**).

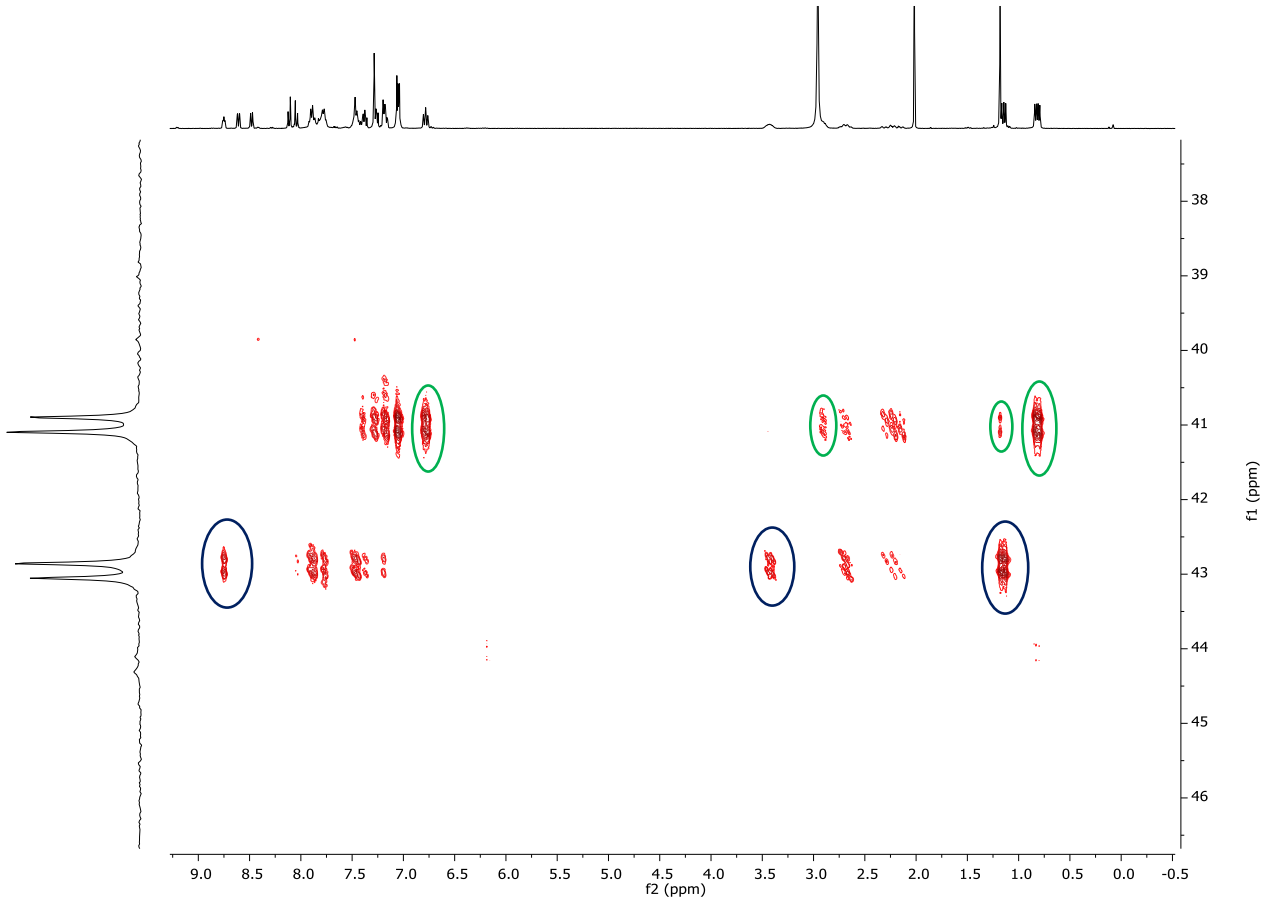

Figure 22. 2D ^{31}P-^{1}H HMBC spectrum of complex **18R** in $CDCl_3$. Circled in blue: long range coupling with P signal at *δ* 42.9 ppm; circled in green: long range coupling with P signal at *δ* 41.0 ppm.

It is worth noting that the 2D ^{31}P-^{1}H HMBC and 2D ^{1}H-^{1}H COSY spectra (**Figure 22** and **23**) show that the triplet at *δ* 6.79 ppm corresponds to the *ortho* protons of one phenyl group linked to the P atom at *δ* 41.0 ppm, and it is *trans* to OAc.

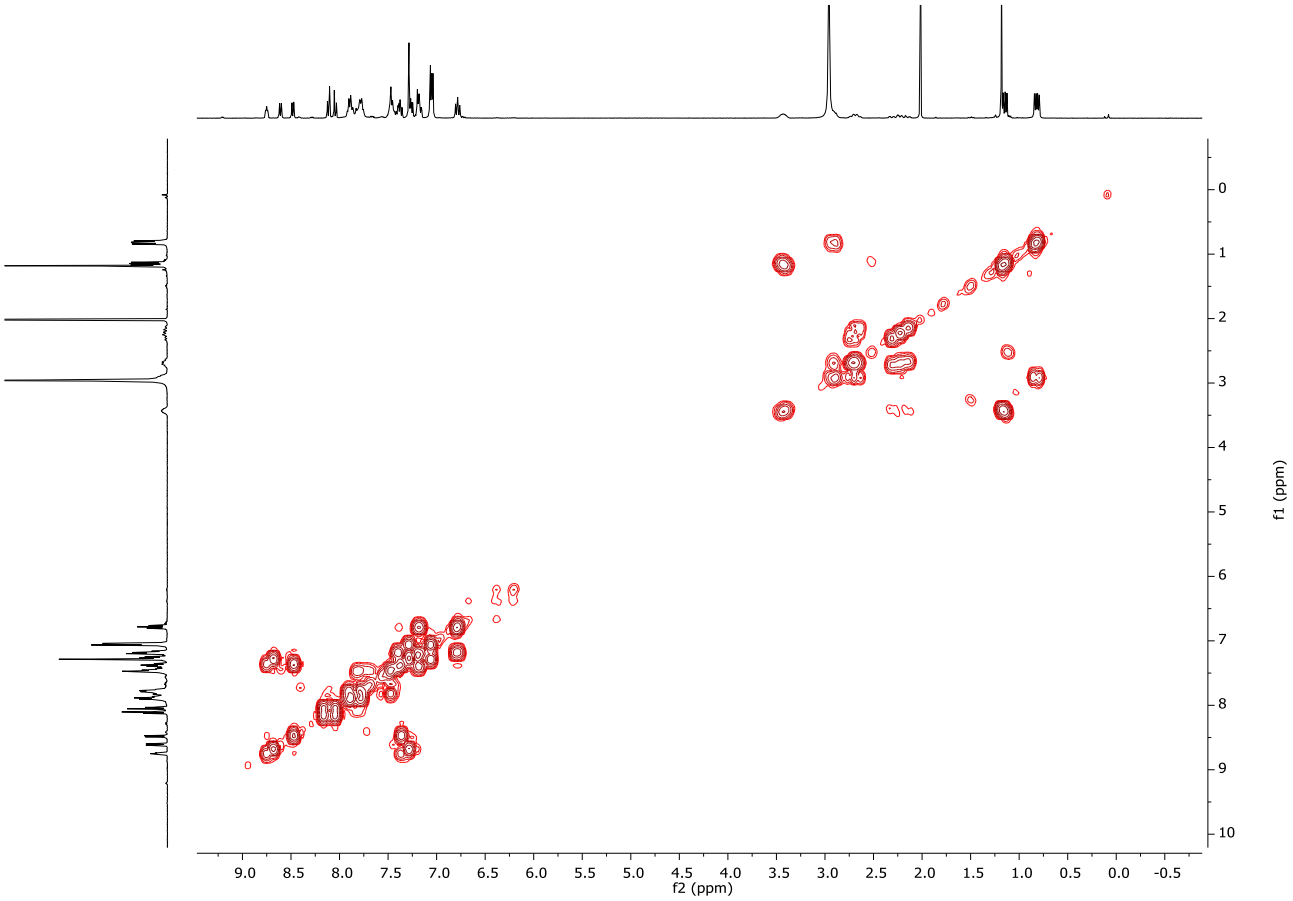

Figure 23. 2D ^{1}H-^{1}H COSY spectrum of complex **18R** in CD_3Cl.

These two *ortho* protons appear up-field shielded with respect to the other ^{1}H NMR phenyl signals and is consistent with an anisotropic effect due to the superimposition of the (R,R)-Skewphos phenyl ring with the phenanthroline ring whose N atom is *trans* to P at *δ* 42.9 ppm, via intramolecular π–π-interactions. The X-Ray analysis of ruthenium complexes bearing Skewphos and DFT calculations (see further part), demonstrate that the diphosphine adopts a three-dimensional structure known as distorted boat conformation, where CH_3 groups appear one axial and one pseudo-equatorial. In this case, the pseudo-equatorial CH_3 with ^{1}H NMR signal at *δ* 0.82, is the one that leads the phenyl groups linked to the P at *δ* 41.0 ppm forward, inducing a stacking effect with a phenanthroline ring. These considerations are also in line with the DFT calculations (see 3.2.3.2 section).

Finally, as confirmation of the proposed conformation, the NOESY ^{1}H-^{1}H NMR spectrum exhibits NOE effect between the *ortho* phen proton at *δ* 8.75 and the *ortho* phenyl protons at *δ* 6.78 ppm, which display NOE effect also with the CH_3 group at *δ* 0.82 ppm (**figure 24** and **25**).

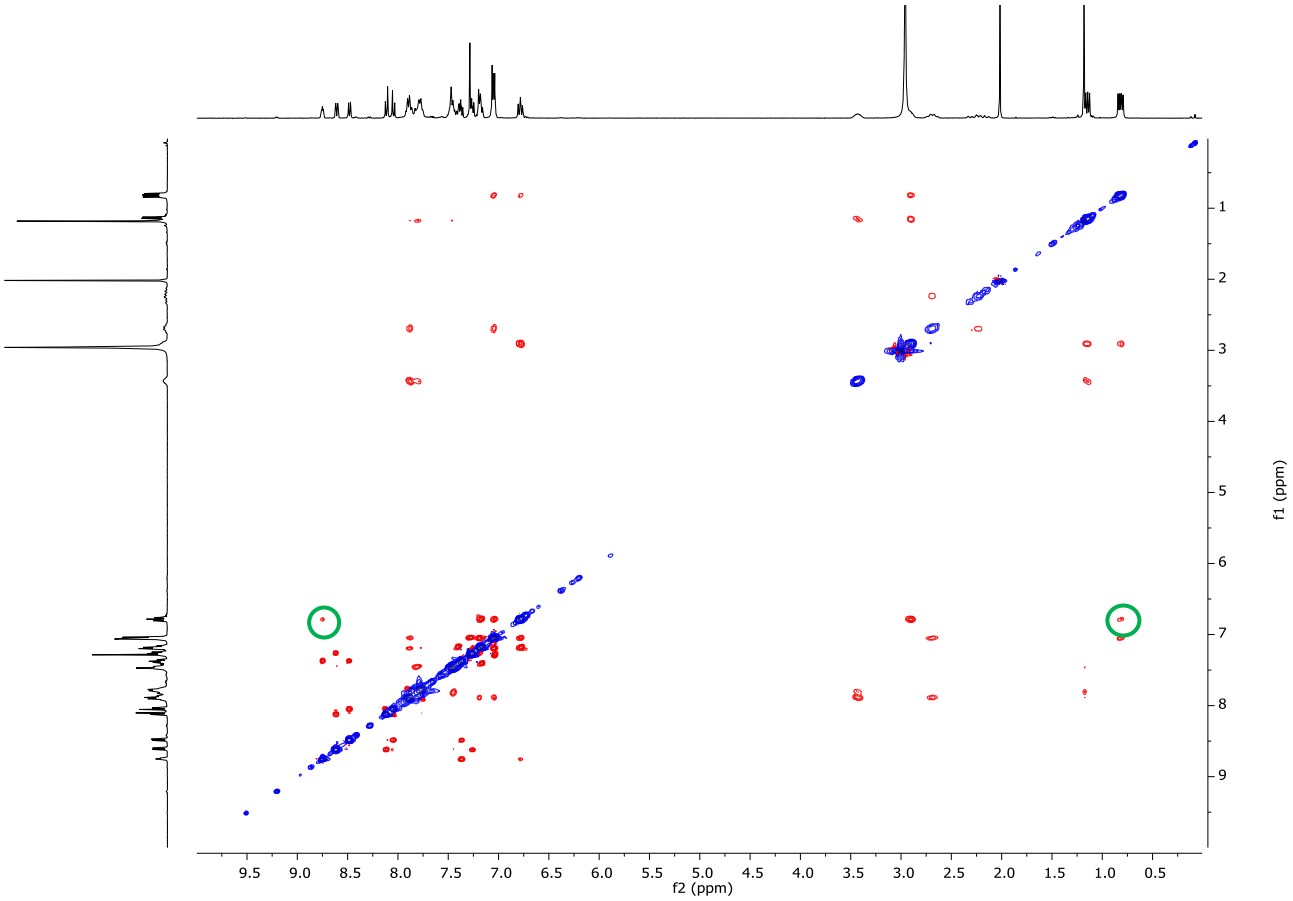

Figure 24. NOESY ^{1}H-^{1}H NMR spectrum of **18R** in $CDCl_3$. Circled in green: NOE effects between the Skewphos *ortho* phenyl protons and phenanthroline *ortho* proton or CH_3 protons at δ 0.82 ppm.

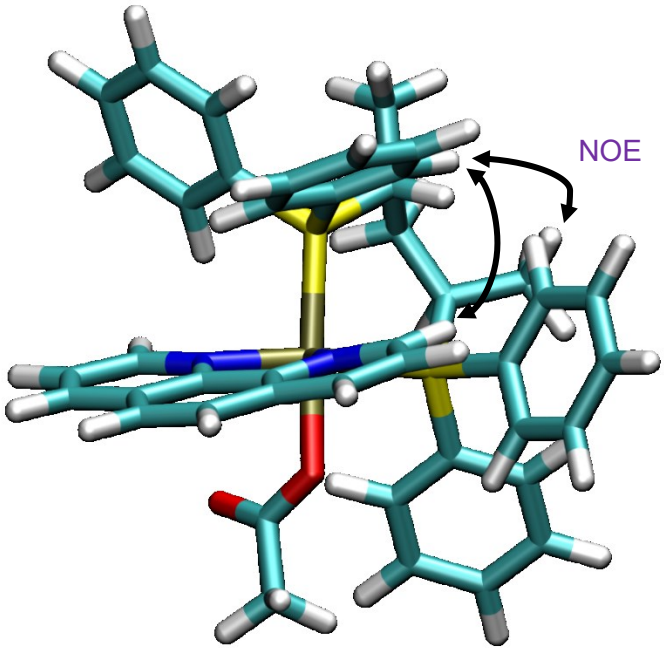

Figure 25. Representation of the most relevant NOE effects related to the **18R** structure.

All these considerations allow the attribution of [Ru(η^1-OAc)(CO)((R,R)-Skewphos)(phen)]OAc conformation as **18R** isomer (see further part), which is obtained as a pure diasteroisomer, as shown in **Scheme 8**.

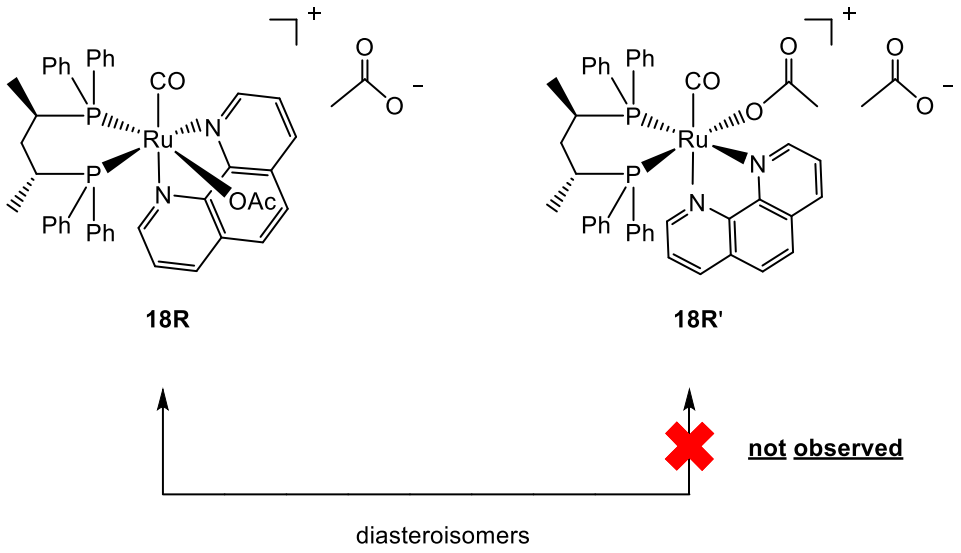

Scheme 8. Conformation of complex Ru(η^1-OAc)(CO)((R,R)-Skewphos)(phen)]OAc which is obtained as pure **18R** isomer. Conversely, the formation of **18R'** diasteroisomer was not observed.

3.2.3.2 Density functional theory (DFT) calculations.

The geometry and the free Gibbs energy of the different stereoisomers of **18R** complex have been investigated through DFT calculations in gas phase and in PMC methanol. Three possible isomers with a fixed fac PPC arrangement, can be envisaged (**Figure 26**).

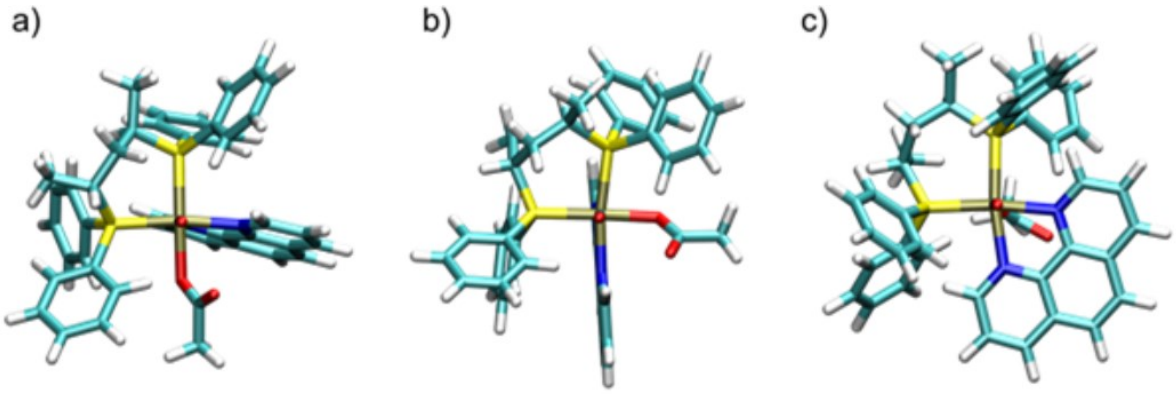

Figure 26. Optimized geometry in PCM methanol for [Ru(η^1-OAc)(CO)((R,R)-Skewphos)(phen)]$^+$ stereoisomers: a) **18R**; b) **18R'**; c) **18R''**.

The distances between Ru---P1 and Ru---P2 present similar values in **18R**, while a progressive difference ($\Delta d = d_{Ru---P1} - d_{Ru---P2}$; from 0.013 to 0.036 Å, see **Table 1**) was observed ranging from **18R'** to **18R''** in the gas phase. The lengths between Ru and N1 were similar in **18R** and **18R'**, while is shorter in **18R''**. An opposite behavior was observed for the Ru---N2 distances (**Table 1** and **Figure 27**).

Table 1 Selected bonds distances (Å) and angles (°) for **18R** stereoisomers in gas phase and methanol.

Bond	Gas phase			Methanol		
	a) **18R**	b) **18R'**	c) **18R''**	a) **18R**	b) **18R'**	c) **18R''**
Ru-P1	2.371	2.386	2.436	2.374	2.392	2.440
Ru-P2	2.369	2.373	2.400	2.379	2.377	2.405
Ru-N1	2.221	2.220	2.180	2.219	2.220	2.193
Ru-N2	2.147	2.147	2.194	2.144	2.146	2.177
Ru-CO	1.849	1.850	1.852	1.842	1.843	1.846
Ru-OAc	2.095	2.098	2.123	2.108	2.110	2.193
Angle						
P1-Ru-P2	92.572	96.995	92.503	92.339	96.514	92.385
N1-Ru-N2	76.479	76.789	76.712	76.561	76.822	76.846

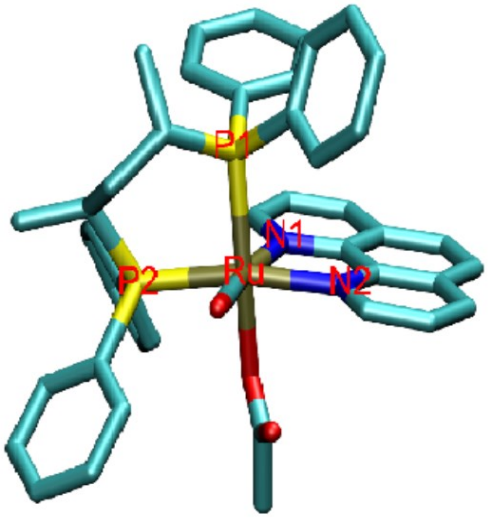

Figure 27. Atom labels, the hydrogen atoms were removed for clarity.

The Ru-OAc presents the same trend of Ru-N1. While the Ru-CO lengths show similar values for all the stereoisomers, the Ru-OAc is similar for **18R** and **18R'** and larger for **18R''**. The N1---Ru---N2 angle shows analogous values in all three complexes, while the P1---Ru---P2 angle values for **18R'** was larger with respect to the other isomers.
In all three stereoisomers, the Skewphos ligand assumes a distorted boat conformation, as reported in **Figure 28**, indicating that the different arrangement of phenanthroline does not significantly affect the geometrical parameters of the complex.

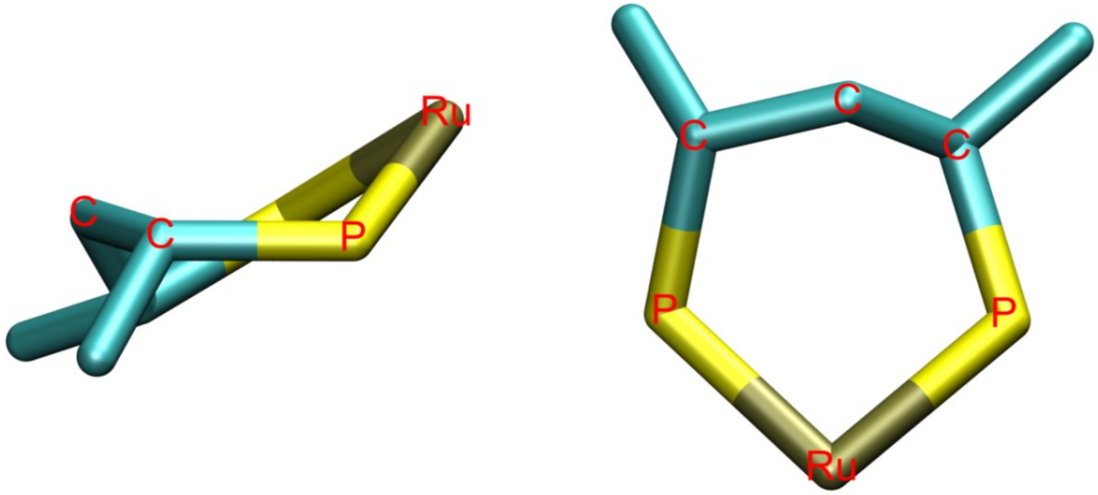

Figure 28. Boat conformation of six-membered-cyclo structures of **18R** diphosphine (the other atoms were removed for clarity).

DFT calculations show that the **18R** species is more stable than **18R'** and **18R''** with ΔG = -4.3 kcal mol^{-1} ($\Delta G = G_{18R'} - G_{18R''}$) and ΔG = -4.4 kcal mol^{-1} ($\Delta G = G_{18R'} - G_{18R'''}$). Moreover, the ΔG between **18R'** and **18R''** is negligible (**Table 2**).

Table 2. Free Gibbs difference in gas phase and in PCM methanol expressed in kcal mol^{-1}.

Difference	ΔG Gas phase	ΔG PCM methanol
18R - 18R'	-4.3	-4.6
18R - 18R''	-4.4	-6.4
18R' - 18R''	-0.1	-1.9

The trend in stability does not change in methanol, the most stable conformer is **18R** with a ΔG ranging from -4.6 and -6.4 kcal mol^{-1}. This result is in agreement with experimental NMR spectra of **18R** (See **Figures 22-24**), indicating that **18R** is the most stable stereoisomer.

3.2.3.3 Synthesis of pivalate and thioacetate chiral ruthenium derivatives.

The pivalate derivative [Ru(η^1-OPiv)(CO)((R,R)-Skewphos)(phen)]OPiv (**19R**) was easily prepared in high yields, by treatment of **18R** with NaOPiv (10 equiv.) in methanol at 60 °C for 24 h via displacement of OAc, following the procedure for **6** (**Scheme 9**).

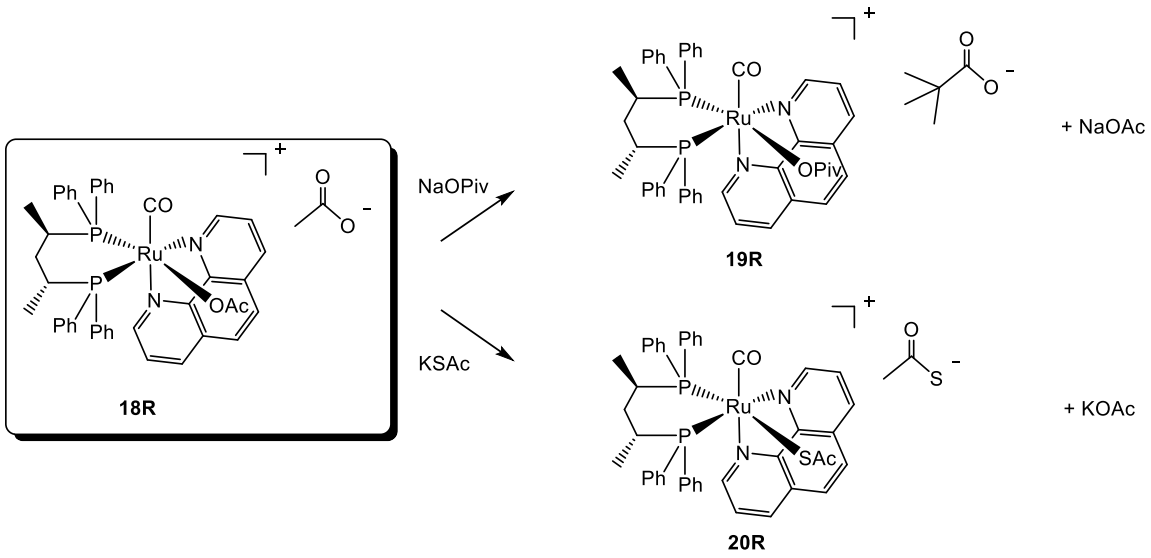

Scheme 9. Synthesis of complexes **19R** and **20R** from **18R** by displacement of the coordinated acetate in MeOH at 60 °C.

The $^{31}P\{^1H\}$ NMR spectrum of **19R** in $CDCl_3$ shows two doublets at *δ* 43.7 and 41.5 ppm ($^2J_{PP}$ = 31.4 Hz), whereas the ^1H NMR singlets at *δ* 1.22 and 0.05 ppm correspond to the methyl groups of the free and coordinated pivalate, respectively. In the $^{13}C\{^1H\}$ NMR spectra, the CO carbon appears as a doublet of doublets at *δ* 204.7 ppm ($^2J_{CP}$ = 20.0 and 15.2 Hz), while the free and coordinated pivalate carbonyl moieties appear as singlets at *δ* 184.0 and 183.6 ppm, respectively. In a similar way, the enantiomer **19S** was prepared from **18S** and NaOPiv.

The thioacetate Ru(η^1-SAc)(CO)((R,R)-Skewphos)(phen)]SAc **20R** was obtained by treatment of the acetate complexes **18R** with KSAc (10 equiv.) in methanol at 60 °C overnight, by displacement of OAc (**Scheme 9**).

The $^{31}P\{^1H\}$ NMR spectrum of **20R** in $CDCl_3$, exhibits a doublet at *δ* 41.1 ppm ($^2J_{PP}$ = 29.6 Hz) for the diphosphine P atom *trans* to the N phenanthroline atom, and a more shielded doublet at *δ* 30.9 ppm for the P *trans* to S thioacetate atom. The ^1H NMR singlets at *δ* 2.09 and 1.90 ppm correspond to the free and coordinated thioacetate methyls. In the $^{13}C\{^1H\}$ NMR spectrum the doublet of doublets at δ 205.5 ppm ($^2J_{CP}$ = 19.5 and 12.2 Hz) corresponds to the CO *cis* to the two P atoms, whereas the singlets at δ 204.1 and 176.1 ppm correspond to the CO carbon atom of the free and coordinated SAc, respectively. As for **20R**, the enantiomer Ru(η^1-SAc)(CO)((S,S)-Skewphos)(phen)]SAc **20S** was obtained from **18S** and KSAc.

3.3 DICATIONIC PHOSPHINE DIIMINE RUTHENIUM COMPLEXES.

3.3.1 State of the art.

In literature, few dicationic ruthenium complexes bearing diphosphine, carbonyl and diimine ligands have been described so far. In 2002 Whittlesey and coworkers[73], described the synthesis of diicationic $[Ru(dppe)(CO)(CH_3CN)_3][OTf]_2$ complex, starting from the aquo complex $[Ru(dppe)(CO)(H_2O)_3][OTf]_2$, exploiting the labile nature of the coordinated water ligands to the metal center. In fact, aquo complexes afford the possibility of studying the lability of the coordinated waters (especially H_2O *trans* to P atoms) with a range of incoming ligands such as unidentate, bidentate, and potentially bridging groups. In 2004, Ooyama[74] synthetized a dicationic ruthenium complex of formula $[Ru(bpy)(dppy)_2(CO)_2](PF_6)_2$ (bpy = 2,2'-bipyridine, dppy = 2-(diphenylphosphino)pyridine) which is an active specie in the reduction of CO_2.

Recently, Alessio *et al.*[75] developed a new class of dicationic water soluble ruthenium complexes with formula $[Ru(bpy)(CO)(PTA)_3](Cl)_2$ and $[Ru(bpy)(CO)_2(PTA)_2](NO_3)_2$ (PTA = 1,3,5-triaza-7-phosphaadamantane and bpy = 2,2'-bipyridine). The monodentate PTA is an amphiphilic and airstable neutral ligand that, besides dissolving in several organic solvents, is characterized by a high solubility in water, thanks to the H-bond with the tertiary amine

nitrogens. This typically imparts excellent water solubility to the metal complexes, which are investigated as potential anticancer drugs and as homogeneous catalysts in aqueous solutions.

3.3.2 Synthesis and characterization of dicationic ruthenium complexes.

The solubility in water of the acetate and pivalate complexes described so far, allows the substitution of the acetate ligand with a water molecule, which eventually leads to the hydroxo complex (see 3.2.2.1 section). This pathway was exploited to exchange the very labile OAc to $^{-}$OH anion, *trans* to P, with neutral species with high electron donor nature, including PTA, acetonitrile (see 3.2.2.1 section) and pyridine, so developing new dicationic ruthenium complexes. Reaction of **5** with PTA (1 equiv.) or pyridine (py) (1 equiv.) in H_2O at 60 °C, after the addition of NH_4PF_6 salt, afforded the dicationic derivatives $[Ru(CO)(dppb)(PTA)(phen)](PF_6)_2$ (**21**) and $[Ru(CO)(dppb)(py)(phen)](PF_6)_2$ (**22**) by displacement of the acetate ligand, isolated in 79 and 80% yield, respectively (eqn. 14 and 15).

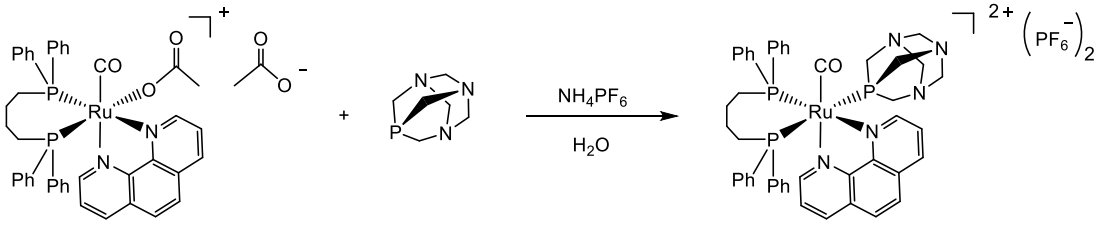

5 **21**

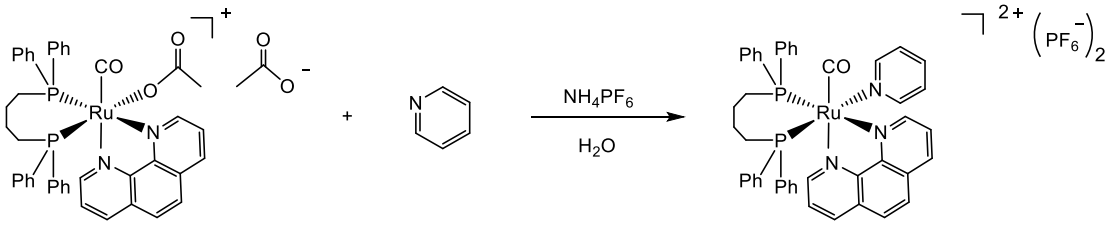

5 **22**

The $^{31}P\{^{1}H\}$ NMR spectrum of **21** in CD_2Cl_2 displays the typical pattern of a phosphorus T system with a triplet at δ 28.9 ppm ($^{2}J_{PP}$ = 24.3 Hz) for the P *trans* to phenanthroline N atom, a doublet of doublets at δ 17.7 ppm ($^{2}J_{PP}$ = 217.6 Hz, $^{2}J_{PP}$ = 25.8 Hz) for the dppb P atom

trans to PTA, and a doublet of doublets at *δ* -65.9 ppm ($^2J_{PP}$ = 217.6 Hz, $^2J_{PP}$ = 23.0) for the PTA. In addition the septuplet at *δ* -144.6 ppm corresponds to the PF_6^- counterion ($^1J_{PF}$ = 711.8 Hz) (**Figure 25**).

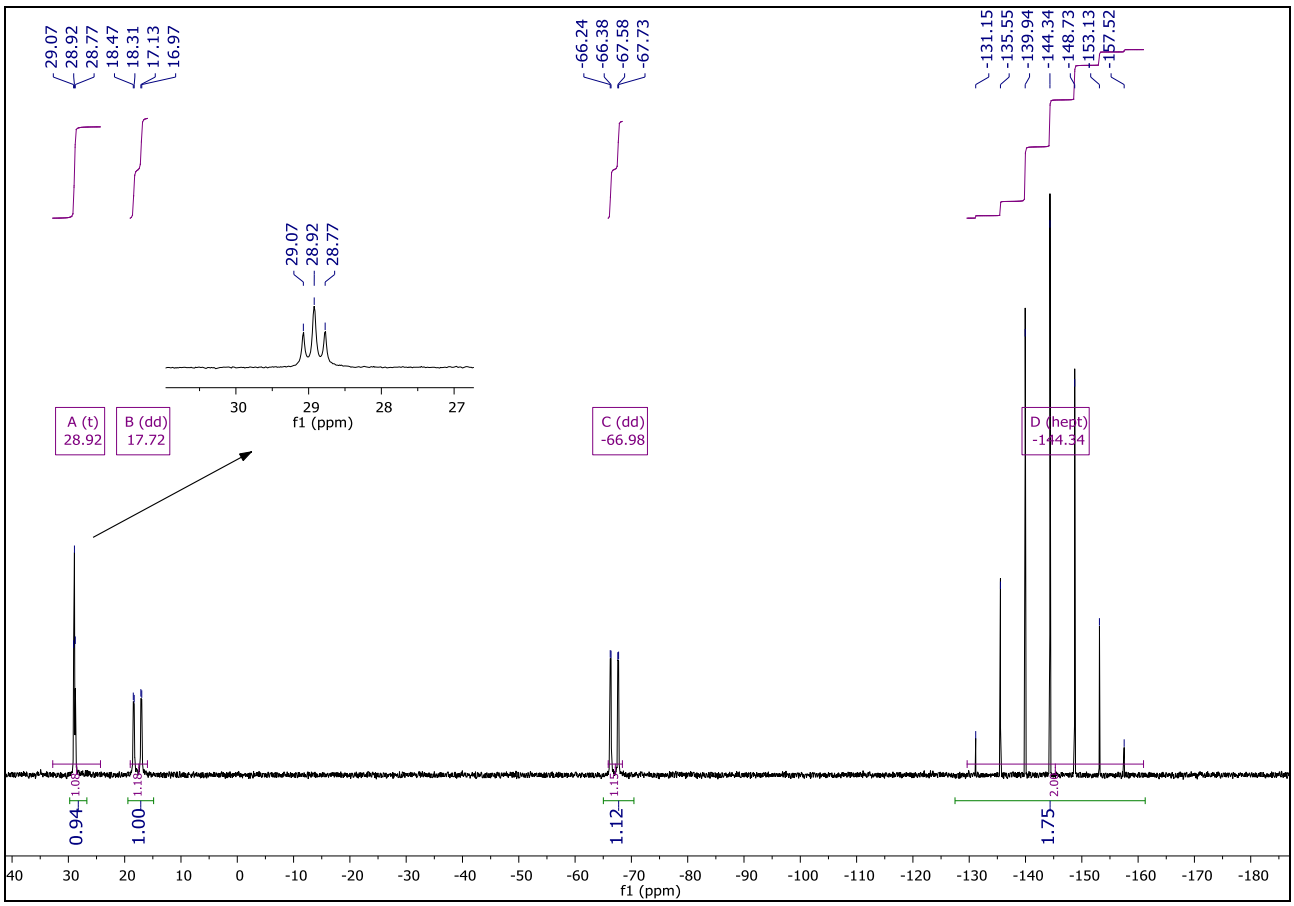

Figure 25. $^{31}P\{^1H\}$ NMR spectrum of **21** in CD_2Cl_2.

The ^1H NMR spectrum shows second order AB q systems with resonances at *δ* 4.12 and 3.94 ppm (J_{AB} = 13.0 Hz, 6H) for the PTA NCH_2N protons, and at 3.28 and 3.19 ppm (J_{AB} = 15.0 Hz, 6H) for the PTA NCH_2P protons. No signal is present in the region between *δ* 2.00 and 1.00 ppm, indicating complete displacement of the coordinated OAc and substitution of the counterion with PF_6^-. In $^{13}C\{^1H\}$ NMR spectrum, the CO signal appears as a quartet at *δ* 202.0 ($^2J_{CP}$ = 12.4 Hz), while the PTA carbon atoms appear at *δ* 71.8 ($^3J_{CP}$ = 6.8 Hz) and 49.7 ppm ($^1J_{CP}$ = 9.3 Hz).

The $^{31}P\{^1H\}$ NMR spectrum of complex **22** in CD_3OD shows two doublets at *δ* 29.0 and 28.8 ppm ($^2J_{PP}$ = 25.3 Hz) for both P atoms, which are *trans* to phen and py N atoms. The septuplet at *δ* -144.6 ppm is for the PF_6^- counterion ($^1J_{PF}$ = 711.8 Hz). Finally, the $^{13}C\{^1H\}$ NMR spectrum, displays the CO triplet at *δ* 203.6 ($^2J_{CP}$ = 15.3 Hz).

Surprisingly, complexes **21** and **22** show poor solubility in water, while are soluble in alcohols, chlorinated solvents, acetone and dmso.

4 BIOLOGICAL ASSAYS

In this study, the in vitro antiproliferative activity of the described ruthenium(II) complexes was firstly evaluated on two anaplastic thyroid cancer cell lines, namely SW1736 and 8505C. Anaplastic thyroid cancer (ATC) is a rare histotype of thyroid tumor characterized by a dramatic poor prognosis[76]. It is the most aggressive thyroid cancer and it is accountable for up to 40% of deaths due to thyroid cancer[77]. ATC is typically diagnosed with local invasion and metastasis and the complete loss of differentiation makes ATC unresponsive to radioiodine treatment[78]. Unfortunately, due to ATC infiltration beyond the thyroid capsule and its invasion of adjacent vital organs, surgical local resection can be performed only in a subset of ATC cases[79]. Nowadays, no effective treatments are available for ATC patients, in fact the use of doxorubicin and cisplatin shows no relevant effects in terms of patients' survival rate[76, 78]. For these reasons, the development of new compounds showing anticancer activity is still challenging in ATC treatment.

Secondly, only the most interesting and promising ruthenium complexes were tested against human colon carcinoma HCT-116 cell line, which is by far the most common malignancy of the gastrointestinal tract and the third most ordinarily diagnosed cancer in males and the second in females[80-81]. Colon carcinoma demonstrate malignant potential only after invasion of the submucosa, where lymphatic vessels are located. An estimated 92% of colon cancer patients undergo surgical resection as the primary modality of treatment. Unfortunately, due to its invasive outcome, surgical resection is not decisive in late-stage colon carcinoma patients and chemotherapy is necessary.

In preliminary cell viability screening, 72-h treatments are commonly carried out wherein cisplatin is used as a reference drug, due to its slow ligand-substitution kinetics. In fact, after 24-h of treatment, cisplatin does not reach its EC_{50} against several cancer cell lines.

The solutions of all compounds were freshly prepared. In particular, all the complexes were tested via dissolution in sterile dmso, followed by dilution with cell culture medium at the defined concentration. Cisplatin was instead dissolved in physiological saline solution to avoid the formation of the less cytotoxic species *cis*-$[PtCl(NH_3)_2(dmso)]+$.[82]

4.1 NEUTRAL RUTHENIUM COMPLEXES

In the first set of experiments, the anticancer effects of complexes **2**, **3** and **4** were evaluated in two human anaplastic thyroid cancer (ATC) cell lines, namely SW1736 and 8505C, and their results have been compared with cisplatin. In order to test the effects of the above mentioned complexes on the cell viability in ATC cell lines, an MTT assay was performed, after the administration of different doses of the compounds for 24, 48 and 72 h (**Figure 26**).

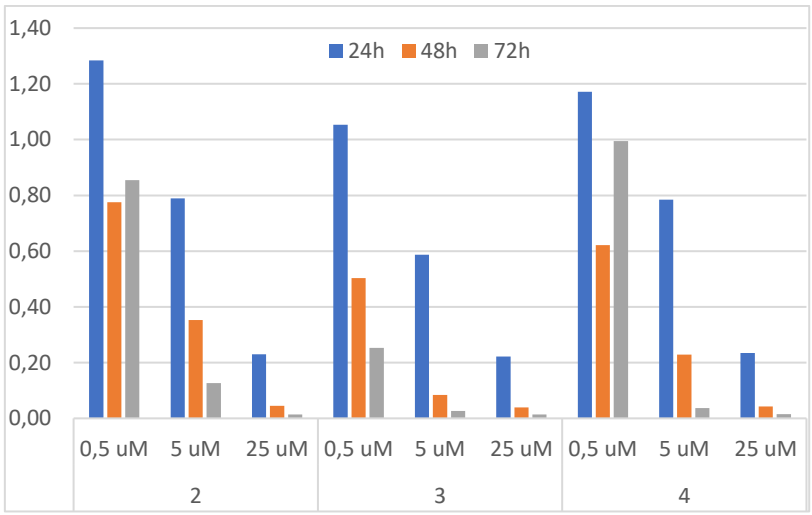

Figure 26. Effect of complexes **2-4** on ATC cell viability in SW1736 cells. Cell viability was evaluated by using the MTT assay and expressed as the percentage of control (dmso). Each point represents the mean value of three-fold determinations. *P < 0.05, **P < 0.01, ***P < 0.001, ****P < 0.0001 by the Student's t-test.

The three complexes demonstrated a moderate cell viability decrease after 72 h of treatment at 5 and 25 μM. The EC_{50} values (dose required to achieve 50% of the theoretical maximal effect) were calculated at 72 h, as reported in **Table 3**:

Table 3. EC_{50} (μM ± SD) of complexes **2-4** and cisplatin in ATC cells.

	EC_{50} of SW1736 cells[a] [μM] at 72 h	**EC_{50} of 8505C cells[a] [μM] at 72 h**
Complex		
2	3.52 ± 0.25	4.75 ± 0.32
3	4.95 ± 0.30	5.76 ± 0.71
4	7.46 ± 0.68	9.54 ± 0.53
Cisplatin	6.40 ± 1.54	5.20 ± 1.82

[a] *Each value represents the mean value of three-fold determinations.*

Complexes **2**-**4** showed EC_{50} values very close to those observed after cisplatin treatment, with any significant improvement in activity. Surprisingly, complex **2** is the most active compared to **3** and **4**, with a EC_{50} of 3.52 μM in SW1736 cell line. The trend of the MTT test suggests that the more the β-diketone ligand is functionalized, the less the complexes are active. In fact, although the purpose was to exploit the biological properties of curcumin, its association with ruthenium complexes results in a decrease of activity with respect to complexes **2** and **3**.

4.2 MONOCATIONIC RUTHENIUM COMPLEXES

4.2.1 The influence on the cell viability

After the substitution of β-diketone ligands with phenanthroline, the effectiveness of complexes **5**-**9**, **5a, 11**-**14** and **17** was evaluated in anaplastic thyroid cancer cell lines, and their results compared with cisplatin[63].

Table 4. EC_{50} (μM ± SD) of complexes **5-9, 5a, 11**-**14**, **17** and cisplatin in ATC cells.

	EC_{50} of SW1736 cells[a] [μM] at 72 h	**EC_{50} of 8505C cells[a] [μM] at 72 h**
Complex		
5	1.24 ± 0.16	2.40 ± 0.54
6	0.19 ± 0.04	0.10 ± 0.02
7	0.21 ± 0.06	0.09 ± 0.03
8	2.77 ± 0.25	2.80 ± 0.28
9	2.80 ± 0.45	2.84 ± 0.15
5a	20.40 ± 0.76	12.10 ± 0.73
11	8.00 ± 0.07	5.80 ± 0.10
12	9.34 ± 0.15	4.68 ± 0.05
13	1.28 ± 0.03	1.65 ± 0.02
14	12.10 ± 0.34	10.30 ± 0.25
17	1.85 ± 0.02	2.1 ± 0.03
Cisplatin	6.40 ± 1.54	5.20 ± 1.82

[a] *Each value represents the mean value of three-fold determinations.*

An MTT assay was performed on SW1736 and 8505C cell lines, after the administration of different doses of the compounds for 24, 48 and 72 h. Complexes **5-9**, **13** and **17** exhibited a strong cell viability decrease at different doses after 72 h of treatment, showing a good effectiveness even when compared with cisplatin administration. Based on these data, the EC_{50} values (dose required to achieve 50% of the theoretical maximal effect) were calculated at 72 h, as reported in **Table 4**.

Interestingly, compounds **5-7** showed an EC_{50} value markedly lower than that observed after cisplatin treatment, with a fold-change ranging from 2 to 58. The acetate **5**, isothiocyanate **8** and chloride **9** show rather similar EC_{50} values in the range 2.84–1.24 μM after 72 h for SW1736 and 8508C cells. Interestingly, pivalate **6** and thioacetate **7** derivatives, reduce the cell viability at significantly lower concentrations in the range of 0.21–0.09 μM, which is more than twenty times lower than that of cisplatin (6.40–5.20 μM). It is worth noting that complex **5a**, compared to its isomer **5**, exhibits a scarce cytotoxicity, confirming that the *facial* PPC geometry of the complexes is the most suitable for a better anticancer activity. The isonitrile derivative **17** displays an EC_{50} of 1.85 μM in SW1736 cell line, value very close to that of the corresponding carbonyl complex **5** (1.24 μM). This result is very encouraging for the future synthesis of ruthenium complexes bearing biological substrates functionalised with isonitrile group, in order to target cancer cells or biomolecules involved in cancer spreading.

Surprisingly, the functionalization of phenanthroline in complexes **11**, **12**, and **14** did not lead to an improvement in activity, with EC_{50} values up to 2 times higher than cisplatin, ranging from 4.68 to 12.10 μM. Only complex **13** demonstrated a good cytotoxic activity with 1.28 and 1.65 μM of EC_{50} in SW1736 and 8505C cell lines, respectively.

Table 5: EC_{50} (μM ± SD) of complexes **5-7**, **14**, **17** and cisplatin in HCT-116 cells.

	EC_{50} of HCT-116 cells[a] [μM] at 72 h
Complex	
5	0.81 ± 0.09
6	1.03 ± 0.06
7	1.20 ± 0.40
14	0.64 ± 0.01
17	0.80 ± 0.20
Cisplatin	15.96 ± 0.08

[a] Each value represents the mean value of three-fold determinations.

Complexes **5**, **6**, **7**, **14** and **17**, were further investigated against HCT-116 cancer cell line and the EC_{50} values, calculated at 72 h, are reported in **table 5**.

Also in HCT-116 cancer cell line, complexes **5**, **6** and **7** demonstrate high cytotoxic activity, reducing the cell viability at concentrations, which are more than 10 times lower than that measured for cisplatin. Contrary to the results obtained on SW1736 and 8505C cell lines, where the thioacetate derivative **7** was the most active with very low EC_{50} values (0.21-0.09 μM), on HCT-116 cell line, complex **7** demonstrates minor but good activity with 1.20 μM of EC_{50}. On the other hand, in HCT-116 cell line, acetate complex **5** displays the lowest EC_{50} value of 0.81 μM, with respect to pivalate **6** and thioacetate **7** derivatives.

Surprisingly, the pyrazinophenanthroline derivative **14** is more active on HCT-116 colon carcinoma cells than on the SW1736 ATC cell line, with 0.64 and 12.10 μM values of EC_{50}, respectively. Moreover, **14** demonstrated to be the most active cytotoxic agent among the tested complexes on HTC-116 cell line, reducing the cell viability at concentration twentyfive times lower than that of cisplatin.

On colon carcinoma cell line, the isonitrile complex **17** exhibits an EC_{50} of 0.80 μM, value, once again, very close to that of the corresponding carbonyl complex **5**, confirming that isonitrile ruthenium complexes are good precursors for the further functionalization of anticancer complexes.

4.2.2 The influence on cell apoptosis

To evaluate whether the cell viability decrease, observed after treatments, was due to apoptotic cell death, a western blot analysis of the cleaved-PARP protein levels was performed[63]. Considering the cell viability results, only carboxylate and thioacetate ruthenium complexes **5-7** which show the lowest EC_{50} values were tested. SW1736 and 8505C cells were treated with complexes **5-7** (each at its EC_{50} value) for 72 h and then the cleaved-PARP level increment was investigated, which is a well-recognized marker of apoptosis. All three tested complexes were able to induce a strong increment of the cleaved-PARP levels in both ATC cell lines. For SW1736 cells, the highest increase was observed with thioacetate complex **7** administration, whereas for 8505C cells carboxylate derivatives **5** and **6** showed the highest response (**figure 27**).

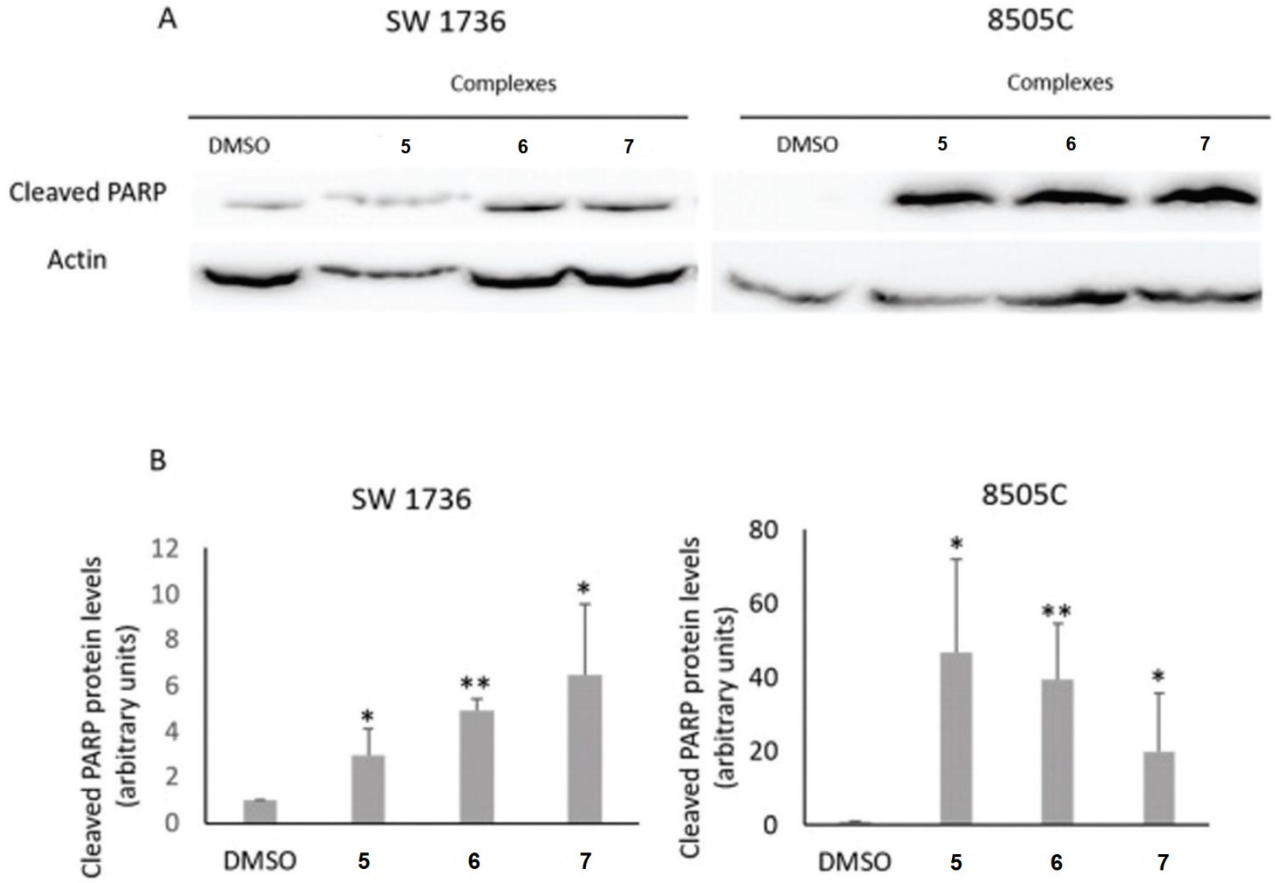

Figure 27. Panel A. SW1736 and 8505C cells were treated with dmso or the ruthenium(II) complexes **5**-**7** at the respective EC_{50} doses for 72 h. Cells were collected and cleaved-PARP or Actin protein levels were analysed by western blot. Panel B. Densitometric analysis of cleaved-PARP fraction levels determined using the western blot assay in ATC cells treated with **5**-**7** at the respective EC_{50} doses or vehicle (dmso) for 72 h. For each cell line, the results were normalized against Actin and expressed as the percentage of control. *P < 0.05, **P < 0.01, ***P < 0.001, ****P < 0.0001 by the Student's t-test.

In addition, the most active complexes **5** and **14** in HCT-116 colon carcinoma cell line, were evaluated in western blot assay of the full-length caspase-3 (pro-caspase). Caspase-3 is an aspartate-specific cysteine protease that belongs to the ICE subfamily of caspases. Caspase-3 exists as inactive proenzymes that undergo proteolytic processing to produce two subunits that during apoptosis dimerize to form the active enzyme. HCT-116 cells were grown to around 75% confluence, and treated with the complexes **5** and **14** at 0.75 μM and or dmso vehicle (0.1% v/v) as a control over 72 h. The western blot assay displays that complex **14** induces a decrease in levels of expression of the full-length caspase-3 to a greater extent compared to **5** and cisplatin (**Figure 28**).

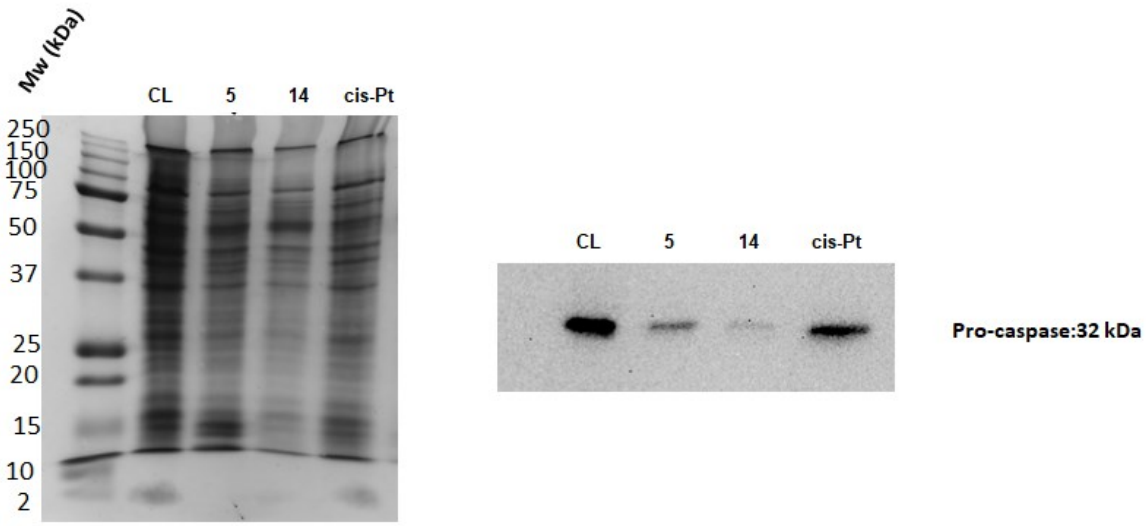

Figure 28. HCT-116 cells were treated with dmso (CL) or cisplatin or the ruthenium(II) complexes **5** and **14** at 0.75 μM for 72 h. Cells were collected and procaspase-3 levels were analysed by western blot.

4.2.3 The influence on tumor aggressiveness

After studying the effects of ruthenium complexes on the cell viability and apoptosis, the ability to modify an in vitro feature of aggressiveness of ATC cells was studied[63]. Thus, the influence of ruthenium compounds on the anchorage-independent growth ability of SW1736 and 8505C cells was evaluated by performing a soft agar colony formation assay. After 72 h of treatment with each EC_{50} dose, a strong significant reduction in the number of colonies was observed in both ATC cells with respect to those treated with dmso only (**Figure 29**).

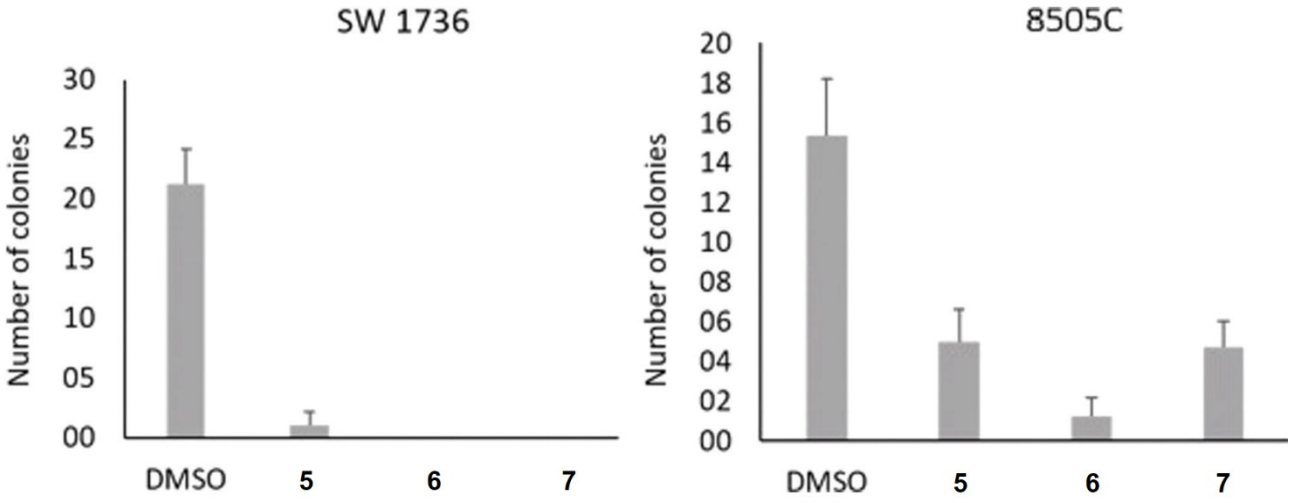

Figure 29. Aggressiveness was evaluated as the clonogenic ability of ATC cells by using the soft agar assay with complexes **5-7** and dmso. The histogram represents the number of colonies per cell line after treatments. For all treatments $P < 0.0001$ by the Student's t-test. All data are representative of three independent experiments.

Interestingly, treatment of SW1736 with derivatives **6** and **7** leads to a complete abrogation of the colony formation with respect to **5**, indicating that the pivalate **6** and the thioacetate **7** derivatives, which have also the lowest EC_{50} values, show the strongest antimetastatic activity. Conversely, for 8505C cells the pivalate **6** shows the highest effect, although no complete abrogation was observed. Therefore, these data indicate that the novel complexes exert effects not only on cell viability and survival, but also on the aggressiveness of cancer cells that escape cell death, suggesting a promising antimetastatic effect.

4.3 CHIRAL MONOCATIONIC RUTHENIUM COMPLEXES

4.3.1 The influence on the cell viability

The effectiveness of the couples of enantiomeric ruthenium complexes **18R/18S**, **19R/19S** and **20R/20S** was evaluated in anaplastic thyroid cancer cell lines (SW1736 and 8505C), and their results compared with cisplatin. In order to test the effects of the above mentioned complexes on the cell viability in ATC cell lines, an MTT assay was performed, after the administration of different doses of the complexes for 24, 48 and 72 h. The EC_{50} values were calculated at 72 h and reported in **Table 6**:

Table 6. EC_{50} (μM ± SD) of complexes **18R**/**18S, 19R**/**19S, 20R**/**20S** and cisplatin in ATC cells.

	EC_{50} of SW1736 cells[a] [μM] at 72 h	**EC_{50} of 8505C cells[a] [μM] at 72 h**
Complex		
18R	0.29 ± 0.03	1.35 ± 0.18
18S	1.98 ± 0.11	2.30 ± 0.26
19R	1.35 ± 0.04	0.35 ± 0.02
19S	2.25 ± 0.23	0.68 ± 0.10
20R	0.65 ± 0.12	0.04 ± 0.01
20S	1.28 ± 0.09	0.58 ± 0.05
Cisplatin	6.40 ± 1.54	5.20 ± 1.82

[a] *Each value represents the mean value of three-fold determinations.*

The influence of chirality on enantiomeric ruthenium complexes induced great differences in activity toward cancer cells and all complexes are considerably more active than cisplatin. As a matter of fact, all the (R,R) enantiomers reduce the cell viability at significantly lower concentrations than the corresponding (S,S) complexes. **18R** demonstrates to be almost 7 times more active than **18S**, exhibiting EC_{50} values of 0.29 and 1.98 μM in SW1736 cells, respectively. Surprisingly, complex **20R** reaches the lowest EC_{50} ever observed in this study, achieving 0.04 μM of EC_{50} in 8505C ATC cell line, value more than 14 times lower with respect to the corresponding enantiomer **20S** (0.58 μM). Contrary, the pivalate derivative **19R** did not exhibit great differences in activity compared to the respective enantiomer **19S**, displaying EC_{50} values of 0.35 and 0.68 μM in 8505C cell line, respectively.

The chiral complexes were further investigated against HCT-116 cancer cell line and the EC_{50} values were calculated at 72 h (**table 7**).

Table 7. EC_{50} (μM ± SD) of complexes **18R**/**18S**, **19R**/**19S**, **20R**/**20S** and cisplatin in HCT-116 cells.

	EC_{50} of HCT-116 cells[a] [μM] at 72 h
Complex	
18R	0.24 ± 0.05
18S	1.20 ± 0.10
19R	0.81 ± 0.08
19S	0.90 ± 0.10
20R	0.37 ± 0.09
20S	1.10 ± 0.30
Cisplatin	15.96 ± 0.08

[a] *Each value represents the mean value of three-fold determinations.*

It is worth highlighting that, also in this case, all compounds are more active than cisplatin. Among all, **18R** and **20R**, exhibiting EC_{50} of 0.24 and 0.37 μM, respectively, show about 50-times higher cytotoxicity compared to the reference drug. Interestingly, once again the (R,R) enantiomers display a most promising activity with **18R** and **20R** exhibiting 3-to-5 times lower EC_{50} values, compared to the (S,S) counterparts (1.20 and 1.10 μM, respectively).

4.3.2 The influence on cell apoptosis

To check whether cell death occurs via apoptosis also after treatment with **18R** and **20R**, Annexin V/Propidium Iodide (PI) assay was carried out. HCT-116 cells were treated at 0.5 μM with the selected complexes for 72 h. Then, cells were harvested and labeled with Annexin–V FITC and PI prior to flow cytometry, aimed at evaluating the percentage of apoptotic cells in suspension. Apoptotic cells at early stage (Q3) occur in the lower right quadrant, while apoptotic cells at late stage (Q2) set in the up-right part. The percentage in the lower left quadrant is due to viable cells (Q4), whereas the upper left part to non-apoptotic cell death (Q1) (**Figure 30**).

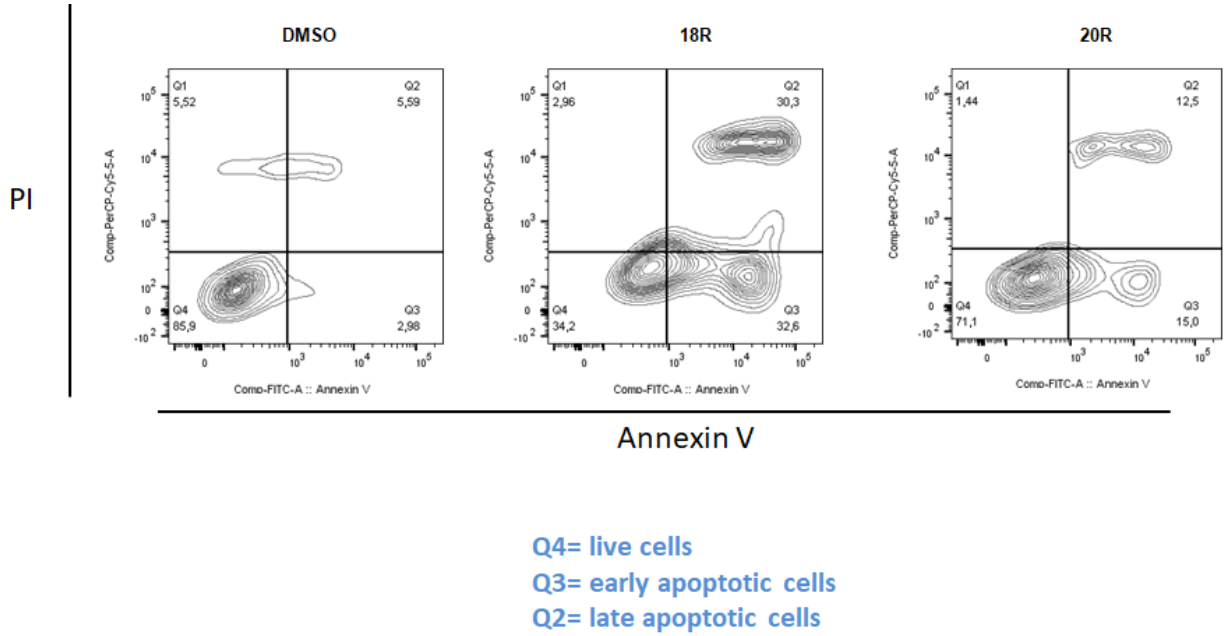

Figure 30. Flow cytofluorimetry assay of complexes **18R** and **20R**. Percentages of viable, apoptotic, and necrotic cells are reported in the corner of each quadrant.

Remarkably, the amount of cells undergoing non-apoptotic cell death was comparable for both treatments to the vehicle (dmso) control. Both complexes trigger apoptotic phenomena with similar percentages between the early-stage-apoptosis cell population and the late-stage one. The **18R**-treated sample is associated with the highest percentage of apoptotic cell death (total 62.9%), confirming its greater potency compared to **20R** (total 27.5% of cells undergoing apoptosis).

4.3.3 Cellular morphology and cell migration assay

Finally, changes in cell morphology after treatment with complexes **18R** and **20R** (72 hours at 0.5 μM) were investigated. Primarily, **18R** and **20R** decreased cell proliferation and in both cases cells changed shape exhibiting apoptotic bodies and cell debris. In addition, **18R** induced a clear cell disaggregation if compared to **20R** complex (**Figure 31**).

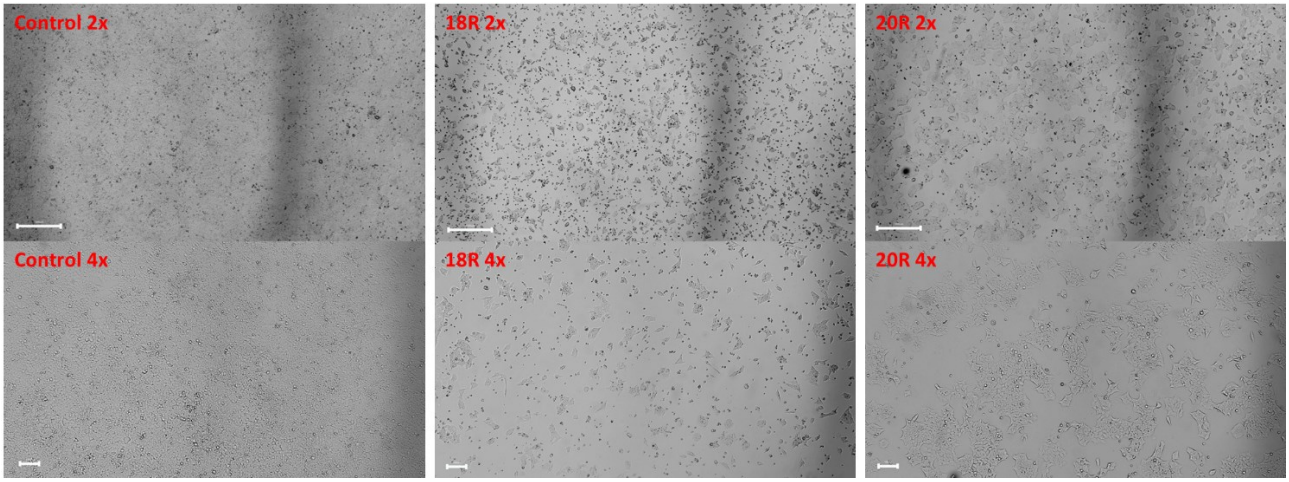

Figure 31. Images collected from Olympus IX70 inverted tissue culture microscope for the evaluation of cellular morphology changes after treatment with dmso (Control), **18R** and **20R**.

Concerning the cell migration assay[83-84], it is worth highlighting that cell migration and invasion are key phenomena in physiologic and pathologic processes, such as wound healing and cancer metastasis. In this work, cells were seeded in a Petri dish and allowed to attach, spread and form a confluent monolayer. A pin tool or needle is usually exploited to scratch and remove cells from a discrete area of the confluent monolayer so to form a cell-free zone.

We examined cell migration in response to the mechanical scratch wound, carried out after treatment (or without treatment for the control) with the model compound **18R**. Collected microscope images pointed out, after a 24-h treatment at 3 μM, a reduction of about 30% of the cell migration rate on the fifth day. In other words, the cells previously treated with the selected Ru(II)-based compound migrated at the edges of the wound to a lesser extent compared to the control (**Figure 32**).

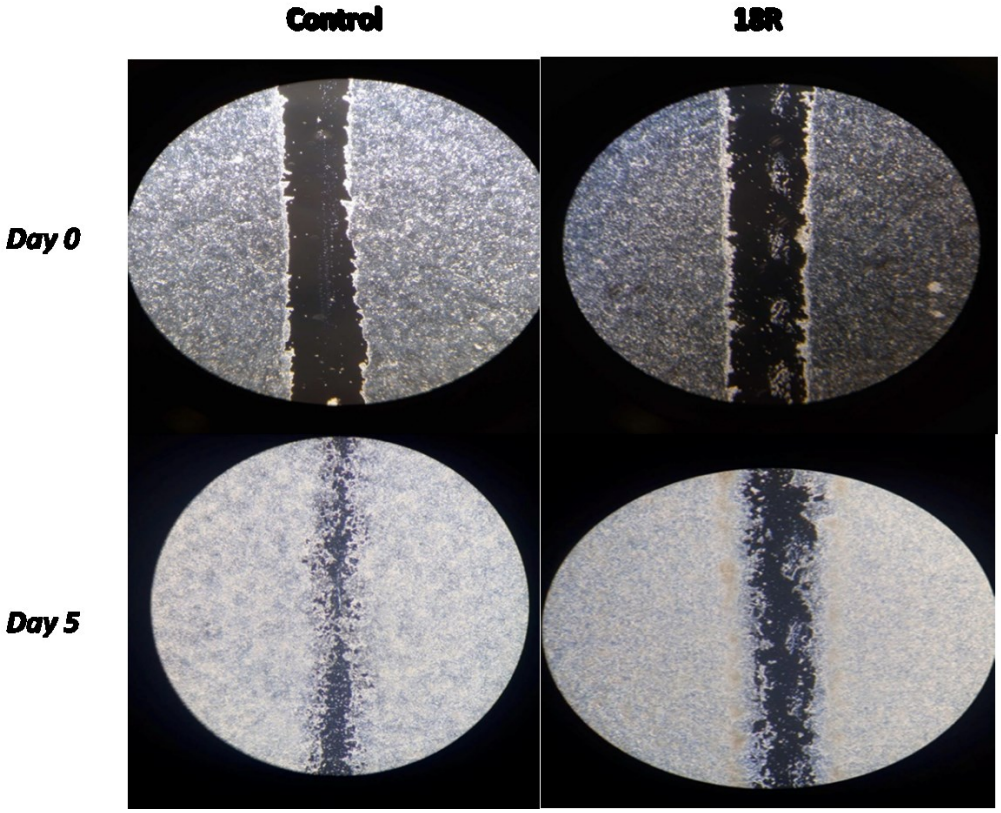

Figure 32. Microscope BIOLAB images of cell migration scratch assay concerning day 0 and day 5 after treatment with and without (Control) complex **18R**.

4.4 DICATIONIC RUTHENIUM COMPLEXES

Finally, the effectiveness of the dicationic ruthenium complexes **21** and **22** was evaluated against SW1736 and 8505C cancer cell lines. The effects of these complexes on the cell viability were evaluated by means of MTT assay after the administration of different doses of the compounds for 24, 48 and 72 h of treatment. The EC_{50} values were calculated at 72h and reposted in **table 8**:

Table 8. EC_{50} (μM ± SD) of complexes **21**, **22** and cisplatin in ATC cells.

	EC_{50} of SW1736 cells[a] [μM] at 72 h	**EC_{50} of 8505C cells[a] [μM] at 72 h**
Complex		
21	13.30 ± 0.12	12.00 ± 0.83
22	10.21 ± 0.90	12.60 ± 0.20
Cisplatin	6.40 ± 1.54	5.20 ± 1.82

[a] *Each value represents the mean value of three-fold determinations.*

Both tested complexes did not exhibit a considerable cell viability decrease if compared with cisplatin administration, displaying quite similar EC_{50} values ranging from 10.21 to 13.30 μM. Additionally, complex **21** was tested against HCT-116 cell lines, confirming its poor activity with a EC_{50} value higher than 15 μM. Probably, even though the dicationic charge would allow an easier uptake throw the negative cell membrane, it's more important that the position *trans* to dppb phosphorus is linked to anionic ligands which can be easily substituted via protonation.
Complexes **21** and **22** were not additionally investigated with cell apoptosis assays.

5 EXPERIMENTAL PART

5.1 GENERAL

All reactions were carried out under an argon atmosphere by using standard Schlenk techniques. The solvents were carefully dried by using standard methods. The precursor [Ru(η^1-OAc)(η^2-OAc)(CO)(dppb)] was prepared according to literature procedures[46], whereas dppb, phen and all other chemicals were purchased from Aldrich and Strem and used without further purification. NMR measurements were performed using a Bruker Advance III HD NMR 400 spectrometer and the chemical shifts, in ppm, are relative to TMS for ^1H and $^{13}C\{^1H\}$ NMR and 85% H_3PO_4 for $^{31}P\{^1H\}$ NMR. Elemental analyses (C, H, and N) were carried out with a Carlo Erba 1106 elemental analyzer, whereas IR analyses were performed with a Bruker Vector 22 FTIR spectrometer. The single crystals of complexes **1** and **4** were obtained by slow diffusion of diethyl ether into a concentrated solution of these species in dichloromethane.

Synthesis of [Ru(OAc)(acac)(CO)(dppb)] (2)
150 mg (0.22 mmol) of [Ru(η^1-OAc)(η^2-OAc)(CO)(dppb)] (**1**) and 27.9 ml of 2,4-pentandione (0.27 mmol) were dissolved in 1.5 ml of methanol and the mixture was stirred at 50 °C, overnight, under argon atmosphere. The solvent was evaporated under reduced pressure and the product was dissolved in 0.5 mL of dichloromethane. Addition of 5 mL of diethyl

ether afforded a colorless precipitate, which was filtered, washed with pentane (2 x 2 mL), diethyl ether (2 x 2 mL) and dried under reduced pressure. Yield: 66 mg (42%). Elemental analysis calcd (%) for $C_{36}H_{38}O_5P_2Ru$: C, 60.60; H, 5.37; found: C, 60.47; H, 4.96; ^{1}H NMR (400 MHz, $CDCl_3$, 298 K): δ 7.87 (t, $^3J_{HH}$ = 8.5 Hz, 2H; Ph), 7.76 (t, $^3J_{HH}$ = 8.1 Hz, 2H; Ph), 7.51-7.25 (m, 16H; Ph), 4.92 (s, 1H; CH), 2.98 (m, 1H; PCH_2), 2.76 (m, 1H; PCH_2), 2.58 (m, 1H; PCH_2), 2.36 (m, 1H; PCH_2), 2.00-1.70 (m, 4H; CH_2), 1.62 (s, 3H, CH_3), 1.56 (s, 3H; CH_3), 1.39 ppm (s, 3H; OCO*C*H_3). ^{13}C{^{1}H} NMR (100.6 MHz, $CDCl_3$, 298 K): δ 204.9 (t, $^2J_{CP}$ = 16.7 Hz; CO), 187.0 (s; O*C*OCH$_3$), 184.3 (s, CH*C*O), 176.6 (s, CH*C*O), 135.1-127.4 (m, Ph), 98.5 (s, CH), 30.7 (d, $^1J_{CP}$ = 31.3 Hz; PCH_2), 29.6 (d, $^1J_{CP}$ = 30.7 Hz; PCH_2), 27.2 (s; OCO*C*H_3), 27.1 (d, $^4J_{CP}$ = 5.5 Hz, CH_3), 24.5 (s; CH_2), 23.4 (d, $^4J_{CP}$ = 4.9 Hz; CH_3), 21.5 ppm (s, CH_2). ^{31}P{^{1}H} NMR (162.0 MHz, $CDCl_3$, 298 K): δ 43.2 (d, $^2J_{PP}$ = 29.5 Hz), 41.9 ppm (d, $^2J_{PP}$ = 29.5 Hz).

Synthesis of [Ru(OAc)(Odbm)(CO)(dppb)] (3)

[Ru(OAc)(Odbm)(CO)(dppb)] was prepared following the procedure described for **2**, starting from *cis*-[Ru(η^1-OAc)(η^2-OAc)(CO)(dppb)] (100.0 mg, 0.15 mmol) and dibenzoylmethane (33.3 mg, 0.15 mmol) in place of 2,4-pentandione, stirring the reaction mixture in MeOH (2 ml) overnight at 60°C. Yield: 79.2 mg (63%). Elemental analysis calcd (%) for $C_{46}H_{42}O_5P_2Ru$: C, 65.94; H, 5.05; found: C, 64.99; H, 4.96; ^{1}H NMR (400 MHz, $CDCl_3$, 298 K): δ 7.91 (m, 2H; Ph), 7.84 (m, 2H; Ph), 7.59-6.99 (m, 26H; Ph), 6.32 (s, 1H, CH), 3.08 (m, 1H; PCH_2), 2.89 (m, 1H; PCH_2), 2.65 (m, 1H; PCH_2), 2.37 (m, 1H; PCH_2), 2.01 (m (overlapped with H_2O signal), 1H; CH_2), 1.79 (m, 2H; CH_2), 1.62 (s, 3H; $COCH_3$), 1.60 ppm (m, 1H; CH_2). ^{13}C{^{1}H} NMR (100.6 MHz, $CDCl_3$, 298 K): δ 205.0 (t, $^2J_{CP}$ = 17.1 Hz; CO), 181.9 (s; O*C*OCH$_3$), 179.3 (s; CH*C*O), 177.2 (s; CH*C*O), 140.0-127.1 (m; Ph), 92.8 (s, *C*HCO), 31.0 (d, $^1J_{CP}$ = 31.9 Hz; PCH_2), 30.0 (d, $^1J_{CP}$ = 31.2 Hz; PCH_2), 24.8 ppm (s; CH_2), 23.4 (d, $^4J_{CP}$ = 4.7 Hz; CO*C*H3), 21.3 ppm (s; CH_2). ^{31}P{^{1}H} NMR (162 MHz, $CDCl_3$, 298 K): δ 44.6 (d, $^2J_{PP}$ = 29.5 Hz), 40.9 ppm (d, $^2J_{PP}$ = 29.5 Hz).

Synthesis of [Ru(OAc)(Ocurc)(CO)(dppb)] (4)

[Ru(OAc)(Ocurc)(CO)(dppb)] was prepared following the procedure described for **3**, starting from *cis*-[Ru(η^1-OAc)(η^2-OAc)(CO)(dppb)] (**1**) (150.0 mg, 0.22 mmol) and curcumin (81.0 mg, 0.22 mmol) in place of 2,4-pentandione. Yield: 114.5 mg (53%). Elemental analysis calcd (%) for $C_{52}H_{50}O_9P_2Ru$: C, 63.60; H, 5.13; found: C, 63.71; H, 5.26; ^{1}H NMR (400 MHz,

$CDCl_3$, 298 K): δ 7.99 (t, $^3J_{HH}$ = 8.7 Hz, 2H; Ph), 7.85 (t, $^3J_{HH}$ = 9.5 Hz, 2H; Ph), 7.67 (t, $^3J_{HH}$ = 8.4 Hz, 2H; Ph), 7.53-6.74 (m, 22H; Ph and CH=CH), 6.27 (d, $^3J_{HH}$ = 4.8 Hz, 1H, CH=CH), 5.97 (d, $^3J_{HH}$ = 15.6 Hz, 1H, CH=CH), 5.26 (s, 1H; CH), 3.97 (s, 3H, OCH_3), 3.87 (s, 3H, OCH_3), 3.13 (m, 1H; PCH_2), 2.89 (m, 1H; PCH_2), 2.72 (m, 1H; PCH_2), 2.29 (m, 1H; PCH_2), 2.16-1.68 (m, 4H; CH_2), 1.78 ppm (s, 3H, $OCOCH_3$). $^{13}C\{^1H\}$ NMR (100.6 MHz, $CDCl_3$, 298 K): δ 204.8 (br m; CO), 179.2 (s; CH*C*O), 178.0 (s; *C*OCH_3), 175.7 (s; CH*C*O), 148.2-122.1 (m; Ph), 115.1 (s; CH=CH), 114.6 (s; CH=CH), 109.9 (s; CH=CH), 108.8 (s; CH=CH), 102.6 (s, CO*C*HCO), 55.9 (s; OCH_3), 31.1 (d, $^1J_{CP}$ = 31.0 Hz; PCH_2), 30.2 (d, $^1J_{CP}$ = 31.7 Hz; PCH_2), 25.3 (s; CH_2), 23.6 (d, $^4J_{CP}$ = 3.8 Hz; OCO*C*H_3), 20.8 ppm (s; CH_2). $^{31}P\{^1H\}$ NMR (162 MHz, $CDCl_3$, 298 K): δ 44.7 (d, $^2J_{PP}$ = 31.0 Hz), 41.1 ppm (d, $^2J_{PP}$ = 31.0 Hz).

Synthesis of *fac PPC*-[Ru(OAc)(CO)(dppb)(phen)]OAc (5)

[Ru(η^1-OAc)(η^2-OAc)(dppb)(CO)] (50.0 mg, 0.074 mmol) and 1,10-phenanthroline (14.0 mg, 0.074 mmol) were dissolved in 1.5 mL of methanol and the mixture was stirred at 60 °C overnight. The solvent was evaporated under reduced pressure and the product was dissolved in 0.5 mL of dichloromethane. Addition of 5 mL of diethyl ether afforded a yellow precipitate, which was filtered and dried under reduced pressure. Yield: 52 mg (83%). Elemental analysis calcd (%) for $C_{45}H_{42}N_2O_5P_2Ru$: C 63.30, H 4.96, N 3.28; found: C 63.15, H 4.83, N 3.18. ^1H NMR (400.1 MHz, CD_2Cl_2, 298 K): δ = 9.47 (br t, $^3J_{HH}$ = 3.6 Hz, 1H; phen), 8.73 (m, 2H; phen), 8.33 (d, $^3J_{HH}$ = 8.1 Hz, 1H; phen), 8.18 (t, $^3J_{HH}$ = 8.7 Hz, 2H; phen), 8.01 (d, $^3J_{HH}$ = 8.8 Hz, 1H; phen), 7.87 (d, $^3J_{HH}$ = 8.8 Hz, 1H; phen), 7.71 (dd, $^3J_{HH}$ = 8.1, $^3J_{HH}$ = 5.3 Hz, 1H; aromatic proton), 7.67-7.55 (m, 4H; Ph), 7.53-7.42 (m, 6H; Ph), 7.40-7.30 (m, 4H; Ph), 6.82 (t, $^3J_{HH}$ = 7.2 Hz, 1H; Ph), 6.57 (t, $^3J_{HH}$ = 6.7 Hz, 2H; Ph), 6.25 (t, $^3J_{HH}$ = 8.7 Hz, 2H; Ph), 3.24 (m, 1H; PCH_2), 3.06 (m, 1H; PCH_2), 2.80 (m, 1H; PCH_2), 2.67 (m, 1H; PCH_2), 2.17 (m, 2H; CH_2), 1.98 (br m, 2H; CH_2), 1.86 (s, 3H; CH_3), 1.63 (m, 1H; CH_2), 1.44 ppm (s, 3H; CH_3). $^{13}C\{^1H\}$ NMR (100.6 MHz, CD_2Cl_2, 298 K): δ = 204.3 (dd, $^2J_{CP}$ = 16.6 Hz, $^2J_{CP}$ = 14.1 Hz; CO), 176.6 (s; *C*OCH_3), 176.0 (s; *C*OCH_3), 155.5-124.4 (m; aromatic carbon atoms), 30.2 (d, $^1J_{CP}$ = 28.0 Hz; P*C*H_2), 27.7 (d, $^1J_{CP}$ = 28.0 Hz; P*C*H_2), 24.6 (s; CH_2), 24.5 (s; CO*C*H_3), 23.2 (d, $^4J_{CP}$ = 4.3 Hz; CO*C*H_3), 21.8 ppm (d, $^2J_{CP}$ = 3.4 Hz; CH_2). $^{31}P\{^1H\}$ NMR (162.0 MHz, CD_2Cl_2, 298 K): δ = 32.4 (d, $^2J_{PP}$ = 22.8 Hz), 29.1 ppm (d, $^2J_{PP}$ = 22.8 Hz). ^1H NMR (400.1 MHz, CD_3OD, 298 K): δ = 9.55 (ddd, $^3J_{HH}$ = 4.7 Hz, $^3J_{HH}$ = 3.1 Hz, $^4J_{HH}$ = 1.2 Hz, 1H; phen), 8.83 (d, $^3J_{HH}$ = 5.3 Hz, 1H; phen), 8.75 (dd, $^3J_{HH}$ = 8.2 Hz, $^4J_{HH}$ = 1.0 Hz, 1H; phen), 8.50 (dd, $^3J_{HH}$ = 8.3 Hz, $^4J_{HH}$ =1.2 Hz, 1H; phen), 8.19 (td, $^3J_{HH}$ = 8.5 Hz, $^4J_{HH}$ = 1.2

Hz, 2H; phen), 8.04 (d, $^{3}J_{HH}$ = 8.8 Hz, 1H; phen), 7.97 (d, $^{3}J_{HH}$ = 8.8 Hz, 1H; phen), 7.77-7.69 (m, 2H; Ph), 7.68-7.62 (m, 3H; Ph), 7.61-7.49 (m, 4H; Ph), 7.47-7.41 (m, 6H; Ph), 6.75 (td, $^{3}J_{HH}$ = 7.4 Hz, $^{4}J_{HH}$ = 1.4 Hz, 1H; Ph), 6.49 (td, $^{3}J_{HH}$ = 8.2 Hz, $^{4}J_{HH}$ = 2.0 Hz, 2H; Ph), 6.22 (t, $^{3}J_{HH}$ = 8.9 Hz, 2H; Ph), 3.29-3.13 (m, 2H; PCH_2), 2.93-2.67 (m, 2H; PCH_2), 2.30-2.13 (m, 2H; CH_2), 2.10-1.94 (m, 1H; CH_2), 1.91 (s, 3H; CH_3), 1.77-1.57 (m, 1H; CH_2), 1.42 ppm (s, 3H; CH_3). IR (Nujol): $\tilde{\nu}$ = 1976 (s) (C≡O), 1608 (s), 1560 (s) (C=O) cm^{-1}.

Synthesis of [Ru(η^{1}-OPiv)(CO)(dppb)(phen)]OPiv (6)

[Ru(η^{1}-OAc)(CO)(dppb)(phen)]OAc (**5**) (50.0 mg, 0.059 mmol) was dissolved in 2 mL of degassed methanol and NaOPiv (76.0 mg, 0.586 mmol, 10 equiv.) was added to the solution. The reaction mixture was stirred for 48 h at 60 °C. The solvent was evaporated, 1 mL of water was added and the product extracted with dichloromethane (1 mL). Addition of diethyl ether (2 mL) to the organic fraction afforded the precipitation of the product as a pale yellow solid that was filtered and washed with diethyl ether (3 x 2 mL), and finally dried under reduced pressure. Yield: 44 mg (79%). Elemental analysis calcd (%) for $C_{51}H_{54}N_2O_5P_2Ru$: C 65.24, H 5.78, N 2.95; found: C 65.12, H 5.55, N 2.81. ^{1}H NMR (400.1 MHz, CD_2Cl_2, 298 K): δ = 9.28 (t, $^{3}J_{HH}$ = 3.9 Hz, 1H; phen), 8.75 (d, $^{3}J_{HH}$ = 8.1 Hz, 1H; phen), 8.60 (d, $^{3}J_{HH}$ = 4.8 Hz, 1H; phen), 8.33 (d, $^{3}J_{HH}$ = 8.1 Hz, 1H; phen), 8.15-8.00 (m, 3H; phen), 7.89 (d, $^{3}J_{HH}$ = 8.8 Hz, 1H; phen), 7.80-7.38 (m, 11H; Ph), 7.36-7.22 (m, 4H; Ph), 6.91 (t, $^{3}J_{HH}$ = 7.3 Hz, 1H; Ph), 6.69 (t, $^{3}J_{HH}$ = 7.0 Hz, 2H; Ph), 6.47 (t, $^{3}J_{HH}$ = 8.8 Hz, 2H; Ph), 3.18 (m, 2H; CH_2), 2.91-2.68 (m, 2H; CH_2), 2.25-2.05 (m, 2H, CH_2), 2.00-1.81 (m, 1H, CH_2), 1.80-1.63 (m, 1H; CH_2), 1.14 (s, 9H; CH_3), 0.31 ppm (s, 9H; CH_3). ^{13}C{^{1}H} NMR (100.6 MHz, CD_2Cl_2, 298 K): δ = 204.4 (t, $^{2}J_{CP}$ = 15.0 Hz; CO), 182.9 (s; *C*OC(CH_3)$_3$), 172.4 (s; *C*OC(CH_3)$_3$), 155.2-124.2 (m; aromatic carbon atoms), 39.0 (s; *C*CH_3), 30.4 (d, $^{1}J_{CP}$ = 27.3 Hz; P*C*H_2), 27.4 (d, $^{1}J_{CP}$ = 27.9 Hz; P*C*H_2), 26.6 (s; CO*C*H_3), 24.7 (s; *C*H_2), 21.6 ppm (s; CH_2). ^{31}P{^{1}H} NMR (162.0 MHz, CD_2Cl_2, 298 K): δ = 32.4 (d, $^{2}J_{PP}$ = 21.5 Hz), 29.1 ppm (d, $^{2}J_{PP}$ = 21.5 Hz). IR (Nujol): $\tilde{\nu}$ = 1976 (s) (C≡O), 1600 (s), 1552 (s) (C=O) cm^{-1}.

Synthesis of [Ru(η^{1}-SAc)(CO)(dppb)(phen)]SAc (7)

[Ru(η^{1}-SAc)(CO)(dppb)(phen)]SAc (**7**) was prepared following the procedure described for **6**, starting from **5** (50.0 mg, 0.059 mmol) and KSAc (67.4 mg, 0.590 mmol, 10 equiv.) in place of NaOPiv, stirring the reaction mixture in MeOH overnight at 60 °C. Yield: 42 mg (80%). Elemental analysis calcd (%) for $C_{45}H_{42}N_2O_3S_2P_2Ru$: C 61.01, H 4.78, N 3.16; found:

C 60.88, H 4.69, N 3.02. ^{1}H NMR (400.1 MHz, CD_2Cl_2, 298 K): δ = 9.38 (t, $^{3}J_{HH}$ = 4.0 Hz, 1H; phen), 8.66 (d, $^{3}J_{HH}$ = 7.8 Hz, 1H; phen), 8.25 (d, $^{3}J_{HH}$ = 7.8 Hz, 1H; phen), 8.17 (br d, $^{3}J_{HH}$ = 4.0 Hz, 1H; phen), 8.00 (d, $^{3}J_{HH}$ = 8.8 Hz, 1H; phen), 7.99-7.91 (m, 4H; aromatic protons), 7.86 (d, $^{3}J_{HH}$ = 8.8 Hz, 1H; phen), 7.75-7.60 (m, 4H; aromatic protons), 7.56-7.42 (m, 5H; Ph), 7.24 (t, $^{3}J_{HH}$ = 6.8 Hz, 1H; Ph), 7.14 (t, $^{3}J_{HH}$ = 7.1 Hz, 1H; Ph), 7.04 (t, $^{3}J_{HH}$ = 7.6 Hz, 2H; Ph), 6.93 (t, $^{3}J_{HH}$ = 6.8 Hz, 2H; Ph), 6.83 (br t, $^{3}J_{HH}$ = 3.8 Hz, 1H; Ph), 6.68 (t, $^{3}J_{HH}$ = 8.5 Hz, 2H; Ph), 3.12 (m, 1H; CH_2), 3.05-2.70 (m, 5H; CH_2), 2.11-1.80 (m, 1H; CH_2), 2.02 (s, 3H; CH_3), 1.97 (s, 3H; CH_3), 1.72 ppm (br m, 1H; CH_2). ^{13}C{^{1}H} NMR (100.6 MHz, CD_2Cl_2, 298 K): δ = 204.2 (dd, $^{2}J_{CP}$ = 17.1 Hz, $^{2}J_{CP}$ = 12.1 Hz; CO), 202.5 (s; S*C*OCH_3), 173.9 (s; S*C*OCH_3), 154.9-124.4 (m; aromatic carbon atoms), 33.40 (d, $^{4}J_{CP}$ = 3.7 Hz; SCO*C*H_3), 31.4 (d, $^{1}J_{CP}$ = 29.6 Hz; P*C*H_2), 29.6 (d, $^{1}J_{CP}$ = 25.6 Hz; P*C*H_2), 25.1 (s; CH_2), 21.5 (s; SCO*C*H_3), 20.8 ppm (d, $^{2}J_{CP}$ = 2.5 Hz; CH_2). ^{31}P{^{1}H} NMR (162.0 MHz, CD_2Cl_2, 298 K): δ = 32.3 (d, $^{2}J_{PP}$ = 21.5 Hz), 21.3 ppm (d, $^{2}J_{PP}$ = 21.5 Hz). IR (Nujol): $\tilde{\nu}$ = 1975 (s) (C≡O), 1600 (s) (C=O) cm^{-1}.

Synthesis of [Ru(NCS)(CO)(dppb)(phen)]SCN (8)

Complex [Ru(NCS)(CO)(dppb)(phen)]SCN (**8**) was prepared following the same procedure described for compound **7** starting from **5** (50.0 mg, 0.059 mmol) and KSCN (56.3 mg, 0.590 mmol, 10 equiv.). The reaction mixture was stirred in MeOH overnight at 60 °C, affording the product as a pale yellow solid, which was filtered, washed with cold methanol (2 x 2 mL) and diethyl ether (2 x 2 mL), and finally dried under reduced pressure. Yield: 40 mg (80%) as a mixture of two isomers: ruthenium isothiocyanate (Ru-NCS; major isomer) and ruthenium thiocyanate (Ru-SCN; minor isomer). Elemental analysis calcd (%) for $C_{43}H_{36}N_4OS_2P_2Ru$: C 60.62, H 4.26, N 6.58; found: C 60.47, H 4.14, N 6.49. ^{1}H NMR (400.1 MHz, $CDCl_3$, 298 K): δ = 9.33 (d, $^{3}J_{HH}$ = 5.1 Hz, 1H; phen minor isomer), 9.22 (d, $^{3}J_{HH}$ = 4.7 Hz, 1H; phen major isomer), 9.16 (d, $^{3}J_{HH}$ = 4.7 Hz, 1H; phen major isomer), 8.68 (d, $^{3}J_{HH}$ = 8.3 Hz, 1H; phen minor isomer), 8.62 (d, $^{3}J_{HH}$ = 8.0 Hz, 1H; phen major isomer), 8.38 (dd, $^{3}J_{HH}$ = 8.2 Hz, $^{4}J_{HH}$ = 1.0 Hz, 1H; phen major isomer), 8.29 (d, $^{3}J_{HH}$ = 8.1 Hz, 1H; phen minor isomer), 8.24 (dd, $^{3}J_{HH}$ = 8.4 Hz, $^{4}J_{HH}$ = 5.6 Hz, 1H; phen minor isomer), 8.12-8.00 (m, 3H; aromatic protons major isomer), 7.96 (d, $^{3}J_{HH}$ = 8.4 Hz, 1H; phen minor isomer), 7.94 (d, $^{3}J_{HH}$ = 8.8 Hz, 1H; phen major isomer), 7.85 (d, $^{3}J_{HH}$ = 8.4 Hz, 1H; phen minor isomer), 7.80 (d, $^{3}J_{HH}$ = 8.8 Hz, 1H; phen major isomer), 7.78-7.71 (m, 2H; aromatic protons), 7,62 (t, $^{3}J_{HH}$ = 9.0 Hz, 1H; aromatic proton major isomer), 7.58-7.43 (m, 10H; Ph), 6.66 (t, $^{3}J_{HH}$ = 7.7 Hz,

1H; Ph minor isomer), 6.58 (t, $^{3}J_{HH}$ = 7.2 Hz, 1H; Ph major isomer), 6.41 (t, $^{3}J_{HH}$ = 7.6 Hz, 2H; Ph minor isomer), 6.35 (t, $^{3}J_{HH}$ = 7.2 Hz, 2H; Ph major isomer), 6.09 (t, $^{3}J_{HH}$ = 8.6 Hz, 2H; Ph), 3.61-3.50 (m, 1H; CH_2), 3.37 (br t, J_{HH} = 12.5 Hz, 1H; CH_2 major isomer), 3.07 (br q, J_{HH} = 12.6 Hz, 1H; CH_2 major isomer), 2.56 (br t, J_{HH} = 15.0 Hz, 1H; CH_2 major isomer), 2.44-2.00 (m, 3H; CH_2), 1.39 (m, 1H; CH_2 major isomer), 1.27 (m, 1H; CH_2 minor isomer), 0.88 ppm (m, 1H; CH_2 minor isomer). $^{31}P\{^{1}H\}$ NMR (162.0 MHz, $CDCl_3$, 298 K): δ = 30.9 (d, $^{2}J_{PP}$ = 21.9 Hz, major isomer), 30.2 (br s, major isomer), 29.7 (d, $^{2}J_{PP}$ = 21.8 Hz, minor isomer), 28.6 ppm (d, $^{2}J_{PP}$ = 21.8 Hz, minor isomer). ^{1}H NMR (400.1 MHz, CD_2Cl_2, 298 K): δ = 9.21 (d, $^{3}J_{HH}$ = 5.3 Hz, 1H; phen), 8.91 (d, $^{3}J_{HH}$ = 5.3 Hz, 1H; phen), 8.69 (dd, $^{3}J_{HH}$ = 8.2 Hz, $^{4}J_{HH}$ = 1.0 Hz, 1H; phen), 8.44 (dd, $^{3}J_{HH}$ = 8.2 Hz, $^{4}J_{HH}$ = 1.0 Hz, 1H; phen), 8.06-7.96 (m, 3H; aromatic protons), 7.93-7.84 (m, 2H; aromatic protons), 7.80-7.71 (m, 3H; aromatic protons), 7.61 (t, $^{3}J_{HH}$ = 6.9 Hz, 1H; aromatic proton), 7.58-7.39 (m, 10H; Ph), 6.76 (t, $^{3}J_{HH}$ = 5.2 Hz, 1H; Ph), 6.50 (t, $^{3}J_{HH}$ = 7.5 Hz, 2H; Ph), 6.15 (t, 2H; $^{3}J_{HH}$ = 8.4 Hz; Ph), 3.40 (m, 1H; CH_2), 3.16-2.95 (m, 2H; CH_2), 2.60 (br t, J_{HH} = 15.9 Hz, 1H; CH_2), 2.29-2.00 (m, 3H; CH_2), 1.49 ppm (m, 1H; CH_2). $^{13}C\{^{1}H\}$ NMR (100.6 MHz, CD_2Cl_2, 298 K): δ = 201.9 (t, $^{2}J_{CP}$ = 14.7 Hz; CO), 155.5 (s; *C*H=N phen), 152.4 (s; *C*H=N phen), 146.5 (s; *ipso*-phen), 145.3 (s; *ipso*-phen), 140.0 (s; Ph), 139.6 (br s; N*C*S), 138.3 (s; Ph), 133.7-125.8 (m; aromatic carbon atoms), 29.3 (d, $^{1}J_{CP}$ = 27.1 Hz; P*C*H_2), 26.5 (d, $^{1}J_{CP}$ = 29.6 Hz; P*C*H_2), 24.4 (s; CH_2), 21.9 ppm (s; CH_2). $^{31}P\{^{1}H\}$ NMR (162.0 MHz, CD_2Cl_2, 298 K): δ = 30.6 ppm (s). IR (Nujol): $\tilde{\nu}$ = 2042 (s) (C=N), 1989 (s) (C≡O) cm^{-1}.

Synthesis of [Ru(Cl)(CO)(dppb)(phen)]PF_6 (9)

[Ru(η^{1}-OAc)(CO)(dppb)(phen)]OAc (**5**) (50.0 mg, 0.059 mmol) was dissolved in 2 mL of degassed methanol and NaCl (34.5 mg, 0.590 mmol, 10 equiv.) was added to the solution. The reaction mixture was stirred overnight at 60 °C. NH_4PF_6 (57.7 mg, 0.354 mmol) was added and the resulting solution was cooled to 0 °C in order to precipitate the product as a yellow solid, which was filtered and washed with cold water (2 x 2 ml), diethyl ether (2 x 2 ml) and finally dried under reduced pressure. Yield: 48 mg (89%). Elemental analysis calcd (%) for $C_{41}H_{36}N_2OClF_6P_3Ru$: C 53.75, H 3.96, N 3.06; found: C 53.33, H 3.51, N 2.86. ^{1}H NMR (400.1 MHz, dmso-d_6, 298 K): δ = 9.42 (br t, $^{3}J_{HH}$ = 4.0 Hz, 1H; phen), 9.06 (d, $^{3}J_{HH}$ = 4.6 Hz, 1H; phen), 8.90 (d, $^{3}J_{HH}$ = 8.0 Hz, 1H; phen), 8.65 (d, $^{3}J_{HH}$ = 8.0 Hz, 1H; phen), 8.19 (t, $^{3}J_{HH}$ = 9.0 Hz, 2H: phen), 8.14 (d, $^{3}J_{HH}$ = 9.0 Hz, 1H; phen), 8.05 (d, $^{3}J_{HH}$ = 8.9 Hz, 1H; phen), 7.92-7.78 (m, 4H; Ph), 7.74 (br t, $^{3}J_{HH}$ = 8.7 Hz, 1H; Ph), 7.65-7.53 (m, 4H; Ph), 7.50-

7.38 (m, 6H; Ph), 6.59 (t, $^3J_{HH}$ = 7.6 Hz, 1H; Ph), 6.29 (t, $^3J_{HH}$ = 7.0 Hz, 2H; Ph), 5.85 (t, $^3J_{HH}$ = 8.7 Hz, 2H; Ph), 3.33 (m (overlapped with H_2O signal), 1H; PCH_2), 3.07 (m, 2H; PCH_2), 2.65 (m, 1H; PCH_2), 2.16 (m, 1H; CH_2), 1.95 (m, 2H; CH_2) 1.41 ppm (br m, 1H; CH_2). $^{13}C\{^1H\}$ NMR (100.6 MHz, dmso-d_6, 298 K): δ = 203.6 (dd, $^2J_{CP}$ = 16.1 Hz, $^2J_{CP}$ = 12.5 Hz; CO), 155.4-125.1 (m; aromatic carbon atoms), 26.9 (d, $^1J_{CP}$ = 26.4 Hz; P*C*H_2), 25.7 (d, $^1J_{CP}$ = 25.7 Hz; P*C*H_2), 24.6 (s; *C*H_2), 21.4 ppm (d, $^2J_{CP}$ = 4.5 Hz; CH_2). $^{31}P\{^1H\}$ NMR (162.0 MHz, dmso-d_6, 298 K): δ = 32.7 (br s), 29.7 ppm (d, $^2J_{PP}$ = 20.5 Hz), -144.2 (sept, $^1J_{PF}$ = 711.7 Hz). IR (Nujol): $\tilde{\nu}$ = 1992 (s) (C≡O) cm^{-1}.

Synthesis of [Ru(OAc)(dppb)(phen)]OAc (10)

[Ru(η^2-OAc)$_2$(dppb)] (50.0 mg, 0.077 mmol) and 1,10-phenanthroline (14.0 mg, 0.077 mmol) were dissolved in 1.5 mL of methanol and the mixture was stirred at 60 °C overnight. The solvent was evaporated under reduced pressure and the product was dissolved in 0.5 mL of dichloromethane. Addition of 5 mL of diethyl ether afforded a yellow precipitate, which was filtered and dried under reduced pressure. Yield: 56 mg (88%). Elemental analysis calcd (%) for $C_{44}H_{42}N_2O_4P_2Ru$: C 63.99, H 5.13, N 3.39; found: C 63.59, H 4.80, N 3.27. ^1H NMR (400.1 MHz, CD_2Cl_2, 298 K): δ = 8.97 (ddd, $^3J_{HH}$ = 5.1 Hz, $^4J_{HH}$ = 2.3 Hz, $^6J_{HH}$ = 1.3 Hz, 1H; phen), 8.46-8.39 (m, 2H; phen), 8.37 (dd, $^3J_{HH}$ = 8.2 Hz, $^4J_{HH}$ = 1.3 Hz, 1H; phen), 8.00-7.85 (m, 6H; aromatic protons), 7.78 (ddd, $^3J_{HH}$ = 8.0 Hz, $^4J_{HH}$ = 5.2 Hz, $^6J_{HH}$ = 0.7 Hz, 1H; phen), 7.73-7.58 (m, 4H; aromatic protons), 7.50 (td, $^3J_{HH}$ = 7.7 Hz, $^4J_{HH}$ = 1.8 Hz, 2H; Ph), 7.45-7.24 (m, 6H; Ph), 6.59 (tq, $^3J_{HH}$ = 7.4 Hz, $^4J_{HH}$ = 1.1 Hz, 1H; Ph), 6.27 (td, $^3J_{HH}$ = 8.3 Hz, $^4J_{HH}$ = 2.2 Hz, 2H; Ph), 5.58 (t, $^3J_{HH}$ = 8.5 Hz, 2H; Ph), 3.23 (m, 1H; PCH_2), 2.67 (m, 1H; PCH_2), 2.41 (m, 2H; PCH_2), 2.20 (m, 2H; CH_2), 1.97 (m, 1H; CH_2), 1.87 (s, 3H; CH_3), 1.66 (m, 1H; CH_2), 1.17 ppm (s, 3H; CH_3). $^{13}C\{^1H\}$ NMR (100.6 MHz, CD_2Cl_2, 298 K): δ = 189.1 (s; *C*OCH_3), 176.4 (s; *C*OCH_3), 159.7-124.1 (m; aromatic carbon atoms), 29.2 (d, $^1J_{CP}$ = 26.7 Hz; P*C*H_2), 26.9 (d, $^1J_{CP}$ = 28.1 Hz; P*C*H_2), 25.0 (s; CH_2), 24.3 (s; CO*C*H_3), 23.7 (s; CO*C*H_3), 22.5 ppm (s; CH_2). $^{31}P\{^1H\}$ NMR (162.0 MHz, CD_2Cl_2, 298 K): δ = 48.9 (d, $^2J_{PP}$ = 33.6 Hz), 47.8 ppm (d, $^2J_{PP}$ = 33.6 Hz). IR (Nujol): $\tilde{\nu}$ = 1976 (s) (C≡O), 1608 (s), 1561 (s) (C=O) cm^{-1}.

Synthesis of *mer PPC*-[Ru(OAc)(CO)(dppb)(phen)]OAc (5a)

[Ru(η^2-OAc)(dppb)(phen)]OAc (50.0 mg, 0.060 mmol) was dissolved in 1.5 mL of methanol and the mixture was stirred at room temperature under CO atmosphere (1 atm) for 5 minutes. The solution was concentrated and the addition of 5 mL of diethyl ether afforded a

yellow precipitate, which was filtered and dried under reduced pressure. Yield: 48 mg (94%). Elemental analysis calcd (%) for $C_{45}H_{42}N_2O_5P_2Ru$: C 63.30, H 4.96, N 3.28; found: C 63.15, H 4.76, N 3.11. ^{1}H NMR (400.1 MHz, CD_3OD, 298 K): δ = 8.82 (d, $^3J_{HH}$ = 5.1 Hz, 1H; phen), 8.70 (d, $^3J_{HH}$ = 7.5 Hz, 2H; phen), 8.57 (d, $^3J_{HH}$ = 8.2 Hz, 1H; phen), 8.10 (t, $^3J_{HH}$ = 8.8 Hz, 2H; Ph), 8.03 (d, $^3J_{HH}$ = 8.9 Hz, 1H; phen), 7.98 (d, $^3J_{HH}$ = 8.9 Hz, 1H; phen), 7.89 (td, $^3J_{HH}$ = 7.2 Hz, $^4J_{HH}$ = 1.8 Hz, 3H; phen), 7.76 (dd, $^3J_{HH}$ = 8.2 Hz, $^4J_{HH}$ = 5.4 Hz, 1H; phen), 7.68-7.37 (m, 13H; aromatic protons), 6.67 (td, $^3J_{HH}$ = 7.5 Hz, $^4J_{HH}$ = 1.0 Hz, 1H; Ph), 5.75 (t, $^3J_{HH}$ = 8.1 Hz, 2H; Ph), 3.20 (m, 2H; PCH_2), 2.71 (m, 1H; PCH_2), 2.47 (m, 2H; CH_2), 2.23-2.03 (m, 2H; CH_2), 1.91 (s, 3H; CH_3), 1.78 (s, 3H; CH_3), 1.70-1.56 ppm (m, 1H; CH_2). ^{13}C{^{1}H} NMR (100.6 MHz, CD_3OD, 298 K): δ = 197.4 (d, $^2J_{CP}$ = 15.5 Hz; CO), 184.0 (s; *C*OCH_3), 178.5 (s; *C*OCH_3), 158.4-124.6 (m; aromatic carbon atoms), 26.9 (d, $^1J_{CP}$ = 24.8 Hz; P*C*H_2), 25.0 (d, $^1J_{CP}$ = 21.1 Hz; P*C*H_2), 24.2 (s; CH_2), 22.6 (s; CO*C*H_3), 22.0 (s; CO*C*H_3), 21.5 ppm (s; CH_2). ^{31}P{^{1}H} NMR (162.0 MHz, CD_3OD, 298 K): δ = 44.6 (d, $^2J_{PP}$ = 29.0 Hz), 2.9 ppm (d, $^2J_{PP}$ = 29.0 Hz).^{1}H NMR (400.1 MHz, CD_2Cl_2, 298 K): δ = 9.13 (ddd, $^3J_{HH}$ = 4.7 Hz, $^4J_{HH}$ = 3.0 Hz, $^6J_{HH}$ = 1.3 Hz, 1H; phen), 8.55 (dd, $^3J_{HH}$ = 8.2 Hz, $^4J_{HH}$ = 1.4 Hz, 1H; phen), 8.34 (d, $^3J_{HH}$ = 7.9 Hz, 1H; phen), 8.24 (d, $^3J_{HH}$ = 5.2 Hz, 1H; phen), 8.03-7.83 (m, 6H; aromatic protons), 7.58-7.24 (m, 18H; Ph), 2.79 (m, 1H; PCH_2), 2.54 (m, 1H; PCH_2), 2.00 (t, $^3J_{HH}$ = 7.7 Hz, 2H; PCH_2), 1.94 (s, 3H; CH_3), 1.41 (s, 3H; CH_3), 1.33 (m, 1H; CH_2), 1.19 (t, $^3J_{HH}$ = 7.0 Hz, 1H; CH_2), 0.92 ppm (t, $^3J_{HH}$ = 7.0 Hz, 1H; CH_2). ^{31}P{^{1}H} NMR (162.0 MHz, CD_2Cl_2, 298 K): δ = 37.3 (s), -16.4 ppm (s).

Synthesis of [Ru(OAc)(CO)(dppb)(IP)] (11)

[Ru(η^1-OAc)(η^2-OAc)(dppb)(CO)] (**1**) (50.0 mg, 0.074 mmol) and 1*H*-imidazo[4,5-*f*][1,10]phenanthroline (IP) (17.0 mg, 0.074 mmol) were dissolved in 1.5 mL of absolute ethanol and the mixture was stirred at 60 °C overnight. The solvent was evaporated under reduced pressure and the residue was dissolved in 0.5 mL of dichloromethane. Addition of 5 mL of diethyl ether afforded a yellow precipitate, which was filtered and dried under reduced pressure. Yield: 47 mg (75%). Elemental analysis calcd (%) for $C_{44}H_{38}N_4O_3P_2Ru$: C 63.38, H 4.59, N 6.72; found: C 63.20, H 4.33, N 6.58. ^{1}H NMR (400.1 MHz, CD_2Cl_2, 298 K): δ = 9.47 (d, $^3J_{HH}$ = 7.8 Hz, 1H; IP), 9.19 (br t, $^3J_{HH}$ = 4.1 Hz, 1H; IP), 8.98 (d, $^3J_{HH}$ = 8.3 Hz, 1H; IP), 8.48 (d, $^3J_{HH}$ = 4.7 Hz, 1H; IP), 8.33 (s, 1H; IP), 8.18 (t, $^3J_{HH}$ = 8.6 Hz, 2H; IP), 7.75-7.19 (m, 15H; Ph), 6.73 (t, $^3J_{HH}$ = 6.7 Hz, 1H; Ph), 6.49 (t, $^3J_{HH}$ = 6.4 Hz, 2H; Ph), 6.21 (t, $^3J_{HH}$ = 8.6 Hz, 2H; Ph), 3.12 (m (overlapped with H_2O signal), 1H; PCH_2), 2.98 (m, 1H;

PCH_2), 2.58 (m, 2H; PCH_2), 2.31-1.79 (m, 3H; CH_2), 1.57 (br m, 1H; CH_2), 1.45 ppm (s, 3H; CH_3). $^{13}C\{^1H\}$ NMR (100.6 MHz, CD_2Cl_2, 298 K): δ = 204.5 (dd, $^2J_{CP}$ = 16.3 Hz, $^2J_{CP}$ = 14.0 Hz; CO), 175.8 (d, $^3J_{CP}$ = 2.6 Hz; *C*OCH_3), 151.7-123.2 (m; aromatic carbon atoms, NCHN), 30.6 (d, $^1J_{CP}$ = 27.2 Hz; P*C*H_2), 28.7 (d, $^1J_{CP}$ = 28.9 Hz; P*C*H_2), 24.9 (s; CH_2), 23.3 (d, $^4J_{CP}$ = 4.4 Hz; CO*C*H_3), 22.1 ppm (d, $^2J_{CP}$ = 2.0 Hz; CH_2). $^{31}P\{^1H\}$ NMR (162.0 MHz, CD_2Cl_2, 298 K): δ = 33.6 (d, $^2J_{PP}$ = 23.0 Hz), 27.6 ppm (d, $^2J_{PP}$ = 23.0 Hz).

Synthesis of [Ru(OAc)(CO)(dppb)(TIP)] (12)

[Ru(OAc)(CO)(dppb)(TIP)] **(12)** was prepared as described for **11**, using 2-(thiophen-2-yl)-1*H*-imidazo[4,5-*f*][1,10]phenanthroline (TIP) (23.0 mg, 0.074 mmol) in place of 1*H*-imidazo[4,5-*f*][1,10]phenanthroline (IP). Yield: 48 mg (71%). Elemental analysis calcd (%) for $C_{48}H_{40}N_4O_3P_2RuS$: C 62.94, H 4.40, N 6.12; found: C 62.77, H 4.28, N 5.80. ^1H NMR (400.1 MHz, CD_3OD, 298 K): δ = 9.40 (t, $^3J_{HH}$ = 3.7 Hz, 1H; TIP), 9.16 (d, $^3J_{HH}$ = 8.1 Hz, 1H; TIP), 8.89 (d, $^3J_{HH}$ = 8.2 Hz, 1H; TIP), 8.76 (d, $^3J_{HH}$ = 4.9 Hz, 1H; TIP), 8.22 (t, $^3J_{HH}$ = 8.6 Hz, 2H; TIP), 7.92 (d, $^3J_{HH}$ = 2.9 Hz, 1H; TIP), 7.74-7.38 (m, 16H; aromatic protons), 7.22 (dd, $^3J_{HH}$ = 5.4 Hz, $^4J_{HH}$ = 3.5 Hz, 1H; TIP), 6.59 (t, $^3J_{HH}$ = 7.2 Hz, 1H; Ph), 6.40 (t, $^3J_{HH}$ = 7.3 Hz, 2H; Ph), 6.18 (t, $^3J_{HH}$ = 8.7 Hz, 2H; Ph), 3.26 (m, 1H; PCH_2), 3.13 (m, 1H; PCH_2), 2.84 (m, 1H; PCH_2), 2.68 (m, 1H; PCH_2), 2.21 (m, 2H; CH_2), 2.02 (br m, 1H; CH_2), 1.60 (br m, 1H; CH_2), 1.47 ppm (s, 3H; CH_3). $^{13}C\{^1H\}$ NMR (100.6 MHz, CD_3OD, 298 K): δ = 204.1 (dd, $^2J_{CP}$ = 16.2 Hz, $^2J_{CP}$ = 14.0 Hz; CO), 177.6 (d, $^3J_{CP}$ = 2.4 Hz; *C*OCH_3), 153.5-123.3 (m; aromatic carbon atoms, NCN, thiophene), 29.1 (d, $^1J_{CP}$ = 28.1 Hz; P*C*H_2), 26.8 (d, $^1J_{CP}$ = 29.3 Hz; P*C*H_2), 24.4 (s; CH_2), 22.4 (d, $^4J_{CP}$ = 4.0 Hz; CO*C*H_3), 21.6 ppm (d, $^2J_{CP}$ = 3.3 Hz; CH_2). $^{31}P\{^1H\}$ NMR (162.0 MHz, CD_3OD, 298 K): δ = 32.5 (d, $^2J_{PP}$ = 24.5 Hz), 28.6 ppm (d, $^2J_{PP}$ = 24.5 Hz).

Synthesis of [Ru(OAc)(CO)(dppb)(p-CF_3PIP)] (13)

[Ru(OAc)(CO)(dppb)(p-CF_3PIP)] **(13)** was prepared as described for **11**, using 2-(4-(trifluoromethyl)phenyl)-1*H*-imidazo[4,5-*f*][1,10]phenanthroline (p-CF_3PIP) (27.0 mg, 0.074 mmol) in place of 1*H*-imidazo[4,5-*f*][1,10]phenanthroline (IP). Yield: 67 mg (92%). Elemental analysis calcd (%) for $C_{51}H_{41}F_3N_4O_3P_2Ru$: C 62.64, H 4.23, N 5.73; found: C 62.46, H 4.13, N 5.61. ^1H NMR (400.1 MHz, CD_2Cl_2, 298 K): δ = 9.25 (d, $^3J_{HH}$ = 8.1 Hz, 1H; PIP), 9.07 (br t, $^3J_{HH}$ = 3.7 Hz, 1H; PIP), 8.88 (d, $^3J_{HH}$ = 8.1 Hz, 1H; PIP), 8.63 (d, $^3J_{HH}$ = 8.1 Hz, 2H; PIP), 8.41 (d, $^3J_{HH}$ = 4.8 Hz, 1H; PIP), 8.21 (t, $^3J_{HH}$ = 8.6 Hz, 2H; CF_3Ph), 7.77-7.29 (m, 17H;

aromatic protons), 6.72 (t, $^{3}J_{HH}$ = 7.3 Hz, 1H; Ph), 6.50 (td, $^{3}J_{HH}$ = 6.7 Hz, $^{4}J_{HH}$ = 2.0 Hz, 2H; Ph), 6.22 (t, $^{3}J_{HH}$ = 8.7 Hz, 2H; Ph), 3.13 (m, 1H; PCH_2), 2.93 (m, 1H; PCH_2), 2.47 (m, 2H; PCH_2), 2.34-1.78 (m, 3H; CH_2), 1.56 (br m, 1H; CH_2), 1.47 ppm (s, 3H; CH_3). $^{13}C\{^{1}H\}$ NMR (100.6 MHz, CD_2Cl_2, 298 K): δ = 204.7 (dd, $^{2}J_{CP}$ = 16.2 Hz, $^{2}J_{CP}$ = 14.0 Hz; CO), 175.7 (d, $^{3}J_{CP}$ = 2.7 Hz; *C*OCH_3), 150.3-122.4 (m; aromatic carbon atoms, NCN, CF_3), 30.6 (d, $^{1}J_{CP}$ = 27.1 Hz; P*C*H_2), 28.6 (d, $^{1}J_{CP}$ = 28.7 Hz; P*C*H_2), 24.9 (s; CH_2), 23.3 (d, $^{4}J_{CP}$ = 4.4 Hz; CO*C*H_3), 22.1 ppm (d, $^{2}J_{CP}$ = 2.3 Hz; CH_2). $^{31}P\{^{1}H\}$ NMR (162.0 MHz, CD_2Cl_2, 298 K): δ = 34.1 (d, $^{2}J_{PP}$ = 23.4 Hz), 27.3 ppm (d, $^{2}J_{PP}$ = 23.4 Hz).

Synthesis of [Ru(OAc)(CO)(dppb)(PzPhen)]OAc (14)

[Ru(η^{1}-OAc)(η^{2}-OAc)(dppb)(CO)] (50.0 mg, 0.074 mmol) and pyrazino[2,3-*f*][1,10]phenanthroline (PzPhen) (17.5 mg, 0.074 mmol) were dissolved in 1.5 mL of methanol and the mixture was stirred at 60 °C overnight. The solvent was evaporated under reduced pressure and the product was dissolved in 0.5 mL of dichloromethane. Addition of 5 mL of diethyl ether afforded a yellow precipitate, which was filtered and dried under reduced pressure. Yield: 60 mg (89%). Elemental analysis calcd (%) for $C_{47}H_{42}N_4O_5P_2Ru$: C 62.32, H 4.67, N 6.18; found: C 62.18, H 4.55, N 6.07. ^{1}H NMR (400.1 MHz, $CDCl_3$, 298 K): δ = 9.68 (br t, $^{3}J_{HH}$ = 3.3 Hz, 1H; PzPhen), 9.63 (d, $^{3}J_{HH}$ = 8.1 Hz, 1H; PzPhen), 9.41 (d, $^{3}J_{HH}$ = 8.0 Hz, 1H; PzPhen), 9.19-9.06 (m, 3H; PzPhen), 8.16 (m, 3H; Ph), 7.76 (dd, $^{3}J_{HH}$ = 8.1 Hz, $^{4}J_{HH}$ = 5.4 Hz, 1H; PzPhen), 7.66-7.35 (m, 13H; Ph), 6.44-6.20 (m, 5H; Ph), 3.47 (m, 1H; PCH_2), 3.29 (br t, 1H; PCH_2), 3.10 (m, 1H; PCH_2), 2.63 (br t, 1H; PCH_2), 2.37-2.04 (m, 3H; CH_2), 1.99 (s, 3H; CH_3), 1.54 (m, 1H; CH_2), 1.50 ppm (s, 3H; CH_3). $^{13}C\{^{1}H\}$ NMR (100.6 MHz, $CDCl_3$, 298 K): δ = 204.1 (t, $^{2}J_{CP}$ = 15.0 Hz; CO), 177.2 (s; *C*OCH_3), 176.5 (s; *C*OCH_3), 157.7-124.9 (m; aromatic carbon atoms), 28.6 (d, $^{1}J_{CP}$ = 26.9 Hz; P*C*H_2), 25.1 (d, $^{1}J_{CP}$ = 30.6 Hz; P*C*H_2), 25.1 (s; CO*C*H_3), 24.1 (s; CH_2), 23.9 (d, $^{4}J_{CP}$ = 3.6 Hz; CO*C*H_3), 21.7 ppm (d, $^{2}J_{CP}$ = 3.4 Hz; CH_2). $^{31}P\{^{1}H\}$ NMR (162.0 MHz, $CDCl_3$, 298 K): δ = 31.7 (d, $^{2}J_{PP}$ = 23.5 Hz), 29.6 ppm (d, $^{2}J_{PP}$ = 23.5 Hz). IR (Nujol): $\tilde{\nu}$ = 1976 (s) (C≡O), 1608 (s), 1562 (s) (C=O) cm^{-1}.

Synthesis of [Ru(η^{1}-OAc)(η^{2}-OAc)(CN-*t*-Bu)(PPh_3)$_2$] (15)

[Ru(OAc)$_2$(PPh_3)] (150.0 mg, 0.202 mmol) was suspended in methanol, *t*-butyl isocyanide (17.0 mg, 0.023 mL, 0.202 mmol) was added under argon atmosphere and stirred for 20 minutes. The orange suspension became white and the product was filtered off, washed with diethyl ether (3 X 2 mL) and dried under reduced pressure. Yield: 150 mg (90%).

Elemental analysis calcd (%) for $C_{45}H_{45}NO_4P_2Ru$: C 65.37, H 5.49, N 1.69; found: C 65.19, H 5.30, N 1.48. ^{1}H NMR (400.1 MHz, CD_2Cl_2, 298 K): δ = 7.56 (m, 10H; Ph), 7.41 (m, 20H; Ph), 0.78 (s, 6H; $OCOCH_3$), 0.75 ppm (s, 9H; *t*-Bu). $^{13}C\{^1H\}$ NMR (100.6 MHz, CD_2Cl_2, 298 K): δ = 180.9 (s; $COCH_3$), 161.1 (br s; $COCH_3$), 134.7 (s; Ph), 132.7 (t, $^2J_{CP}$ = 19.8 Hz; CN), 129.4 (s; Ph), 127.8 (s; Ph), 56.4 (s; $C(CH_3)_3$), 30.2 (s; $C(CH_3)_3$), 22.4 ppm (s; $COCH_3$). $^{31}P\{^1H\}$ NMR (162.0 MHz, CD_2Cl_2, 298 K): δ = 41.2 ppm (s).

Synthesis of [Ru(η^1-OAc)(η^2-OAc)(CN-*t*-Bu)(dppb)] (16)

Complex **15** (150.0 mg, 0.181 mmol) and 1,4-bis(diphenylphosphino)butane (dppb) (77.5 mg, 0.181 mmol) were dissolved in 1.5 mL of toluene and the mixture was stirred at 100 °C overnight. The solvent was concentrated under reduced pressure and addition of 5 mL of *n*-heptane afforded a white precipitate, which was filtered, washed with *n*-heptane (3 X 2 mL) and dried under reduced pressure. Yield: 110 mg (83%). Elemental analysis calcd (%) for $C_{37}H_{43}NO_4P_2Ru$: C 60.98, H 5.95, N 1.92; found: C 60.60, H 5.76, N 1.71. ^{1}H NMR (400.1 MHz, CD_2Cl_2, 298 K): δ = 7.77-7.34 (m, 20H; Ph), 2.78 (br m, 2H; PCH_2), 2.37 (br m, 2H; PCH_2), 1.78 (d, $^3J_{HH}$ = 17.8 Hz, 4H; CH_2), 1.46 (s, 6H; $OCOCH_3$), 1.32 ppm (s, 9H; *t*-Bu). $^{13}C\{^1H\}$ NMR (100.6 MHz, CD_2Cl_2, 298 K): δ = 158.5 (t, $^2J_{CP}$ = 18.0 Hz; CN), 133.9-127.1 (m; aromatic carbon atoms), 57.3 (s; $C(CH_3)_3$), 30.3 (s; $C(CH_3)_3$), 29.6 (d, $^1J_{CP}$ = 31.2 Hz; PCH_2), 24.2 (s; $COCH_3$), 23.2 ppm (s; CH_2). $^{31}P\{^1H\}$ NMR (162.0 MHz, CD_2Cl_2, 298 K): δ = 51.9 ppm (br s).

Synthesis of [Ru(OAc)(CN-*t*-Bu)(dppb)(phen)]OAc (17)

Complex **16** (50.0 mg, 0.069 mmol) and 1,10-phenanthroline (12.5 mg, 0.069 mmol) were dissolved in 1.5 mL of methanol and the mixture was stirred at 60 °C overnight. The solvent was evaporated under reduced pressure and the product was dissolved in 0.5 mL of dichloromethane. Addition of 5 mL of diethyl ether afforded a yellow precipitate, which was filtered and dried under reduced pressure. Yield: 50 mg (79%). Elemental analysis calcd (%) for $C_{49}H_{51}N_3O_4P_2Ru$: C 64.75, H 5.66, N 4.62; found: C 64.57, H 5.37, N 4.41. ^{1}H NMR (400.1 MHz, CD_2Cl_2, 298 K): δ = 9.29 (ddd, $^3J_{HH}$ = 4.7 Hz, $^4J_{HH}$ = 3.1 Hz, $^6J_{HH}$ = 1.2 Hz, 1H; phen), 8.60 (dd, $^3J_{HH}$ = 8.2, $^4J_{HH}$ = 1.1 Hz, 1H; phen), 8.53 (d, $^3J_{HH}$ = 4.5 Hz, 1H; phen), 8.21 (dd, $^3J_{HH}$ = 8.2 Hz, $^4J_{HH}$ = 1.3 Hz, 1H; phen), 8.19 (m, 2H; phen), 8.00 (d, $^3J_{HH}$ = 8.8 Hz, 1H; phen), 7.86 (d, $^3J_{HH}$ = 8.8 Hz, 1H; phen), 7.82 (m, 2H; Ph), 7.60 (td, $^3J_{HH}$ = 7.3 Hz, $^4J_{HH}$ = 1.3 Hz, 1H; Ph), 7.54-7.44 (m, 6H; Ph), 7.42-7.35 (m, 2H; Ph), 7.21 (t, $^3J_{HH}$ = 7.0 Hz, 2H; Ph),

7.13 (br t, 2H; Ph), 6.98 (t, $^{3}J_{HH}$ = 7.0 Hz, 1H; Ph), 6.76 (t, $^{3}J_{HH}$ = 7.1 Hz, 2H; Ph), 6.45 (t, $^{3}J_{HH}$ = 8.2 Hz, 2H; Ph), 3.02 (m, 2H; PCH_2), 2.64 (m, 1H; PCH_2), 2.37 (m, 1H; PCH_2), 2.21-190 (m, 2H; CH_2), 1.84 (s, 3H; CH_3), 1.82-1.53 (m, 2H; CH_2), 1.44 (s, 9H; CH_3), 1.40 ppm (s, 3H; CH_3). $^{13}C\{^{1}H\}$ NMR (100.6 MHz, CD_2Cl_2, 298 K): δ = 176.6 (s; *C*OCH_3), 176.4 (s; *C*OCH_3), 155.0 (s; *C*H=N phen), 154.8 (s; *C*H=N phen), 154.2 (t, $^{2}J_{CP}$ = 18.4 Hz; CN), 151.4-123.0 (m; aromatic carbon atoms), 58.5 (s; *C*$(CH_3)_3$), 31.2 (d, $^{1}J_{CP}$ = 27.2 Hz; P*C*H_2), 29.9 (s; C(*C*$H_3)_3$), 29.4 (d, $^{1}J_{CP}$ = 29.2 Hz; P*C*H_2), 25.4 (s; CH_2), 24.4 (s; CO*C*H_3), 24.3 (d, $^{4}J_{CP}$ = 4.6 Hz; CO*C*H_3), 21.8 ppm (s; CH_2). $^{31}P\{^{1}H\}$ NMR (162.0 MHz, CD_2Cl_2, 298 K): δ = 41.8 (d, $^{2}J_{PP}$ = 26.5 Hz), 29.9 ppm (d, $^{2}J_{PP}$ = 26.5 Hz).

Synthesis of [Ru(η^{1}-OAc)(CO)((R,R)-Skewphos)(phen)]OAc (18R)

Complex [Ru(η^{1}-OAc)(η^{2}-OAc)((R,R)-Skewphos)(CO)] (**1R**) (100.0 mg; 0.145 mmol) and 1,10-phenanthroline (20.8 mg; 0.115 mmol) were dissolved in methanol (1.5 mL) and the mixture was stirred at 60 °C overnight. The solvent was evaporated under reduced pressure and the product was dissolved in dichloromethane (0.5 mL). Addition of diethyl ether (5 mL) afforded a pale yellow precipitate, which was filtered off and dried under reduced pressure. Yield: 115 mg (91%). Elemental analysis (%) calc for $C_{46}H_{44}N_2O_5P_2Ru$: C 63.66, H 5.11, N 3.23; found: C 63.50, H 4.99, N 3.11. ^{1}H NMR (400.1 MHz, $CDCl_3$, 298 K): δ = 8.75 (t, $^{3}J_{HH}$ = 4.3 Hz, 1H; phen), 8.68 (d, $^{3}J_{HH}$ = 8.1 Hz, 1H; phen), 8.47 (d, $^{3}J_{HH}$ = 7.9 Hz, 1H; phen), 8.16 (d, $^{3}J_{HH}$ = 8.8 Hz, 1H; phen), 8.04 (d, $^{3}J_{HH}$ = 8.8 Hz, 1H; phen), 7.95-7.74 (m, 7H; Ph), 7.48 (m, 4H; Ph), 7.38 (m, 2H; aromatic protons), 7.28 (m, 1H; phen), 7.18 (m, 3H; Ph), 7.06 (m, 4H; aromatic protons), 6.79 (t, $^{3}J_{HH}$ = 8.6 Hz, 2H; Ph), 3.43 (br m, 1H; PCH), 2.91 (br m, 1H; PCH), 2.69 (m, 1H; CH_2), 2.35 – 2.08 (m, 1H; CH_2), 2.02 (s, 3H; $COCH_3$) 1.19 (s, 3H; $COCH_3$), 1.16 (dd, $^{3}J_{HP}$ = 15.1 Hz, $^{3}J_{HH}$ = 7.5 Hz, 3H; CH_3), 0.82 (dd, $^{3}J_{HP}$ = 13.0 Hz, $^{3}J_{HH}$ = 6.8 Hz, 3H; CH_3). $^{13}C\{^{1}H\}$ NMR (100.6 MHz, $CDCl_3$, 298 K): δ = 204.7 (dd, $^{2}J_{CP}$ = 20.0 Hz, $^{2}J_{CP}$ = 15.2 Hz; CO), 177.3 (d; $^{3}J_{CP}$ = 2.5 Hz *C*OCH_3), 177.2 (s; *C*OCH_3), 154.0-122.7 (m; aromatic carbon atoms), 37.2 (t, $^{2}J_{CP}$ = 4.1 Hz; *C*H_2), 32.8 (d, $^{1}J_{CP}$ = 30.4 Hz; P*C*H), 24.8 (s; CO*C*H_3), 23.6 (d, $^{4}J_{CP}$ = 4.3 Hz; CO*C*H_3), 22.9 (dd, $^{1}J_{CP}$ = 31.6, $^{3}J_{CP}$ = 2.3 Hz; P*C*H), 18.5 (d, $^{2}J_{CP}$ = 5.9 Hz; CH*C*H_3), 17.2 (d, $^{2}J_{CP}$ = 1.8 Hz; CH*C*H_3). $^{31}P\{^{1}H\}$ NMR (162 MHz, $CDCl_3$, 298 K): δ 42.9 (d, $^{2}J_{PP}$ = 32.2 Hz), 41.0 ppm (d, $^{2}J_{PP}$ = 32.2 Hz). IR (Nujol): $\tilde{\nu}$ = 1957 (s) (C≡O), 1602 (s), 1579 (s) (C=O) cm^{-1}.

Synthesis of [Ru(η^1-OAc)(CO)((S,S)-Skewphos)(phen)]OAc (18S)

Complex [Ru(η^1-OAc)(CO)((S,S)-Skewphos)(phen)]OAc **(18S)** was prepared following the procedure described for **18R**, starting from [Ru(η^1-OAc)(η^2-OAc)((S,S)-Skewphos)(CO)] (**1S**) in place of **1R**. Yield: 110 mg (87%). Elemental analysis (%) calc for $C_{46}H_{44}N_2O_5P_2Ru$: C 63.66, H 5.11, N 3.23; found: C 63.42, H 4.87, N 3.09.

Synthesis of [Ru(η^1-OPiv)(CO)((R,R)-Skewphos)(phen)]OPiv (19R)

Complex **18R** (50.0 mg, 0.058 mmol) was dissolved in degassed methanol (2 mL) and then NaOPiv (66.0 mg, 0.576 mmol, 10 equiv.) was added to the solution. The reaction mixture was stirred for 48 h at 60 °C. The solvent was evaporated, dichloromethane (2 mL) was added and then the excess of salt was filtered off. The resulting solution was concentrated and precipitated by the addition of diethylether (2 mL). The orange solid was filtered, washed with diethylether (2 x 2 mL) and dried under reduced pressure. Yield: 45 mg (82%). Elemental analysis (%) calc for $C_{52}H_{56}N_2O_5P_2Ru$: C 65.60, H 5.93, N 2.94; found: C 65.37, H 5.62, N 2.45. ^{1}H NMR (400.1 MHz, $CDCl_3$, 298 K): δ = 8.88 (dd, $^3J_{HH}$ = 8.2 Hz, $^4J_{HH}$ = 0.5 Hz, 1H; phen), 8.60 (t, $^3J_{HH}$ = 3.5 Hz, 1H; phen), 8.51 (dd, $^3J_{HH}$ = 8.2 Hz, $^4J_{HH}$ = 1.2 Hz, 1H; phen), 8.27 (d, $^3J_{HH}$ = 8.8 Hz, 1H; phen), 8.06 (d, $^3J_{HH}$ = 8.8 Hz, 1H; phen), 7.93-7.67 (m, 7H; Ph), 7.48-7.33 (m, 6H; aromatic protons), 7.31-7.18 (m, 3H; aromatic protons), 7.16-7.04 (m, 5H; Ph), 6.96 (t, $^3J_{HH}$ = 8.8 Hz, 2H; Ph), 3.48 (br m, 1H; PC*H*), 2.91 (m, 1H; PC*H*), 2.80 (m, 1H; CH_2), 2.41-2.17 (m, 1H; CH_2), 1.22 (s, 9H; $COC(CH_3)_3$), 1.20 (dd, $^3J_{HP}$ = 15.0 Hz, $^3J_{HH}$ = 7.4 Hz, 3H; CH_3), 0.89 (dd, $^3J_{HP}$ = 12.9 Hz, $^3J_{HH}$ = 6.8 Hz, 3H; CH_3), 0.05 ppm (s, 9H; $COC(CH_3)_3$). ^{13}C{^{1}H} NMR (100.6 MHz, $CDCl_3$, 298 K): δ = 204.7 (dd, $^2J_{CP}$ = 20.0 Hz, $^2J_{CP}$ = 15.2 Hz; CO), 184.0 (br s; *C*$OC(CH_3)_3$), 183.6 (s; *C*$OC(CH_3)_3$), 153.9-123.6 (m; aromatic carbon atoms), 65.9 (s; *C*$(CH_3)_3$), 37.3 (br s; *C*H_2), 32.7 (d, $^1J_{CP}$ = 30.3 Hz; P*C*H), 28.9 (br s; $COC(CH_3)_3$), 27.3 (s; $COC(CH_3)_3$), 23.1 (d, $^1J_{CP}$ = 31.2; P*C*H), 18.5 (d, $^2J_{CP}$ = 5.8 Hz; CH*C*H_3), 16.9 (s; CH*C*H_3). ^{31}P{^{1}H} NMR (162 MHz, $CDCl_3$, 298 K): δ 43.7 (d, $^2J_{PP}$ = 31.4 Hz), 41.5 ppm (d, $^2J_{PP}$ = 31.4 Hz). IR (Nujol): $\tilde{\nu}$ = 1965 (s) (C≡O), 1600 (s), 1556 (s) (C=O) cm^{-1}.

Synthesis of [Ru(η^1-OPiv)(CO)((S,S)-Skewphos)(phen)]OPiv (19S)

Complex [Ru(η^1-OPiv)(CO)((S,S)-Skewphos)(phen)]OPiv **(19S)** was prepared following the procedure described for **19R**, starting from **18S** in place of **18R**. Yield: 43 mg (78%).

Elemental analysis (%) calc for $C_{52}H_{56}N_2O_5P_2Ru$: C 65.60, H 5.93, N 2.94; found: C 65.22, H 5.56, N 2.68.

Synthesis of [Ru(η^1-SAc)(CO)((R,R)-Skewphos)(phen)]SAc (20R)

Complex **18R** (50.0 mg, 0.058 mmol) was dissolved in degassed methanol (2 mL) and KSAc (63.4 mg, 0.565 mmol, 10 equiv.) was added to the solution. The reaction mixture was stirred for 24 h at 60 °C. The solvent was evaporated, acetone (2 mL) was added and the excess of salt was filtered off. The resulting solution was concentrated and precipitated by the addition of pentane (2 mL), affording an orange solid which was filtered, washed with pentane (2 x 2 mL) and dried under reduced pressure. Yield: 40 mg (77%). Elemental analysis (%) calc for $C_{46}H_{44}N_2O_3P_2RuS_2$: C 61.39, H 4.93, N 3.11; found: C 61.23, H 4.73, N 2.89. ^{1}H NMR (400.1 MHz, $CDCl_3$, 298 K): δ = 8.63 (d, $^3J_{HH}$ = 8.0 Hz, 1H; phen), 8.56 (m, 2H; phen), 8.17 (s, 2H; phen), 7.93 (m, 3H; Ph), 7.81 (br m, 3H; Ph), 7.53 – 7.25 (m, 8H; aromatic protons), 7.15 (td, $^3J_{HH}$ = 7.9 Hz, $^4J_{HH}$ = 2.4 Hz, 2H; Ph), 7.07 (td, $^3J_{HH}$ = 7.9 Hz, $^4J_{HH}$ = 2.1 Hz, 2H; Ph), 6.97 (t, $^3J_{HH}$ = 8.5 Hz, 2H; Ph), 6.92 (d, $^3J_{HH}$ = 5.3 Hz, 1H; Ph), 6.62 (t, $^3J_{HH}$ = 8.4 Hz, 2H; Ph), 3.35 (br m, 1H; PCH), 3.07 (m, 1H; PCH), 2.63 (m, 1H; CH_2), 2.28 – 2.04 (m, 1H; CH_2), 2.09 (s, 3H; $COCH_3$) 1.90 (s, 3H; $COCH_3$), 1.09 (dd, $^3J_{HP}$ = 15.0 Hz, $^3J_{HH}$ = 7.4 Hz, 3H; CH_3), 0.80 (dd, $^3J_{HP}$ = 12.5 Hz, $^3J_{HH}$ = 6.9 Hz, 3H; CH_3). ^{13}C{^{1}H} NMR (100.6 MHz, $CDCl_3$, 298 K): δ = 205.5 (dd, $^2J_{CP}$ = 19.5 Hz, $^2J_{CP}$ = 12.2 Hz; CO), 204.1 (s; *C*OCH_3), 176.1 (s; *C*OCH_3), 152.9 - 121.8 (m; aromatic carbon atoms), 37.4 (br t; *C*H_2), 34.3 (d, $^1J_{CP}$ = 28.9 Hz; P*C*H), 33.4 (d, $^4J_{CP}$ = 2.8 Hz; CO*C*H_3), 23.3 (s; CO*C*H_3), 21.9 (d, $^1J_{CP}$ = 28.5; P*C*H), 18.8 (d, $^2J_{CP}$ = 6.1 Hz; CH*C*H_3), 17.6 (s; CH*C*H_3). ^{31}P{^{1}H} NMR (162 MHz, $CDCl_3$, 298 K): δ 41.1 (d, $^2J_{PP}$ = 29.6 Hz), 30.9 ppm (d, $^2J_{PP}$ = 29.6 Hz). IR (Nujol): $\tilde{\nu}$ = 1967 (s) (C≡O), 1620 (s), 1587 (s) (C=O) cm^{-1}.

Synthesis of [Ru(η^1-SAc)(CO)((S,S)-Skewphos)(phen)]SAc (20S)

Complex [Ru(η^1-SAc)(CO)((S,S)-Skewphos)(phen)]SAc **(20S)** was prepared following the procedure described for **20R**, starting from **18S** in place of **18R**. Yield: 38 mg (75%). Elemental analysis (%) calc for $C_{46}H_{44}N_2O_3P_2RuS_2$: C 61.39, H 4.93, N 3.11; found: C 61.21, H 4.78, N 2.96.

Synthesis of $[Ru(CO)(dppb)(PTA)(phen)](PF_6)_2$ (21)

Complex **5** (50.0 mg, 0.059 mmol) and 1,3,5-triaza-7-phosphaadamantane (PTA) (9.2 mg, 0.059 mmol) were dissolved in H_2O (2 mL) and stirred at 80 °C for one hour under argon atmosphere. The addition of NH_4PF_6 (95.4 mg, 0.586 mmol) immediately afforded a white precipitate, which was filtered, washed with water (2 x 2 mL) and dried under reduced pressure. Yield: 55 mg (79%). Elemental analysis calcd (%) for $C_{47}H_{48}F_{12}N_5OP_5Ru$: C 47.72, H 4.09, N 5.92; found: C 47.51, H 3.88, N 5.63. ^{1}H NMR (400.1 MHz, CD_2Cl_2, 298 K): δ = 9.47 (dtd, $^3J_{HH}$ = 4.1 Hz, $^4J_{HH}$ = 2.0 Hz, $^6J_{HH}$ = 0.8 Hz, 1H; phen), 8.92 (d, $^3J_{HH}$ = 5.2 Hz, 1H; phen), 8.89 (d, $^3J_{HH}$ = 8.3 Hz, 1H; phen), 8.50 (d, $^3J_{HH}$ = 8.3 Hz, 1H; phen), 8.18 (dd, $^3J_{HH}$ = 8.2 Hz, $^4J_{HH}$ = 5.4 Hz, 1H; phen), 8.14 (d, $^3J_{HH}$ = 8.9 Hz, 1H; phen), 8.07 (ddd, $^3J_{HH}$ = 8.2 Hz, $^4J_{HH}$ = 5.3 Hz, $^6J_{HH}$ = 0.6 Hz, 1H; phen), 7.95 (d, $^3J_{HH}$ = 8.9 Hz, 1H; phen), 7.93-7.82 (m, 3H; Ph), 7.74-7.49 (m, 8H; Ph), 7.41 (td, $^3J_{HH}$ = 7.9 Hz, $^4J_{HH}$ = 2.6 Hz, 2H; Ph), 7.24 (t, $^3J_{HH}$ = 8.8 Hz, 2H; Ph), 7.03 (td, $^3J_{HH}$ = 7.4 Hz, $^4J_{HH}$ = 1.3 Hz, 1H; Ph), 6.70 (td, $^3J_{HH}$ = 8.0 Hz, $^4J_{HH}$ = 2.5 Hz, 2H; Ph), 6.02 (t, $^3J_{HH}$ = 8.9 Hz, 2H; Ph), 4.12, 3.94 (AB q, J_{AB} = 13.0 Hz, 6H; NCH_2N (PTA)), 3.28, 3.19 (AB q, J_{AB} = 15.0 Hz, 6H; NCH_2P (PTA)), 3.15 (m, 1H; dppb PCH_2), 2.98 (m, 1H; dppb PCH_2), 2.68 (m, 2H; dppb PCH_2), 2.10-1.68 ppm (m (overlapped with H_2O signal), 4H; dppb CH_2). $^{13}C\{^1H\}$ NMR (100.6 MHz, CD_2Cl_2, 298 K): δ = 202.0 (q, $^2J_{CP}$ = 12.4 Hz; CO), 155.6-127.1 (m; aromatic carbon atoms), 71.8 (d, $^1J_{CP}$ = 6.8 Hz; PTA *C*H_2), 49.7 (d, $^1J_{CP}$ = 9.3 Hz; PTA *C*H_2), 34.0 (d, $^1J_{CP}$ = 28.4 Hz; dppb P*C*H_2), 29.1 (d, $^1J_{CP}$ = 23.6 Hz; dppb P*C*H_2), 23.3 (s; dppb CH_2), 22.8 ppm (s; dppb CH_2). $^{31}P\{^1H\}$ NMR (162.0 MHz, CD_2Cl_2, 298 K): δ = 28.9 (t, $^2J_{PP}$ = 24.3 Hz; dppb), 17.7 (dd, $^2J_{PP}$ = 217.6 Hz, $^2J_{PP}$ = 25.8 Hz; dppb), -65.9 (dd, $^2J_{PP}$ = 217.6 Hz, $^2J_{PP}$ = 23.0; PTA), -144.6 ppm (hept, $^1J_{PF}$ = 711.8 Hz; PF_6^-).

Synthesis of $[Ru(CO)(dppb)(py)(phen)](PF_6)_2$ (22)

Complex $[Ru(CO)(dppb)(py)(phen)](PF_6)_2$ (**22**) was synthetized as described for **21**, using pyridine (py) (4.0 mg, 0.059 mmol) in place of PTA. Yield: 53 mg (80%). Elemental analysis calcd (%) for $C_{47}H_{44}F_{12}N_3OP_4Ru$: C 50.41, H 3.96, N 3.75; found: C 50.28, H 3.70, N 3.43. ^{1}H NMR (400.1 MHz, CD_3OD, 298 K): δ = 9.81 (ddd, $^3J_{HH}$ = 5.2 Hz, $^4J_{HH}$ = 2.4 Hz, $^6J_{HH}$ = 1.2 Hz, 1H; phen), 9.61 (d, $^3J_{HH}$ = 4.6 Hz, 1H; phen), 8.99 (dd, $^3J_{HH}$ = 8.3 Hz, $^4J_{HH}$ = 1.1 Hz, 1H; phen), 8.57 (dd, $^3J_{HH}$ = 8.4 Hz, $^4J_{HH}$ = 1.2 Hz, 1H; phen), 8.35 (dd, $^3J_{HH}$ = 8.3 Hz, $^4J_{HH}$ = 5.3 Hz, 1H; phen), 8.19 (m, 1H; py), 8,08 (d, $^3J_{HH}$ = 8.9 Hz, 1H; phen), 7.98 (dd, $^3J_{HH}$ = 5.5 Hz, $^4J_{HH}$ = 2.7 Hz, 1H; py), 7.93 (d, $^3J_{HH}$ = 8.9, 1H; phen), 7.80-7.39 (m, 17H; aromatic protons), 6.96 (t, $^3J_{HH}$ = 7.1 Hz, 2H; Ph), 6.81 (t, $^3J_{HH}$ = 7.6 Hz, 1H; Ph), 6.52 (td, $^3J_{HH}$ = 8.4 Hz, $^4J_{HH}$

= 2.4 Hz, 2H; Ph), 6.17 (t, $^{3}J_{HH}$ = 8.5 Hz, 2H; Ph), 3.59 (m, 1H; PCH_2), 3.15 (m, 1H; PCH_2), 2.86 (m, 2H; PCH_2), 2.38-2.06 ppm (m, 4H; CH_2). $^{13}C\{^{1}H\}$ NMR (100.6 MHz, CD_3OD, 298 K): δ = 203.6 (7, $^{2}J_{CP}$ = 15.3 Hz; CO), 156.1-124.2 (m; aromatic carbon atoms), 29.1 (d, $^{1}J_{CP}$ = 28.3 Hz; P*C*H_2), 26.8 (d, $^{1}J_{CP}$ = 29.8 Hz; P*C*H_2), 22.0 (s; CH_2), 21.3 ppm (s; CH_2). $^{31}P\{^{1}H\}$ NMR (162.0 MHz, CD_3OD, 298 K): δ = 29.0 (d, $^{2}J_{PP}$ = 25.3 Hz; dppb), 28.8 (d, $^{2}J_{PP}$ = 25.3 Hz; dppb), -144.3 ppm (hept, $^{1}J_{PF}$ = 711.8 Hz; PF_6^-).

5.2 SINGLE CRYSTAL X-RAY STRUCTURE DETERMINATION

Data were obtained at 100 K using an x-ray single crystal diffractometer equipped with a CMOS detector (Bruker APEX III, κ-CMOS), a TXS rotating anode with MoK_α radiation (λ = 0.71073 Å) and a Helios optic using the APEX3 software package[85]. Measurements were performed on single crystals coated with perfluorinated ether. The crystals were fixed on top of a kapton micro sampler and frozen under a stream of cold nitrogen. A matrix scan was used to determine the initial lattice parameters. Reflections were corrected for Lorentz and polarization effects, scan speed, and background using SAINT. Absorption correction, including odd and even ordered spherical harmonics was performed using SADABS. Space group assignment was based upon systematic absences, E statistics, and successful refinement of the structures. The structures were solved using SHELXT with the aid of successive difference Fourier maps, and were refined against all data using SHELXL[86] in conjunction with SHELXLE[87]. Hydrogen atoms were calculated in ideal positions as follows: Methyl hydrogen atoms were refined as part of rigid rotating groups with a C–H distance of 0.98 Å and $U_{iso(H)} = 1.5 \cdot U_{eq(C)}$. Other H atoms were placed in calculated positions and refined using a riding model, with methylene and aromatic C–H distances of 0.99 Å and 0.95 Å, respectively, and other C–H distances of 1.00 Å, all with $U_{iso(H)} = 1.2 \cdot U_{eq(C)}$. Non-hydrogen atoms were refined with anisotropic displacement parameters. Full-matrix least-squares refinements were carried out by minimizing $\Sigma w(F_o^2 - F_c^2)^2$ with the SHELXL weighting scheme. Neutral atom scattering factors for all atoms and anomalous dispersion corrections for the non-hydrogen atoms were taken from *International Tables for Crystallography*. A split layer refinement was used for disordered groups and additional restraints on geometries and anisotropic displacement parameters were used, if necessary. The unit cell of **5** contains 8 disordered molecules of water and the unit cell of **8** contains a mixture of disordered solvents which were treated as a diffuse contribution to the overall scattering without specific

atom positions using the PLATON/SQUEEZE procedure. Images of the crystal structures were generated with Mercury[88].

5.3 DFT CALCULATION METHODS

All density functional theory (DFT) calculations were performed using the B3LYP functional, composed of Becke's three-parameter hybrid exchange functional (B3)[89] and the correlation functional of Lee, Yang, and Parr (LYP)[90-91], using Gaussian 16 program[92]. Moreover the Grimme's dispersion contribution correction (D3) was added[93]; previous works have shown that B3LYP-D3 scheme provides reliable results for thermochemistry of organometallic compounds[94-97]. Geometry optimizations were carried out in vacuum with a def2SVP basis set[97-99] for all atoms, the pseudopotential was applied for ruthenium atom. Due to the key role of solvation in influencing thermodynamic and kinetic properties of metal complexes, geometries have been also obtained including environmental effects by means of the polarizable continuum method (PCM)[100].

No imaginary frequencies were obtained for the complexes investigated, Gibbs free energies (G) have been calculated by adding the zero-point energy and thermal correction terms to the electronic energy of the complex.

5.4 CELL LINES

Human anaplastic thyroid cancer cell lines SW1736 and 8505C carry the same BRAF V600E and TERT gene promoter mutations[101-102]. The cell lines have been validated by short tandem repeat and tested whether they are mycoplasma-free. SW1736 and 8505C cells were cultivated as described in literature[103]. Cultured cells were treated with either cisplatin (Cayman Chemical, Ann Arbor, MI) solubilized in N,N-dimethylformamide (DMF)[82] (Sigma Aldrich, Saint Louis, MO, USA) or ruthenium(II) complexes solubilized in dmso (0.04–0.25% in RPMI 1640 medium) and then diluted in RPMI 1640 medium (EuroClone) supplemented with 10% fetal bovine serum (Gibco Invitrogen, Milan, Italy).

Human colon carcinoma HCT-116 cells were obtained from American Type Culture Collection (Manassas, VA) and grown in DMEM supplemented with 10% fetal bovine serum. Cells were grown in a humidified incubator with 5% CO_2 at 37 °C. Cells were seeded in 96-well plates (5500 cells/well; volume = 100 µL) and grown to 70%–75% confluence, followed

by treatment with dmso (control) or each compound (dissolved in dmso) in fresh medium at different concentrations in the micromolar or sub-micromolar domain (both in control and in treatment wells a final dmso concentration of 0.1% v/v; quadruplicate conditions). Likewise, cells were plated in quadruplicate in 96-well plates and grown to the same confluence to be treated with cisplatin (dissolved in 0.9% w/v NaCl(aq)) in fresh medium at different concentrations, for comparison purposes. After 72-h incubation at 37 °C, inhibition of cell proliferation was measured by MTT assay, as previously described[104]. The cytotoxicity of the compounds was quantified as the percentage of surviving cells compared to untreated cells. At least three MTT tests for each compound were carried out in order to evaluate the corresponding IC_{50} values. DMEM W/GLUTAMAX^{TM}-I (pyruvate 1X) cell growth medium was purchased from Life Technologies Italia while fetal bovine serum, sterile dmso, *cis*-diammineplatinum(II) dichloride (herein after, cisplatin) and 3-(4,5-dimethyl-2-thiazolyl)-2,5-diphenyl-2H-tetrazolium bromide (MTT) were from Merck. Penicillin-streptomycin (solution; 5000 U/mL) were acquired from Thermofisher Life Technologies.

5.5 PROTEIN EXTRACTION AND WESTERN BLOT

ATC cells were treated with dmso or ruthenium(II) compounds at the respective EC_{50} doses for 72 h. Briefly, SW1736 and 8505C cells have been collected by scraping and lysed with total lysis buffer (50 mM Tris·HCl, pH 8.0, 120 mM NaCl, 5 mM EDTA, 1% Triton, 1% NP40, and 1 mM DTT) supplemented with phenyl-methylsulphonyl fluoride and protease inhibitors. Lysates were then centrifuged at 13000*g* for 10 min at 4 °C and the supernatants were quantified by using the Bradford assay. Western blot analysis was performed as previously described[104]. Proteins were electrophoresed on SDS-PAGE and then transferred onto nitrocellulose membranes (GE Healthcare, Little Chalfont, UK), saturated with 5% non-fat dry milk in PBS/0.1% Tween 20. The membranes were then incubated overnight with a rabbit polyclonal anti-cleaved-PARP antibody (Abcam, Cambridge, United Kingdom) or a rabbit anti-actin antibody (Merck KGaA). The day after, the membranes were incubated with anti-rabbit or anti-mouse immunoglobulin coupled to peroxidase (Merck KGaA) for 2 h. Blots were developed using UVITEC Alliance LD (UVITecLimited, Cambridge, UK) with the SuperSignal Technology (Thermo Scientific Inc Waltham, MA, USA).

HCT-116 cells were grown to around 75% confluence, and treated with the Ru(II)-based complexes at 0.75 μM or dmso vehicle (0.1% v/v) as a control over 72 h. Colon cancer cells

were then subjected to immunoblotting analysis using the following protocol. Proteins were extracted in RIPA buffer (Sigma-Aldrich) containing protease inhibitor cocktail tablets 1X (Roche), sonicated 10 min and then lysates were clarified by centrifugation at 8000 x g for 10 min at 4 °C. Supernatants were harvested and protein content was determined by BCA assay (Sigma-Aldrich). Protein samples were diluted 1:1 with Laemmli's sample buffer (62.5 mM Tris–HCl, pH 6.8, 25% glycerol, 2% SDS, 0.01% bromophenol blue), heated for 5 min at 90°C, and separated by SDS/polyacrylamide gel electrophoresis (PAGE) on 12% T acrylamide gels in tris/glycine/SDS buffer. Proteins were then electroblotted onto polyvinylidene fluoride membranes (PVDF) (Bio-Rad) at 80 V for 1 h and 30 min at 4 °C. Amido Black staining (Sigma-Aldrich) was used to confirm equal protein loading in different lanes. Non-specific sites were blocked by incubating the membranes with 5% non-fat dried milk and 0.05% Tween-20 (Sigma-Aldrich) in tris-buffered saline for 1h at room temperature. Membranes were incubated with the different primary antibodies at the appropriate dilutions in 1% non-fat dried milk, 0.05% Tween-20 in tris-buffered saline overnight at 4°C. Blots were then incubated 1 h at room temperature with the appropriate HRP-conjugated secondary antibody. The immunocomplexes were visualized by chemiluminescence using the ChemidocMP imaging system (Bio-Rad) and the intensity of the chemiluminescence response was measured by processing the image with Image Lab software (Bio-Rad).
Mouse monoclonal antibodies against caspase-3 (sc 7272, 1:1000) was purchased from Santa Cruz Biotechnology, Inc. (Santa Cruz, CA). Horseradish peroxidase (HRP)-conjugated secondary antibody (sc-2005, 1:2000) against primary antibody was purchased from Santa Cruz Biotechnology, Inc. (Santa Cruz, CA). FITC Annexin V apoptosis detection kit I was purchased ThermoFisher Scientific, (Waltham, MA, USA). All chemicals were of high-grade pureness and used as purchased without any further purification.

5.6 SOFT AGAR ASSAY

The soft agar colony formation assay was used to evaluate the cellular transformation in vitro of SW1736 and 8505C cells after being treated with vehicle or ruthenium(II) complexes at the respective EC50 doses. As previously described[105], after 72 h of treatment, cells were collected, and 10000 cells per plate were suspended in 4 mL of complete medium containing 0.25% agarose and then seeded to the top of a 1% agarose complete medium layer in 6 cm

plates. After 30 days, the colonies were counted by using an inverted microscope Leica DMI-600B (Leica Microsystems Ltd, Heerbrugg, Switzerland).

5.7 STATISTICAL ANALYSIS

The evaluated cell viability, cleaved PARP or Caspase-3 protein level and colony forming capacity data were expressed as mean ± SD, and significances were analysed by performing the Student's *t*-test using GraphPad Software for Science (San Diego, CA, USA): *p* values lower than 0.05 were considered to be statistically significant.

5.8 FLOW CYTOFLUORIMETRY ASSAY

Apoptosis indexes were measured using the Annexin-V fluorescein isothiocyanate (FITC) apoptosis detection kit I from by ThermoFisher Scientific, (Waltham, MA, USA). HCT-116 cells were grown to around 75% confluence, treated with the most promising chiral complexes **18R** and **20R** (at 0.5 μM) or dmso vehicle as a control (0.1% v/v) for 72 h, harvested by trypsinization and centrifugation. Cell pellets were washed twice with ice cold PBS 1X and cells were then resuspended in binding buffer 1X at a concentration of 3 $x10^6$ cells/mL. 200 μL of the suspension was then transferred to a 5 mL flow cytometry tube. Cells were stained with 5 μL of anti-annexin V-FITC for 10 minutes in the dark. 10 μL of propidium iodide (PI) was added, in each tube, just before the acquisition of the sample on flow cytometry instrument. For annexin V/PI assay analysis, approximately 1.0 $x10^4$-gated events were acquired for each sample by a FACSCanto flow cytometer (Becton Dickinson). Flow cytometry data were processed using FlowJo software (v10 TreeStar). The excitation wavelength was 488 nm and the detection wavelengths were 530 ± 15 and 620 ± 21 nm for Annexin V and PI, respectively.

Data (**Figure 31**) are shown as density plots of Annexin-V (x-axis) and propidium iodide (PI, y-axis) staining. Viable cells were defined as annexin V-negative and PI-negative. Early apoptotic cells were defined as annexin V-positive and PI-negative, late apoptotic cells were defined as annexin V- and PI-positive, whereas cells positive for PI only were considered dead by a necrotic pathway.

5.9 CELLULAR MORPHOLOGY AND CELL MIGRATION ASSAY

An Olympus IX70 inverted tissue culture microscope was used for evaluating cellular morphology changes upon treatment and microscopic imaging with phase contrast. Cell migration was assessed using the scratch wound healing assay, as described in literature[106]. Cells were grown to confluence in tissue culture dishes, then the most promising compound DL92 (final concentration= 3 μM) or drug-free medium were added. After 24 h, cells were washed twice with PBS and scraped up using a sterile 1,000 μL pipette tip, then cultured in the abovementioned medium. The migration rate is associated with change of the distance between the edges of the wound (defined by the lines), indicating the cell-free surface area. Pictures here reported are representative of one of three different experiments (original magnification 4X; scale bar = 100 μm).

6 CONCLUSIONS AND FUTURE PERSPECTIVES

In summary, in this PhD work we have reported the straightforward synthesis of novel ruthenium complexes bearing bidentate phosphine and diimine ligands, which exhibit high cytotoxicity against cancer cell lines, namely human anaplastic thyroid cancer (SW1736 and 8505C) and colon carcinoma (HCT-116). The obtained complexes have been characterized using NMR, IR and X-ray diffraction measurements.

Firstly, the reaction between the versatile precursor [Ru(OAc)(η^2-OAc)(CO)(dppb)] (**1**) and β-diketones ligands, afforded the neutral complexes of general formula [Ru(η^1-OAc)(CO)(dppb)(dkt)] (where dkt = acetylacetonate, dibenzoylmethane and curcumin), by protonation and displacement of one acetate ligand. The three complexes demonstrated a moderate cell viability decrease after 72 h of treatment in ATC cell lines, with EC_{50} values comparable to those of cisplatin (6.40-5.20 μM), ranging from 3.52 to 9.54 μM.

The precursor [Ru(OAc)(η^2-OAc)(CO)(dppb)] (**1**) in combination with the bidentate phen ligand, led to the synthesis of the monocationic complex [Ru(OAc)(CO)(dppb)(phen)]OAc (**5**), which proved to be a suitable starting compound for substitution reactions in alcohol media with different anions, giving access to the new class of complexes [RuX(CO)(dppb)(phen)]Y (X = Y = OAc, OPiv, SAc, and NCS; X = Cl and Y = PF_6). Acetate and pivalate derivatives are water soluble, leading to the protonation of acetate or pivalate by H_2O and the formation of the corresponding hydroxo-complex. These cationic complexes

display high cytotoxic activity on ATC and HCT-116 cell lines, with EC_{50} values ranging from 2.84 to 0.09 μM, which are markedly lower than that of cisplatin, with a fold-change ranging from 2 to 58. Cleaved-PARP analysis shows that a large part of the effects on the decrease of cell viability is due to apoptosis increment. It is worth noting that in addition to a decrease in cell proliferation and induction of apoptosis, a nearly complete abrogation of the colony formation ability is observed, exhibiting a promising effect also as antimetastatic agents. Conversely, the meridional (*mer*) PPC isomer **5a** of complex **5** highlighted a different behaviour as cytotoxic agent, leading to a poor effectiveness in cell viability studies (EC_{50} in SW1736 cell line = 20.40 μM).

The substitution of the phenanthroline ligand with functionalized imidazophenanthroline did not improve the cytotoxic activity of these complexes, except for the acetate complex bearing the pyrazinophenanthroline ligand (**14**), which demonstrated to be approximately as active as the corresponding phenanthroline complex **5** in HCT-116 cell line, with 0.64 and 0.81 μM values of EC_{50}, respectively. Likewise, the substitution of the carbonyl group with *t*-butyl isocyanide in complex **17**, led to a stable and water soluble specie, exhibiting a EC_{50} of 1.85 μM in SW1736 and 0.80 μM in HCT-116 cell lines, values very close to those of the corresponding carbonyl complex **5** (1.24 and 0.81 μM for SW1736 and HCT-116 cancer cell lines, respectively).

The control of the configuration at the ruthenium center was achieved by inserting a chiral diphosphine, such as (R,R)-Skewphos or (S,S)-Skewphos, in order to obtain the enantiomeric acetate complexes [Ru(η^1-OAc)(CO)((R,R)-Skewphos)(phen)]OAc (**18R**), [Ru(η^1-OAc)(CO)((S,S)-Skewphos)(phen)]OAc (**18S**) and their corresponding pivalate and thioacetate derivatives by displacement of the acetate anion in methanol. The influence of chirality on each couple of enantiomeric ruthenium complexes induced a large differences in activity toward anaplastic thyroid cancer and colon carcinoma cell lines. All the R,R enantiomers reduce the cell viability at significantly lower concentrations than the corresponding S,S enantiomers, demonstrating to be even up to ten times more active. Complex [Ru(η^1-SAc)(CO)((R,R)-Skewphos)(phen)]SAc (**20R**) showed the lowest EC_{50} observed in this study, reaching 0.04 μM of EC_{50} in 8505C ATC cell line.

Finally, the synthesis of dicationic ruthenium complexes has been studied. Complexes **21** and **22** were obtained by reaction of the monocationic acetate complex **5** and neutral ligands (PTA or pyridine), exploiting the lability of the Ru-OAc bond in water, due to the *trans* influence exerted by the diphosphine ligand. None of the obtained dicationic complexes

displayed promising anticancer activity toward ATC and colon carcinoma cell lines, ranging from 10.21 to 15.00 μM of EC_{50} values.

Due to their versatile behavior, high stability and promising anticancer activity, the monocationic ruthenium complexes are suitable candidates for further evaluation studies under biological conditions. In particular, considering the high affinity demonstrated with sulfur species, such as thioacetate, GSH and cysteine, the mechanisms of action of these complexes as redox catalysts inside the cells, will be evaluated in the future.

In addition, considering also the stability and high cytotoxicity of the isonitrile ruthenium complex, the functionalization of biological substrates with an isonitrile group and their coordination to the ruthenium centre, will be evaluated in order to target selectively cancer cells or biomolecules involved in cancer development.

7 BIBLIOGRAPHY

1. *Metalloproteins and Metalloenzymes*. WORLD SCIENTIFIC: 2014; p 400.

2. Casini, A.; Vessières, A.; Meier-Menches, S. M., Metal-based Anticancer Agents. *Royal Society of Chemistry* **2019**, P001-355.

3. Guo, Z.; Sadler, P. J., Metals in Medicine. *Angewandte Chemie International Edition* **1999,** *38* (11), 1512-1531.

4. Silva, H. V. R.; Dias, J. S. M.; Ferreira-Silva, G. Á.; Vegas, L. C.; Ionta, M.; Corrêa, C. C.; Batista, A. A.; Barbosa, M. I. F.; Doriguetto, A. C., Phosphine/diimine ruthenium complexes with Cl^-, CO, NO^+, NO_2-, NO_3- and pyridine ligands: Pro-apoptotic activity on triple-negative breast cancer cells and DNA/HSA interactions. *Polyhedron* **2018,** *144*, 55-65.

5. Schatzschneider, U., Bioinorganic Medicinal Chemistry. Edited by Enzo Alessio. *Angewandte Chemie International Edition* **2011,** *50* (46), 10765-10767.

6. Lloyd, N. C.; Morgan, H. W.; Nicholson, B. K.; Ronimus, R. S., The Composition of Ehrlich's Salvarsan: Resolution of a Century-Old Debate. *Angewandte Chemie International Edition* **2005,** *44* (6), 941-944.

7. Alderden, R. A.; Hall, M. D.; Hambley, T. W., The Discovery and Development of Cisplatin. *Journal of Chemical Education* **2006,** *83* (5), 728.

8. Rosenberg, B.; Vancamp, L.; Trosko, J. E.; Mansour, V. H., Platinum Compounds: a New Class of Potent Antitumour Agents. *Nature* **1969,** *222* (5191), 385-386.

9. Stathopoulos, G. P., Liposomal cisplatin: a new cisplatin formulation. *Anti-Cancer Drugs* **2010,** *21* (8).

10. Reedijk, J.; Lohman, P. H. M., Cisplatin: Synthesis, antitumour activity and mechanism of action. *Pharmaceutisch Weekblad* **1985,** *7* (5), 173-180.

11. Ishida, S.; Lee, J.; Thiele, D. J.; Herskowitz, I., Uptake of the anticancer drug cisplatin mediated by the copper transporter Ctr1 in yeast and mammals. *Proceedings of the National Academy of Sciences* **2002,** *99* (22), 14298.

12. Pinato, O.; Musetti, C.; Sissi, C., Pt-based drugs: the spotlight will be on proteins. *Metallomics* **2014,** *6* (3), 380-395.

13. Tornaghi, E.; Andreoni, W.; Carloni, P.; Hutter, J.; Parrinello, M., Carboplatin versus cisplatin: density functional approach to their molecular properties. *Chemical Physics Letters* **1995,** *246* (4), 469-474.

14. Extra, J. M.; Espie, M.; Calvo, F.; Ferme, C.; Mignot, L.; Marty, M., Phase I study of oxaliplatin in patients with advanced cancer. *Cancer Chemotherapy and Pharmacology* **1990,** *25* (4), 299-303.

15. Los, G.; Mutsaers, P. H. A.; Ruevekamp, M.; McVie, J. G., The use of oxaliplatin versus cisplatin in intraperitoneal chemotherapy in cancers restricted to the peritoneal cavity in the rat. *Cancer Letters* **1990,** *51* (2), 109-117.

16. Schreiber-Brynzak, E.; Pichler, V.; Heffeter, P.; Hanson, B.; Theiner, S.; Lichtscheidl-Schultz, I.; Kornauth, C.; Bamonti, L.; Dhery, V.; Groza, D.; Berry, D.; Berger, W.; Galanski, M.; Jakupec, M. A.; Keppler, B. K., Behavior of platinum(iv) complexes in models of tumor hypoxia: cytotoxicity, compound distribution and accumulation. *Metallomics* **2016,** *8* (4), 422-433.

17. Platinum-containing cytostatic drugs. In *Meyler's Side Effects of Drugs (Sixteenth Edition)*, Aronson, J. K., Ed. Elsevier: Oxford, 2016; pp 810-833.

18. Zeng, L.; Gupta, P.; Chen, Y.; Wang, E.; Ji, L.; Chao, H.; Chen, Z.-S., The development of anticancer ruthenium(II) complexes: from single molecule compounds to nanomaterials. *Chemical Society Reviews* **2017,** *46* (19), 5771-5804.

19. Southam, H. M.; Butler, J. A.; Chapman, J. A.; Poole, R. K., Chapter One - The Microbiology of Ruthenium Complexes. In *Advances in Microbial Physiology*, Poole, R. K., Ed. Academic Press: 2017; Vol. 71, pp 1-96.

20. Wei, S.; Yuchun, L.; Peiyuan, L., Design of Ru-arene Complexes for Antitumor Drugs. *Mini-Reviews in Medicinal Chemistry* **2018,** *18* (2), 184-193.

21. Clarke, M. J.; Bitler, S.; Rennert, D.; Buchbinder, M.; Kelman, A. D., Reduction and Subsequent Binding of Ruthenium Ions Catalyzed by Subcellular Components. *Journal of Inorganic Biochemistry* **1980,** *12* (1), 79-87.

22. Quiles, J. L.; Sánchez-González, C.; Vera-Ramírez, L.; Giampieri, F.; Navarro-Hortal, M. D.; Xiao, J.; Llopis, J.; Battino, M.; Varela-López, A., Reductive Stress, Bioactive Compounds, Redox-Active Metals, and Dormant Tumor Cell Biology to Develop Redox-Based Tools for the Treatment of Cancer. *Antioxidants & Redox Signaling* **2020**.

23. Ahmed-Ouameur, A.; Diamantoglou, S.; Sedaghat-Herati, M. R.; Nafisi, S.; Carpentier, R.; Tajmir-Riahi, H. A., The effects of drug complexation on the stability and conformation of human serum albumin. *Cell Biochemistry and Biophysics* **2006,** *45* (2), 203-213.

24. Guo, W.; Zheng, W.; Luo, Q.; Li, X.; Zhao, Y.; Xiong, S.; Wang, F., Transferrin Serves As a Mediator to Deliver Organometallic Ruthenium(II) Anticancer Complexes into Cells. *Inorganic Chemistry* **2013,** *52* (9), 5328-5338.

25. Tanaka, Y.; Akita, M., Organometallic radicals of iron and ruthenium: Similarities and dissimilarities of radical reactivity and charge delocalization. *Coordination Chemistry Reviews* **2019,** *388*, 334-342.

26. Alessio, E.; Messori, L., NAMI-A and KP1019/1339, Two Iconic Ruthenium Anticancer Drug Candidates Face-to-Face: A Case Story in Medicinal Inorganic Chemistry. *Molecules* **2019,** *24* (10).

27. Alessio, E., Thirty Years of the Drug Candidate NAMI-A and the Myths in the Field of Ruthenium Anticancer Compounds: A Personal Perspective. *European Journal of Inorganic Chemistry* **2017,** *2017* (12), 1549-1560.

28. Novohradský, V.; Bergamo, A.; Cocchietto, M.; Zajac, J.; Brabec, V.; Mestroni, G.; Sava, G., Influence of the binding of reduced NAMI-A to human serum albumin on the pharmacokinetics and biological activity. *Dalton Transactions* **2015,** *44* (4), 1905-1913.

29. Adeniyi, A. A.; Ajibade, P. A., Development of ruthenium-based complexes as anticancer agents: toward a rational design of alternative receptor targets. *Reviews in Inorganic Chemistry* **2016,** *36* (2), 53-75.

30. Morris, R. E.; Aird, R. E.; del Socorro Murdoch, P.; Chen, H.; Cummings, J.; Hughes, N. D.; Parsons, S.; Parkin, A.; Boyd, G.; Jodrell, D. I.; Sadler, P. J., Inhibition of Cancer Cell Growth by Ruthenium(II) Arene Complexes. *Journal of Medicinal Chemistry* **2001,** *44* (22), 3616-3621.

31. Berndsen, R. H.; Weiss, A.; Abdul, U. K.; Wong, T. J.; Meraldi, P.; Griffioen, A. W.; Dyson, P. J.; Nowak-Sliwinska, P., Combination of ruthenium(II)-arene complex [Ru(η^6-p-cymene)Cl_2(pta)] (RAPTA-C) and the epidermal growth factor receptor inhibitor erlotinib results in efficient angiostatic and antitumor activity. *Scientific Reports* **2017,** *7* (1), 43005.

32. Chatterjee, S.; Kundu, S.; Bhattacharyya, A.; Hartinger, C. G.; Dyson, P. J., The ruthenium(II)–arene compound RAPTA-C induces apoptosis in EAC cells through mitochondrial and p53–JNK pathways. *JBIC Journal of Biological Inorganic Chemistry* **2008,** *13* (7), 1149.

33. Clavel, C. M.; Păunescu, E.; Nowak-Sliwinska, P.; Griffioen, A. W.; Scopelliti, R.; Dyson, P. J., Modulating the Anticancer Activity of Ruthenium(II)–Arene Complexes. *Journal of Medicinal Chemistry* **2015,** *58* (8), 3356-3365.

34. Scolaro, C.; Bergamo, A.; Brescacin, L.; Delfino, R.; Cocchietto, M.; Laurenczy, G.; Geldbach, T. J.; Sava, G.; Dyson, P. J., In Vitro and in Vivo Evaluation of Ruthenium(II)−Arene PTA Complexes. *Journal of Medicinal Chemistry* **2005,** *48* (12), 4161-4171.

35. Bergamo, A.; Masi, A.; Dyson, P. J.; Sava, G., Modulation of the metastatic progression of breast cancer with an organometallic ruthenium compound. *Int J Oncol* **2008,** *33* (6), 1281-1289.

36. Adhireksan, Z.; Davey, G. E.; Campomanes, P.; Groessl, M.; Clavel, C. M.; Yu, H.; Nazarov, A. A.; Yeo, C. H. F.; Ang, W. H.; Dröge, P.; Rothlisberger, U.; Dyson, P. J.; Davey, C. A., Ligand substitutions between ruthenium–cymene compounds can control protein versus DNA targeting and anticancer activity. *Nature Communications* **2014,** *5* (1), 3462.

37. Adhireksan, Z.; Palermo, G.; Riedel, T.; Ma, Z.; Muhammad, R.; Rothlisberger, U.; Dyson, P. J.; Davey, C. A., Allosteric cross-talk in chromatin can mediate drug-drug synergy. *Nature Communications* **2017,** *8* (1), 14860.

38. Li, G.; Sun, L.; Ji, L.; Chao, H., Ruthenium(II) complexes with dppz: from molecular photoswitch to biological applications. *Dalton Transactions* **2016,** *45* (34), 13261-13276.

39. Dwyer, F. P.; Gyarfas, E. C.; Rogers, W. P.; Koch, J. H., Biological Activity of Complex Ions. *Nature* **1952,** *170* (4318), 190-191.

40. Zeng, Z.-P.; Wu, Q.; Sun, F.-Y.; Zheng, K.-D.; Mei, W.-J., Imaging Nuclei of MDA-MB-231 Breast Cancer Cells by Chiral Ruthenium(II) Complex Coordinated by 2-(4-Phenyacetylenephenyl)-1H-imidazo[4,5f][1,10]phenanthroline. *Inorganic Chemistry* **2016,** *55* (11), 5710-5718.

41. Tan, C.; Wu, S.; Lai, S.; Wang, M.; Chen, Y.; Zhou, L.; Zhu, Y.; Lian, W.; Peng, W.; Ji, L.; Xu, A., Synthesis, structures, cellular uptake and apoptosis-inducing properties of highly cytotoxic ruthenium-Norharman complexes. *Dalton Transactions* **2011,** *40* (34), 8611-8621.

42. Friedman, A. E.; Chambron, J. C.; Sauvage, J. P.; Turro, N. J.; Barton, J. K., A molecular light switch for DNA: $Ru(bpy)_2(dppz)_2^+$. *Journal of the American Chemical Society* **1990,** *112* (12), 4960-4962.

43. Wachter, E.; Moyá, D.; Parkin, S.; Glazer, E. C., Ruthenium Complex “Light Switches” that are Selective for Different G-Quadruplex Structures. *Chemistry – A European Journal* **2016,** *22* (2), 550-559.

44. Chelucci, G.; Baldino, S.; Baratta, W., Ruthenium and osmium complexes containing 2-(aminomethyl)pyridine (Ampy)-based ligands in catalysis. *Coordination Chemistry Reviews* **2015,** *300*, 29-85.

45. Baratta, W.; Chelucci, G.; Herdtweck, E.; Magnolia, S.; Siega, K.; Rigo, P., Highly Diastereoselective Formation of Ruthenium Complexes for Efficient Catalytic Asymmetric Transfer Hydrogenation. *Angewandte Chemie International Edition* **2007,** *46* (40), 7651-7654.

46. Giboulot, S.; Comuzzi, C.; Del Zotto, A.; Figliolia, R.; Lippe, G.; Lovison, D.; Strazzolini, P.; Susmel, S.; Zangrando, E.; Zuccaccia, D.; Baldino, S.; Ballico, M.; Baratta, W., Preparation of monocarbonyl ruthenium complexes bearing bidentate nitrogen and phosphine ligands and their catalytic activity in carbonyl compound reduction. *Dalton Transactions* **2019,** *48* (33), 12560-12576.

47. Ohkuma, T.; Koizumi, M.; Muñiz, K.; Hilt, G.; Kabuto, C.; Noyori, R., trans-RuH(η-BH_4)(binap)(1,2-diamine): A Catalyst for Asymmetric Hydrogenation of Simple Ketones under Base-Free Conditions. *Journal of the American Chemical Society* **2002,** *124* (23), 6508-6509.

48. Kitamura, M.; Ohkuma, T.; Inoue, S.; Sayo, N.; Kumobayashi, H.; Akutagawa, S.; Ohta, T.; Takaya, H.; Noyori, R., Homogeneous asymmetric hydrogenation of functionalized ketones. *Journal of the American Chemical Society* **1988,** *110* (2), 629-631.

49. Ohkuma, T.; Ooka, H.; Ikariya, T.; Noyori, R., Preferential hydrogenation of aldehydes and ketones. *Journal of the American Chemical Society* **1995,** *117* (41), 10417-10418.

50. Ohkuma, T.; Ooka, H.; Yamakawa, M.; Ikariya, T.; Noyori, R., Stereoselective Hydrogenation of Simple Ketones Catalyzed by Ruthenium(II) Complexes. *The Journal of Organic Chemistry* **1996,** *61* (15), 4872-4873.

51. Baratta, W.; Ballico, M.; Esposito, G.; Rigo, P., Role of the NH_2 Functionality and Solvent in Terdentate CNN Alkoxide Ruthenium Complexes for the Fast Transfer Hydrogenation of Ketones in 2-Propanol. *Chemistry – A European Journal* **2008,** *14* (18), 5588-5595.

52. Hatcher, H.; Planalp, R.; Cho, J.; Torti, F. M.; Torti, S. V., Curcumin: From ancient medicine to current clinical trials. *Cellular and Molecular Life Sciences* **2008,** *65* (11), 1631-1652.

53. Refat, M. S., Synthesis and characterization of ligational behavior of curcumin drug towards some transition metal ions: Chelation effect on their thermal stability and biological activity. *Spectrochimica Acta Part A: Molecular and Biomolecular Spectroscopy* **2013,** *105*, 326-337.

54. Skopenko, V. V.; Amirkhanov, V. M.; Sliva, T. Y.; Vasilchenko, I. S.; Anpilova, E. L.; Garnovskii, A. D., Various types of metal complexes based on chelating β-diketones and their structural analogues. *Russian Chemical Reviews* **2004,** *73* (8), 737-752.

55. Fernández, R.; Melchart, M.; Habtemariam, A.; Parsons, S.; Sadler, P. J., Use of Chelating Ligands to Tune the Reactive Site of Half-Sandwich Ruthenium(II)–Arene Anticancer Complexes. *Chemistry – A European Journal* **2004,** *10* (20), 5173-5179.

56. Bonfili, L.; Pettinari, R.; Cuccioloni, M.; Cecarini, V.; Mozzicafreddo, M.; Angeletti, M.; Lupidi, G.; Marchetti, F.; Pettinari, C.; Eleuteri, A. M., Arene–RuII Complexes of Curcumin Exert Antitumor Activity via Proteasome Inhibition and Apoptosis Induction. *ChemMedChem* **2012,** *7* (11), 2010-2020.

57. Caruso, F.; Rossi, M.; Benson, A.; Opazo, C.; Freedman, D.; Monti, E.; Gariboldi, M. B.; Shaulky, J.; Marchetti, F.; Pettinari, R.; Pettinari, C., Ruthenium–Arene Complexes of Curcumin: X-Ray and Density Functional Theory Structure, Synthesis, and Spectroscopic Characterization, in Vitro Antitumor Activity, and DNA Docking Studies of (p-Cymene)Ru(curcuminato)chloro. *Journal of Medicinal Chemistry* **2012,** *55* (3), 1072-1081.

58. Barbosa, M.; Correa, R.; Bastos, T.; Pozzi, L.; Moreira, D.; Ellena, J.; Doriguetto, A.; Silveira, R.; Oliveira, C.; Kuznetsov, A.; Malta, V.; Soares, M.; Batista, A., Structural isomerism of Ru(II)-carbonyl complexes: Synthesis, characterization and their antitrypanosomal activities. *New J. Chem.* **2017,** *41*.

59. Barolli, J. P.; Corrêa, R. S.; Miranda, F. S.; Ribeiro, J. U.; Jr., C. B.; Ellena, J.; Moreno, V.; Cominetti, M. R.; Batista, A. A., Polypyridyl Ruthenium Complexes: Novel DNA-Intercalating Agents against Human Breast Tumor. *Journal of the Brazilian Chemical Society* **2017,** *28*, 1879-1889.

60. Popolin, C. P.; Reis, J. P. B.; Becceneri, A. B.; Graminha, A. E.; Almeida, M. A. P.; Corrêa, R. S.; Colina-Vegas, L. A.; Ellena, J.; Batista, A. A.; Cominetti, M. R., Cytotoxicity and anti-tumor effects of new ruthenium complexes on triple negative breast cancer cells. *PLOS ONE* **2017,** *12* (9), e0183275.

61. Spencer, A.; Wilkinson, G., Reactions of μ3-oxo-triruthenium carboxylates with π-acid ligands. *Journal of the Chemical Society, Dalton Transactions* **1974,** (8), 786-792.

62. Dobson, A.; Robinson, S. D.; Uttley, M. F., Complexes of the platinum metals. Part V. Perfluorocarboxylato-derivatives. *Journal of the Chemical Society, Dalton Transactions* **1975,** (5), 370-377.

63. Lovison, D.; Allegri, L.; Baldan, F.; Ballico, M.; Damante, G.; Jandl, C.; Baratta, W., Cationic carboxylate and thioacetate ruthenium(II) complexes: synthesis and cytotoxic activity against anaplastic thyroid cancer cells. *Dalton Transactions* **2020,** *49* (24), 8375-8388.

64. Arikawa, Y.; Nakamura, T.; Higashi, T.; Horiuchi, S.; Sakuda, E.; Umakoshi, K., Reactivity of a Methoxido–Ruthenium Complex Bearing a Pincer-Type Bis(carbene) Ligand toward Thiocyanate, Carbon Disulfide, and Isothiocyanate. *European Journal of Inorganic Chemistry* **2017,** *2017* (5), 881-884.

65. Brewster, T. P.; Ding, W.; Schley, N. D.; Hazari, N.; Batista, V. S.; Crabtree, R. H., Thiocyanate linkage isomerism in a ruthenium polypyridyl complex. *Inorganic chemistry* **2011,** *50* (23), 11938-11946.

66. Baer, C.; Pike, J., Infrared Spectroscopic Analysis of Linkage Isomerism in Metal−Thiocyanate Complexes. *Journal of Chemical Education* **2010,** *87* (7), 724-726.

67. Meot-Ner, M., The Ionic Hydrogen Bond. *Chemical Reviews* **2005,** *105* (1), 213-284.

68. Meot-Ner, M.; Elmore, D. E.; Scheiner, S., Ionic Hydrogen Bond Effects on the Acidities, Basicities, Solvation, Solvent Bridging, and Self-Assembly of Carboxylic Groups. *Journal of the American Chemical Society* **1999,** *121* (33), 7625-7635.

69. Smith, M. B., Organic Chemistry: An Acid-Base Approach. **2011,** *6*, 207.

70. Naruto, M.; Saito, S., Cationic mononuclear ruthenium carboxylates as catalyst prototypes for self-induced hydrogenation of carboxylic acids. *Nature Communications* **2015,** *6* (1), 8140.

71. Stumper, A.; Lämmle, M.; Mengele, A. K.; Sorsche, D.; Rau, S., One Scaffold, Many Possibilities – Copper(I)-Catalyzed Azide–Alkyne Cycloadditions, Strain-Promoted Azide–Alkyne Cycloadditions, and Maleimide–Thiol Coupling of Ruthenium(II) Polypyridyl Complexes. **2018,** *2018* (5), 586-596.

72. Sanhueza, L.; Cortés, D.; González, I.; Loeb, B., Condensation Reaction between Phenanthroline-5,6-diones and Ethylenediamine and Its Optimization through Dialogue between Theory and Experiment. In *Stereochemistry and Global Connectivity: The Legacy of Ernest L. Eliel Volume 2*, American Chemical Society: 2017; Vol. 1258, pp 79-89.

73. Hargreaves, M. D.; Mahon, M. F.; Whittlesey, M. K., Substitution Reactions of [Ru(dppe)(CO)(H2O)3][OTf]2. *Inorganic Chemistry* **2002,** *41* (12), 3137-3145.

74. Ooyama, D.; Sato, M., Crystallographic report: A synthetic precursor for hetero-binuclear metal complexes, $[Ru(bpy)(dppy)_2(CO)_2](PF_6)_2$ (bpy = 2,2′-bipyridine, dppy = 2-(diphenylphosphino)pyridine). *Applied Organometallic Chemistry* **2004,** *18* (8), 380-381.

75. Battistin, F.; Vidal, A.; Balducci, G.; Alessio, E., Investigating the reactivity of neutral water-soluble Ru(II)–PTA carbonyls towards the model imine ligands pyridine and 2,2′-bipyridine. *RSC Advances* **2020,** *10* (45), 26717-26727.

76. Denaro, N.; Nigro, C. L.; Russi, E. G.; Merlano, M. C., The role of chemotherapy and latest emerging target therapies in anaplastic thyroid cancer. *Onco Targets Ther* **2013,** *9*, 1231-1241.

77. Perri F, L. G., Scarpati GDV, Buonerba C. , Anaplastic thyroid carcinoma: A comprehensive review of current and future therapeutic options. . *World J Clin Oncol* **2011,** *2(3)*, 150-157.

78. Schlumberger, M.; Lacroix, L.; Russo, D.; Filetti, S.; Bidart, J.-M., Defects in iodide metabolism in thyroid cancer and implications for the follow-up and treatment of patients. *Nature Clinical Practice Endocrinology & Metabolism* **2007,** *3* (3), 260-269.

79. Sugitani, I.; Onoda, N.; Ito, K.-I.; Suzuki, S., Management of Anaplastic Thyroid Carcinoma: the Fruits from the ATC Research Consortium of Japan. *J Nippon Med Sch* **2018,** *85* (1), 18-27.

80. B. Stewart, C. P. W., IARC, World Cancer Report, WHO Press,. **2014**.

81. Torre, L. A.; Bray, F.; Siegel, R. L.; Ferlay, J.; Lortet-Tieulent, J.; Jemal, A., Global cancer statistics, 2012. *CA: A Cancer Journal for Clinicians* **2015,** *65* (2), 87-108.

82. Hall, M. D.; Telma, K. A.; Chang, K.-E.; Lee, T. D.; Madigan, J. P.; Lloyd, J. R.; Goldlust, I. S.; Hoeschele, J. D.; Gottesman, M. M., Say no to DMSO: dimethylsulfoxide inactivates cisplatin, carboplatin, and other platinum complexes. *Cancer Res* **2014,** *74* (14), 3913-3922.

83. Yarrow, J. C.; Perlman, Z. E.; Westwood, N. J.; Mitchison, T. J., A high-throughput cell migration assay using scratch wound healing, a comparison of image-based readout methods. *BMC Biotechnology* **2004,** *4* (1), 21.

84. Friedl, P. H., Y.; Tusch, M., Collective cell migration in morphogenesis and cancer. *Int. J. Dev. Biol.* **2004,** *48*, 441-449.

85. APEX suite of crystallographic software, APEX 3, Version 2015.5 2, Bruker AXS Inc., Madison, Wisconsin, USA, 2015.

86. Sheldrick, G., Crystal structure refinement with SHELXL. *Acta Crystallogr., Sect. A: Found. Adv* **2015,** *71*, 3-8.

87. C. B. Hubschle, G. M. S. a. B. D., ShelXle: a Qt graphical user interface for SHELXL. *J. Appl. Crystallogr.* **2011,** *44*, 1281–1284.

88. C. F. Macrae, I. J. B., J. A. Chisholm, P. R. Edgington, P. McCabe, E. Pidcock, L. Rodriguez-Monge, R. Taylor, J. van de Streek and P. A. Wood, Mercury CSD 2.0 – new features for the visualization and investigation of crystal structures. *J. Appl. Crystallogr.* **2008,** *41*, 466-470.

89. Becke, A. D., A new mixing of Hartree–Fock and local density-functional theories. *The Journal of Chemical Physics* **1993,** *98* (2), 1372-1377.

90. Lee, C.; Yang, W.; Parr, R. G., Development of the Colle-Salvetti correlation-energy formula into a functional of the electron density. *Physical Review B* **1988,** *37* (2), 785-789.

91. Miehlich, B.; Savin, A.; Stoll, H.; Preuss, H., Results obtained with the correlation energy density functionals of becke and Lee, Yang and Parr. *Chemical Physics Letters* **1989,** *157* (3), 200-206.

92. M. J. Frisch, G. W. T., H. B. Schlegel, G. E. Scuseria, M. A. Robb, J. R. Cheeseman, G. Scalmani, V. Barone, G. A. Petersson, H. Nakatsuji, X. Li, M. Caricato, A. V. Marenich, J. Bloino, B. G. Janesko, R. Gomperts, B. Mennucci, H. P. Hratchian, J. V Ortiz, A. F. Izmaylov, J. L. Sonnenberg, D. Williams-Yung, F. Ding, F. Lipparini, F. Egidi, J. Goings, B. Peng, A. Petrone, T. Henderson, D. Ranasinghe, V. G. Zakrzewski, J. Gao, N. Rega, G. Zheng, W. Liang, M. Hada, M. Ehara, K. Toyota, R. Fukuda, J. Hasegawa, M. Ishida, T. Nakajima, Y. Honda, O. Kitao, H. Nakai, T. Vreven, K. Throssell, J. A. Montgomery Jr., J. E. Peralta, F. Ogliaro, M. Bearpark, J. J. Heyd, E. Brothers, K. N. Kudin, V. N. Staroverov, T. A. Keith, R. Kobayashi, J. Normand, K. Raghavachari, A. Rendell, J. C. Burant, S. S. Iyengar, J. Tomasi, M. Cossi, J. M. Millam, M. Klene, C. Adamo, R. Cammi, J. W. Ochterski, R. L. Martin, K. Morokuma, O. Farkas, J. B. Foresman and D. J. Fox, Gaussian 16 Revis. A 03. **2016**.

93. Grimme, S.; Ehrlich, S.; Goerigk, L., Effect of the damping function in dispersion corrected density functional theory. *Journal of Computational Chemistry* **2011,** *32* (7), 1456-1465.

94. Veclani, D.; Melchior, A.; Tolazzi, M.; Cerón-Carrasco, J. P., Using Theory To Reinterpret the Kinetics of Monofunctional Platinum Anticancer Drugs: Stacking Matters. *Journal of the American Chemical Society* **2018,** *140* (43), 14024-14027.

95. Dabbish, E.; Russo, N.; Sicilia, E., Rationalization of the Superior Anticancer Activity of Phenanthriplatin: An In-Depth Computational Exploration. *Chemistry – A European Journal* **2020,** *26* (1), 259-268.

96. Du, J.; Jiang, G., Adsorption of actinide ion complexes on C60O: An all-electron ZORA-DFT-D3 study. *Spectrochim Acta A Mol Biomol Spectrosc* **2019,** *223*, 117375.

97. Mendizabal, F.; Miranda-Rojas, S., Electronic and optical properties of $[Au(CH_3CSS)]_4$ cluster. A quantum chemistry study. *RSC Advances* **2020,** *10* (55), 33549-33557.

98. Weigend, F., Accurate Coulomb-fitting basis sets for H to Rn. *Physical Chemistry Chemical Physics* **2006,** *8* (9), 1057-1065.

99. Weigend, F.; Ahlrichs, R., Balanced basis sets of split valence, triple zeta valence and quadruple zeta valence quality for H to Rn: Design and assessment of accuracy. *Physical Chemistry Chemical Physics* **2005,** *7* (18), 3297-3305.

100. Tomasi, J.; Mennucci, B.; Cammi, R., Quantum Mechanical Continuum Solvation Models. *Chemical Reviews* **2005,** *105* (8), 2999-3094.

101. Maggisano, V.; Celano, M.; Lombardo, G. E.; Lepore, S. M.; Sponziello, M.; Rosignolo, F.; Verrienti, A.; Baldan, F.; Puxeddu, E.; Durante, C.; Filetti, S.; Damante, G.; Russo, D.; Bulotta, S., Silencing of hTERT blocks growth and migration of anaplastic thyroid cancer cells. *Mol Cell Endocrinol* **2017,** *448*, 34-40.

102. Schweppe, R. E.; Klopper, J. P.; Korch, C.; Pugazhenthi, U.; Benezra, M.; Knauf, J. A.; Fagin, J. A.; Marlow, L. A.; Copland, J. A.; Smallridge, R. C.; Haugen, B. R., Deoxyribonucleic Acid Profiling Analysis of 40 Human Thyroid Cancer Cell Lines Reveals Cross-Contamination Resulting in Cell Line Redundancy and Misidentification. *The Journal of Clinical Endocrinology & Metabolism* **2008,** *93* (11), 4331-4341.

103. Allegri, L.; Mio, C.; Russo, D.; Filetti, S.; Baldan, F., Effects of HuR downregulation on anaplastic thyroid cancer cells. *Oncol Lett* **2018,** *15* (1), 575-579.

104. Daniel KG, C. D., Orlu S, Cui QC, Miller FR, et al. , Clioquinol and pyrrolidine dithiocarbamate complex with copper to form proteasome inhibitors and apoptosis inducers in human breast cancer cells. . *Brest Cancer Res* **2005,** *7*, R897–908.

105. Allegri, L.; Rosignolo, F.; Mio, C.; Filetti, S.; Baldan, F.; Damante, G., Effects of nutraceuticals on anaplastic thyroid cancer cells. *Journal of Cancer Research and Clinical Oncology* **2018,** *144* (2), 285-294.

106. Liang, C.-C.; Park, A. Y.; Guan, J.-L., In vitro scratch assay: a convenient and inexpensive method for analysis of cell migration in vitro. *Nature Protocols* **2007,** *2* (2), 329-333.

Acknowlegments

I would like to express my deep gratitude to my research supervisor, Professor Walter Baratta, for giving me this opportunity, for his patient guidance, enthusiastic encouragement and for the constructive teachings during the planning and development of this research work.

I would like to express my very great appreciation to Professor Giuseppe Damante and Dr. Lorenzo Allegri, for the biological work regarding this project, for trying to connect medicine with chemistry, even though sometimes hard to achieve.

I would also like to extend my thanks to my close collaborator Dr. Maurizio Ballico, for his useful and constructive recommendations on this project, leading me to reach new ideas, for his help day by day. My thanks are extended also to Dr. Rosario Figliolia, my friend and colleague, for his support, his suggestions and encouragement throughout my study.

I am particularly grateful to the following people for their contribution to this project: Dr. Paolo Martinuzzi and Pierluigi Polese for their valuable technical support helping me in handling the analytical instruments (NMR, IR, etc.); Professor Andrea Melchior and Dr. Daniele Veclani, for their participation to this project with DFT calculations; Dr. Christian Jandl of the Technische Universität München (TUM) for the crystal x-ray structure determinations; and Dr. Chiara Nardon for her participation in the extension of biological studies with her support and great experience.